CELL-BASED AND BIOCHEMICAL SCREENS FOR SMALL-MOLECULE INHIBITORS OF DYNEIN AND OF HSP70

by

Guangyu Zhu

B.S., Peking University, 2002

Submitted to the Graduate Faculty of

School of Arts and Sciences in partial fulfillment

of the requirements for the degree of

Doctor of Philosophy

University of Pittsburgh

2007

UNIVERSITY OF PITTSBURGH

SCHOOL OF ARTS AND SCIENCES

This dissertation was presented

by

Guangyu Zhu

It was defended on

June 25th, 2007

and approved by

Dennis P. Curran, Ph.D.

Christian E. Schafmeister, Ph.D.

Donald B. DeFranco, Ph.D.

Billy W. Day, Ph.D.
Dissertation Major Adviser

CELL-BASED AND BIOCHEMICAL SCREENS FOR SMALL-MOLECULE INHIBITORS OF DYNEIN AND OF HSP70

Guangyu Zhu, Ph.D.

University of Pittsburgh, 2007

Dyneins are protein motor complexes that generate force towards the minus ends of microtubules, and cytoplasmic dynein plays a variety of important roles in cell. A small library of synthetic chemicals based on the natural product purealin was first examined for inhibition of cytoplasmic dynein heavy chain and cell growth. The compounds showed effective antiproliferative activity against a mouse leukemia cell line, but selective activities against a small panel of human carcinoma cell lines. Purealin and some of its analogues showed concentration-dependent inhibitory effects against the microtubule-stimulated ATPase activity of both bovine cytoplasmic dynein heavy chain as well as the recombinant motor domain of human cytoplasmic dynein in an uncompetitive pattern, indicating that they do not compete with the binding of ATP. Purealin also weakly inhibited p53 nuclear accumulation after DNA damage. Small interfering RNAs of cytoplasmic dynein heavy chain were also tested as a positive control in this assay, although the lifetime of the protein turned out to be too long for the siRNA approach to be useful in a screening protocol.

A strategy was built to screen for dynein inhibitors based on a GFP-GR nuclear translocation assay by using a mouse mammary adenocarcinoma cell line (3617.4) stably expressing the fluorescent protein. A small library of synthetic compounds was screened for inhibition of hormone-stimulated GFP-GR nuclear translocation. Several compounds were found to elicit the desired phenotype, and these compounds inhibited the ATPase activity of

cytoplasmic dynein heavy chain motor domain without competing for the hydrolyzable ATP-binding site. Biochemical specificity tests showed that the compounds did not compete for GR binding nor inhibit the ATPase activities of Hsp70, Hsp90 or myosin.

Libraries of compounds designed to be Hsp70-perturbing agents were also evaluated. Previous data showed that the Hsp70 chaperone class is induced in certain breast cancer cells and that antisense-mediated knockdown of Hsp70 triggers apoptosis, indicating that Hsp70s represent a new target for breast cancer therapy. A small molecule inhibitor of Hsp70 co-chaperone interaction (MAL3-101), as well as several analogues, showed antiproliferative activity against SK-BR3 breast cancer cells.

TABLE OF CONTENTS

TABLE OF CONTENTS VI
LIST OF TABLES IX
LIST OF FIGURES XI
ABBREVIATIONS XV
PREFACE XVII
1.0 **INTRODUCTION** 1
1.1 Microtubule and microtubule-associated proteins 1
1.2 Motor proteins and motor protein inhibitors 3
1.3 Dynein as a molecular target 6
1.3.1 Cytoplasmic dynein 6
1.3.2 The dynein transportation system 10
1.3.3 Known dynein inhibitors 12
1.3.4 Purealin and purealin library 13
1.4 Hsp70 as a chemotherapeutic target 16
1.4.1 Hsp70 as a molecular chaperone 16
1.4.2 Compounds targeting Hsp70 18
2.0 **MATERIALS AND EXPERIMENTAL PROCEDURES** 21
2.1 Materials 21
2.2 Experimental procedures 22
2.2.1 Antiproliferative assay 22
2.2.2 Dynein purification from bovine brain 23
2.2.3 Glycerol-based dynein purification 24
2.2.4 Colorimetric ATPase assay 25
2.2.5 Western blotting 25

2.2.6 SDS-PAGE 26
2.2.7 In-gel digestion with trypsin 26
2.2.8 Mass spectrometry 27
2.2.9 Dynein ATPase inhibition assay 27
2.2.10 P53 nuclear translocation assay 28
2.2.11 Dynein heavy chain siRNA experiment 29
2.2.12 GFP-glucocorticoid receptor nuclear translocation assay 31
2.2.13 Glucocorticoid receptor ligand binding domain competitor assay 32
2.2.14 *In vitro* glucocorticoid receptor binding assay 32
2.2.15 Recombinant cytoplasmic dynein motor domain expression and purification 33
2.2.16 Kinetics of cytoplasmic dynein heavy chain motor domain inhibition 34
2.2.17 Hsp70 and Hsp90 ATPase assays 35
2.2.18 Myosin Ca^{2+}-ATPase assay 35
2.2.19 Cellular levels of soluble and polymerized tubulin 36
2.2.20 Tubulin polymerization assay 37
3.0 **BIOLOGICAL EVALUATION OF A PUREALIN LIBRARY** 38
3.1 Introduction 38
3.2 Antiproliferative activities of purealin library components 43
3.3 Dynein isolation and purification 45
3.3.1 Purification of bovine brain cytoplasmic dynein heavy chain 45
3.3.2 Characterization of bovine cytoplasmic dynein by mass spectrometry 49
3.3.3 Expression and purification of dynein motor domain 54
3.4 Biochemical evaluation of purealin library component 56
3.5 P53 nuclear translocation experiments 62
3.6 siRNA-based knockdown of dynein heavy chain 71
3.7 Discussion 75
4.0 **DISCOVERY OF NEW SMALL-MOLECULE INHIBITORS OF CYTOPLASMIC DYNEIN BY A PHENOTYPIC SCREEN** 78
4.1 Introduction 78
4.2 Chemical Libraries for screening 78

4.3 GFP-GR nuclear translocation screening results 79
4.3.1 Inhibitory effect of EHNA on GFP-GR nuclear translocation 79
4.3.2 Inhibition by purealin of GFP-GR nuclear translocation 82
4.3.3 Inhibitory effect of the UPCMLD library compounds on GFP-GR nuclear translocation 82
4.4 *in vitro* GR binding assay results 88
4.5 Inhibition of dynein motor domain ATPase 90
4.6 Kinetics study on the new dynein inhibitors 91
4.7 Specificity studies 96
4.7.1 Hsp70 and Hsp90 ATPase assay results 96
4.7.2 Myosin ATPase assay results 98
4.7.3 Microtubule polymerization assay results 99
4.8 Antiproliferative activity of the UPCMLD hit compounds 104
4.9 Discussion 104
5.0 **BIOLOGICAL EALUATION OF HSP70 INHIBITORS** 107
5.1 Introduction 107
5.2 Antiproliferative activity of the first library 108
5.3 Antiproliferative activity of Ugi-Biginelli compounds 111
5.4 Conclusions and discussion 115
6.0 **CONCLUSIONS AND DISCUSSIONS** 118
BIBLIOGRAPHY 123

LIST OF TABLES

Table 1. Antiproliferative activities of the purealin/purealidin library. 44
Table 2. Peak assignments of mass spectrum of spot 1 50
Table 3. Protein identification results by MALDI-TOFMS. 53
Table 4. Fifty percent dynein heavy chain ATPase inhibitory concentrations of the purealin library. 58
Table 5. The V^{app}_{max}, K^{app}_{M} and Ki values of dynein ATPase with and without different inhibitors. 62
Table 6. Dynein heavy chain siRNA sequences. 71
Table 7. The V^{app}_{max}, K^{app}_{M} and K_i values of the ATPase activity of recombinant cytoplasmic dynein heavy chain motor domain in the presence of 2, 10 and 50 μM PSI002049. 93
Table 8. The V^{app}_{max}, K^{app}_{M} and K_i values of the ATPase activity of recombinant cytoplasmic dynein heavy chain motor domain in the presence of 50μM CMC002042, PSI002042, STW001222 and PSI002043 94
Table 9. The V^{app}_{max}, K^{app}_{M} and K_i values of the microtubule-stimulated ATPase activity of recombinant cytoplasmic dynein heavy chain motor domain in the presence of 50μM STW001222, PSI002049 and PSI002049. 95
Table 10. Effects of the compounds on the rate of Hsp70 ATP hydrolysis 97
Table 11. Effects of the compounds on the rate of Hsp90 ATP hydrolysis 97
Table 12. Effects of the compounds (100 μM) on the rate of myosin Ca^{2+}-stimulated ATPase activity of rabbit muscle myosin II (25 μg/mL). 98
Table 13. Antiproliferative activities of the test agents against 3617.4 cells. 104
Table 14. Antiproliferative activity of MAL3-101 and structural related compounds against SK-BR3 cells. 110

Table 15. Antiproliferative activity of MAL3-101 against MDA-MB468 and WI-38 cell proliferation..... 110

LIST OF FIGURES

Figure 1. Chemical structures of two microtubule depolymerization inhibitors: paclitaxel and discodermolide 2
Figure 2. Schematic rendition of the intramolecular communication within one motor domain of myosin (a), kinesin (b) and dynein (c), and translation into a conformational change that leads to movement. 3
Figure 3. Chemical structures of the kinesin inhibitors AS-2 and monastrol, and the myosin inhibitors blebbistatin and BTS. 5
Figure 4. Organization of the dynein motor domain. 7
Figure 5. A speculative model for the dynein cross-bridge cycle. 8
Figure 6. Structure and power stroke of dynein c. 9
Figure 7. Model of links between cytosolic dynein heavy chain to p53. 11
Figure 8. Chemical structures of the known dynein inhibitors EHNA, AMP-PNP and NEM. 12
Figure 9. Structures of the only known non-ATP-mimicking dynein inhibitor, purealin, and other related dibromotyrosine-derived natural products. 13
Figure 10. Bromotyrosine-derived alkaloids. 14
Figure 11. Structures of 16 purealidin A analogues. 15
Figure 12. Chemical structures of DSG and NSC-630668-R/1. 18
Figure 13. (A) Chemical structure of MAL3-101 and (B) superimposed molecular models of R/1 (yellow) and MAL3-101 (white). 19
Figure 14. Flow diagram illustrating the preparation of brain cytoplasmic dynein. 39
Figure 15. SDS-PAGE of bovine cytoplasmic dynein after sucrose gradient centrifugation. 40
Figure 16. Schematic of MALDI (A) and structure of the matrix molecule α-cyano-4-hydroxycinnamic acid (B). 42

Figure 17. Coomassie blue-stained SDS-PAGE (A) and anti-dynein heavy chain Western blot (B) analysis of sucrose density gradient fractions in the standard purification of dynein heavy chain. 46
Figure 18. Anti-dynein intermediate chain Western blot analysis of sucrose density gradient fractions 3-8. 46
Figure 19. The protein concentration (A) and ATPase activity (B) of different dynein purification fractions 5-7. 47
Figure 20. ATPase activity of brain cytoplasmic dynein as a function of microtubule concentration. 47
Figure 21. Inhibitory effect of EHNA on bovine cytoplasmic dynein ATPase activity. 48
Figure 22. Coomassie blue-stained SDS-PAGE analysis of sucrose density gradient fractions in the glycerol-based dynein purification. 48
Figure 23. Coomassie blue-stained SDS-PAGE gel used in the mass spectrometric analysis of dynein fractions 49
Figure 24. MALDI-TOF mass spectrum of spot 1 50
Figure 25. MALDI-TOF- mass spectrum of spot 2 52
Figure 26. MALDI-TOF mass spectrum of spot 3 52
Figure 27. MALDI-TOF mass spectrum of spot 4. 53
Figure 28. SDS-PAGE analysis of protein samples from the baculovirus/Hi5 cell cytoplasmic dynein heavy chain motor domain expression system. 55
Figure 29. Inhibition by purealin of ATPase activity of axonemes and outer-arm-depleted axonemes. 56
Figure 30. Inhibition of bovine brain dynein ATPase activity by purealin and purealidin A. 57
Figure 31. Dynein motor domain ATPase inhibitory activities of purealin, purealidin A and *para*/chlorophenyl/H-purealidin A. 59
Figure 32. Inhibition by purealin of dynein ATPase activity. 59
Figure 33. Michaelis-Menten curve (A) and Hanes-Woolf curve (B) of dynein in the presence of difference inhibitors: purealin, purealidin A and *para*/chlorophenyl/H-purealidin A. 61
Figure 34. Overexpression of dynamitin inhibits p53 movement to the nucleus. 63
Figure 35. Dynein-driven nuclear uptake of wild type p53 in A549 cells treated with camptothecin (data courtesy of Dr. Kenneth Giuliano). 64

Figure 36. EHNA blocks p53 translocation into the nucleus after DNA damage. 65
Figure 37. Inhibitory activity of purealin and *para*/chlorophenyl/H-purealidin A on p53 translocation into the nucleus after DNA damage 67
Figure 38. Representative composite immunofluorescent images from p53 nuclear translocation high content screening experiments. 68
Figure 39. Average florescent intensity in A549 cells after treatment with camptothecin (CPT).69
Figure 40. Average florescent intensity in A549 cell upon the treatment of EHNA. 69
Figure 41. Average florescent intensity in A549 cells after treatment with purealin. 70
Figure 42. siRNA knockdown of dynein heavy chain. 73
Figure 43. Immunostaining of nuclei, p53 and dynein heavy chain in A549 cells uppn treatment of scrambled siRNA or DyHC siRNA. 74
Figure 44. Structural classes within the UPCMLD initial discovery library. 79
Figure 45. EHNA blocks GFP-GR nuclear translocation. 80
Figure 46. Time-dependent inhibitory effect of 2.5mM EHNA against GFP-GR nuclear translocation. 81
Figure 47. Purealin inhibition effect of GFP-GR nuclear translocation. 82
Figure 48. GFP-GR nuclear translocation inhibitory effect of JUN266. 83
Figure 49. GFP-GR nuclear translocation inhibitory activity of the UPCMLD compounds. 84
Figure 50. The nuclear translocation scores of the active UPCMLD compounds (left) and chemical structures of the compounds (right). 85
Figure 51. Representative images of GFP-GR nuclear translocation assay by IN Cell Analyzer 1000 system. 86
Figure 52. Quantification of GFP-GR nuclear translocation assay by IN Cell Analyzer 1000. ... 87
Figure 53. Low potency of the GFP-GR translocation-inhibitory compounds in an *in vitro* GR competition assay as compared to DEX (mean ± SD, N = 4). 89
Figure 54. Low potency of the compounds in affecting hormone-specific GR binding as compared to DEX (mean ± SD, N = 2). 89
Figure 55. Inhibitory activities of UMCMLD compounds against recombinant dynein heavy chain motor domain. 91
Figure 56. Inhibition by PSI002049 of recombinant rat cytoplasmic dynein heavy chain motor domain-catalyzed release of free phosphate from ATP. 92

Figure 57. Michaelis-Menten (*left*) and Hanes-Woolf (*right*) plots of basal dynein motor domain ATPase activity in the presence of different concentrations of PSI002049. 93
Figure 58. Michaelis-Menten (left) and Hane-Woolf (right) plots of basal dynein motor domain ATPase activity in the presence of 50μM CMC002042, PSI002042, STW001222 and PSI002043. 94
Figure 59. Michaelis-Menten (left) and Hane-Woolf (right) plots of microtubule-stimulated dynein motor domain ATPase activity in the presence of 50μM STW001222, PSI002049 and PSI002049. 95
Figure 60. Western blot analysis of polymerized (p) and soluble (s) tubulin fractions of 3617.4 cells with treatment of colchicine or paclitaxel. 100
Figure 61. Western blot analysis of polymerized (p) and soluble (s) tubulin fractions of 3617.4 cells with treatment of dynein inhibitors. 101
Figure 62. Turbidity profiles of tubulin polymerization assay with stepwise temperature changes in the presence of PSI002049. 103
Figure 63. Dynein motor domain ATPase in the presence of different concentration of PSI002049 fractions. 106
Figure 64. General synthetic scheme of MAL3-101 analogues. 108
Figure 65. Chemical structure of MAL3-101 structural related compounds. 109
Figure 66. Antiproliferative activity of Ugi-1 compounds. 111
Figure 67. Antiproliferative activity of Ugi-2 compounds. 112
Figure 68. Antiproliferative activity of Ugi-3 compounds. 113
Figure 69. Antiproliferative activity of Biginelli acids. 114
Figure 70. Antiproliferative activity of Biginelli esters. 115
Figure 71. Structure-activity relationship of MAL3-101 analogues. 117

ABBREVIATIONS

AAA	ATPase-associated diverse cellular activities
ATP	Adenosine triphosphate
CHCA	α-Cyano-4-hydroxycinnamic acid
DCD	Discodermolide
DyHC	Dynein heavy chain
DMEM	Dulbecco's modified eagle's medium
DMSO	Dimethylsulfoxide
DSS	Dissuccinimidyl suberate
DTT	Dithiothreitol
EDTA	Ethylenediaminetetraacetic acid
EGTA	Ethyleneglycoltetraacetic acid
EHNA	*erythro*-9-(2-Hydroxy-3-nonyl)adenine
GFP-GR	Green fluorescent protein-glucocorticoid receptor
GTP	Guanosine triphosphate
HEPES	4-(2-Hydroxyethyl)-1-piperazineethanesulfonic acid
IC	Intermediate chain
LC	Light chain
MALDI-TOF/TOF-MS/MS	Matrix-assisted laser desorption ionization-time of flight/time of flight-mass spectrometry/mass spectrometry
MAPs	Microtubule-associated proteins
MTS	3-(4,5-Dimethylthiazol-2-yl)-5-(3-carboxymethoxyphenyl)-2-(4-sulfophenyl)-2*H*-tetrazolium
MTs	Microtubules
PI	Protease inhibitors

PIPES	Piperazine-*N*,*N*′-bis(2-ethanesulfonic acid)
PMSF	Phenylmethylsufonyl fluoride
PVDF	Polyvinylidene difluoride
SAR	Structure-activity relationship
QSAR	Quantitative structure-activity relationship
SDS-PAGE	Sodium dodecyl sulfate-polyacrylamide gel electrophoresis

PREFACE

I would like to take this opportunity to thank people who gave me great help during my Ph.D. study. First and foremost, I would like to thank my adviser, Prof. Billy W. Day for choosing me as his Ph.D. student and offering me a great project at the interface of chemistry and biology, and for training me in the aspects of cell biology, biochemistry, cutting-edge proteomics and computational chemistry. He gave me so much help in this context. He is a great mentor to let me have the freedom to explore my ability to uncover the mystery of the research work. I would like to thank my committee members, Prof. Dennis P. Curran, Prof. Christian E. Schafmeister and Prof. Donald B. DeFranco for their being on my committee, their support and all the useful discussions I have had with them.

I would like to thank Dr. Raghanvan Balachandran, a senior scientist in Prof. Day's group, for giving me so much support in learning cell culture, biochemistry, protein purification and other cell biology techniques. I would like to thank all other Day group members, Charitha Madiraju, Jelena Janjic, Brianne Raccor, Miranda Sarachine, Weixiang Dai, Zhe Zhang, Yun Fan and Jie Gao, for their help.

There are many collaborators in my research work, and it was my great pleasure to work with them. I would like to thank Prof. Richard B. Vallee at Columbia University Medical Center, as well as his group members, Drs. Peter Hook, Jennifer Litowski, Helen Bremner and Pascale Monzo, and Richard McKenny, Stephanie Stehman, Dileep Varma and Jin-Wu Tsai, for their

great support in the dynein motor domain expression and purification, as well as biochemical evaluations of dynein inhibitors. I greatly appreciate Prof. Vallee's invitations to visit his laboratory and all of the techniques I learned while there. I would also like to thank Prof. Donald B. DeFranco as well as his lab members Marcia Lewis, Xinjia Wang, Terry McGuire, Marjet Heitzer, Louisa Ho and Yue Luo for their support in the context of GFP-GR assays. I would like to thank Prof. Jeffrey Brodsky and his lab members Christine Wright and Ping Zhang for their help with the HSP70/90 assays.

I would also like to extend my acknowledgement to Prof. Dennis P. Curran and Dr. Fanglong Yang for the synthesis of purealin and its analogues, Profs. Peter Wipf and Kay Brummond and Dr. Stefan Werner for their support and the UPCMLD compounds, Prof. Andreas Vogt for help on the ArrayScan system, and Drs. Dwayne W. Dexter and Ann del Campo for their help with data analysis.

At last, I would like to thank my family members, for their support all over the years. Especially, I would like to sincerely thank my beautiful, lovely wife, Mo Ji. It is Mo who encourages me when I meet difficulties. It is Mo who gives me wonderful suggestions when I need them. It is Mo as well who ignites my romantic life in the United States and gives me hope to pursue my scientific career road. I could accomplish nothing without her.

1.0 INTRODUCTION

The aims of cancer researchers is not only to identify new structural classes of agents to selectively attack the disease, but also to aim at new targets. In this work, cytoplasmic dynein and Hsp70 were chosen as drug targets that are both unique and challenging. The first goal of this project was to develop a high throughput and high information content screening system for examining libraries of compounds as potential inhibitors of the molecular motor cytoplasmic dynein. Through wise selection of screening strategies and new methods for compound evaluation, chemical biology tools and even novel therapeutic agents could be found. The second goal of this project was to evaluate Hsp70-targeting agents as anti-breast cancer agents. In both cases, the biological activities measured for library members will allow structure-activity relationship (SAR) development, which should aid in the discovery of more portent and/or selective agents. Also, the biological character of the drug target as well as the molecular mechanisms of action for a given agent could be evaluated. This results from this project will provide a cornerstone for these goals.

1.1 Microtubule and microtubule-associated proteins

Microtubules (MTs) are intracellular tubes of regular circumference that form cytoskeletal lattices and the mitotic spindle. They are built and dismantled by the dynamic

assembly/disassembly of heterodimers of the ~50 kDa proteins α- and β- tubulin, of which several isotypes for each monomer exist in mammalian systems[1]. The tubulin/microtubule system is a proven clinically useful antitumor target. Examples of chemotherapeutics that act via perturbation of tubulin polymerization include paclitaxel, docetaxel, vinblastine and discodermolide[2-5] (Figure 1).

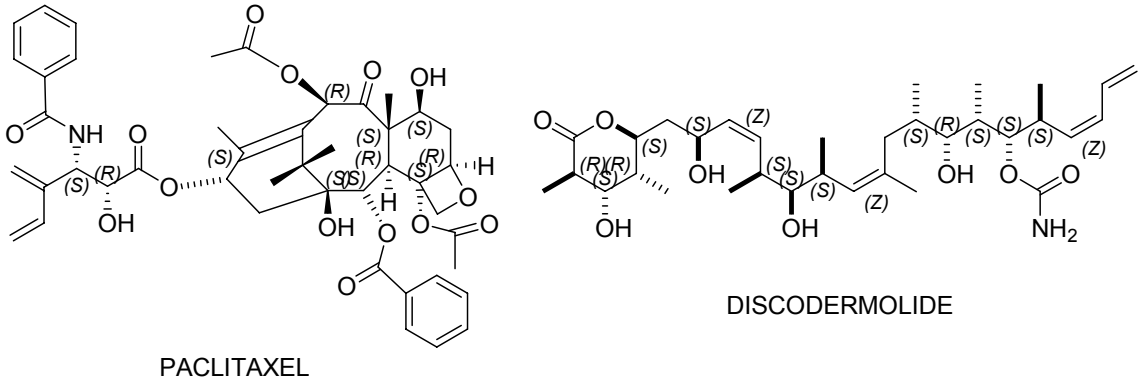

Figure 1. Chemical structures of two microtubule depolymerization inhibitors: paclitaxel and discodermolide

There is a large group of microtubule(MT)-associated proteins, or MAPs[6], that bind microtubules, acting mainly to stabilize them against disassembly. The binding of MAPs to microtubules is largely dependent on MAP phosphorylation status, making them targets for protein kinases. Major MAPs include MAP1, MAP2, MAP4 and tau. MAP4 is the most abundant and ubiquitous MAP in non-neuronal cells that stabilizes microtubules[7].

1.2 Motor proteins and motor protein inhibitors

Motor proteins are amazing biological machines that are responsible for most forms of movement in cells. Motor proteins utilizing the cytoskeleton as the railway for their movement fall into two categories: Actin motors, such as myosin, move along microfilaments through interaction with actin; Microtubule motors, such as dynein and kinesin, move along microtubules through interaction with tubulin. There are two basic types of microtubule motors: plus end-motors and minus end-directed motors, depending on the direction in which they "walk" along the microtubule cables within the cell. Motor proteins utilize ATP hydrolysis to generate the power they use to “walk”, which causes a small conformational change in the global motor domain (Figure 2).

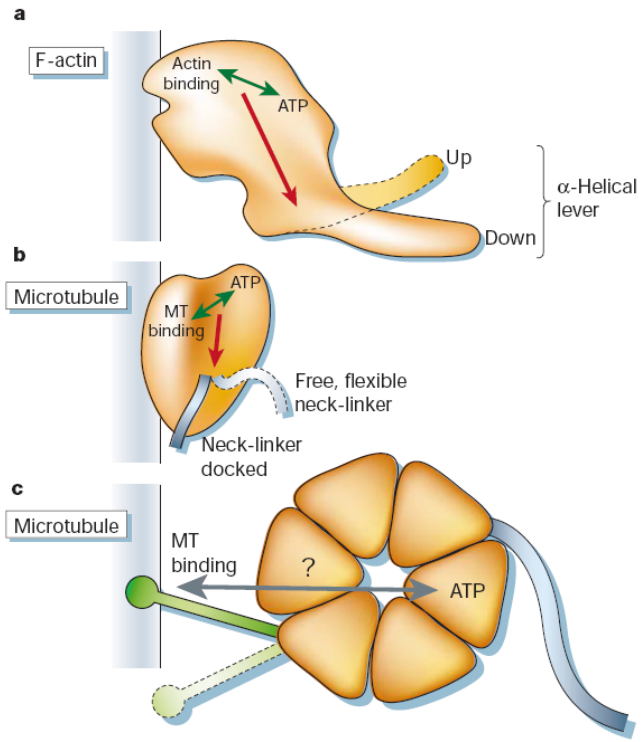

Figure 2. Schematic rendition of the intramolecular communication within one motor domain of myosin (a), kinesin (b) and dynein (c), and translation into a conformational change that leads to movement.
[From Schlwa, M et al. Nature 422, 759 (2003). Ref. [8]]

Motor proteins are involved in protein, organelle and vesicle transport in cells, and non-motor domains and associated proteins play a key role in this process. The protein myosin plays important roles in the contraction of muscle fibers in animals. Kinesins and dyneins play essential roles in the formation of the mitotic spindle apparatus and the separation of chromosomes during mitosis and meiosis. Dynein is also found in flagella and is crucial for cell motility.

Much effort has been expended in the pursuit of small molecule inhibitors of kinesins and myosins (Figure 3). In 1998, a small molecule known as adociasulfate-2 (AS-2), from the active extract of marine sponge, was found to disrupt microtubule attachment to the kinesin-coated surface in a motility assay and to completely inhibit the MT-stimulated kinesin ATPase activity with an IC_{50} of 2.7 μM[9]. Specificity tests with various ATPases showed that the only enzymes substantially inhibited by AS-2 were kinesin superfamily members. However, tests with cells in grown in culture demonstrated that AS-2 has no effect on the proliferation of HeLa cells. AS-2 was then injected into early *Drosophila* embryos. Arrest of nuclear division was observed with high concentrations of AS-2, and some distinct abnormalities (e.g., spindles and MT asters without chromosomes, mats of unattached MTs, etc.) were found with lower concentrations.

The small molecule monastrol is an example of a cell-permeable, kinesin-specific inhibitor[10]. It was identified from a phenotypic screen in which monastrol caused monoastral spindles in mitotic cells. Monastrol inhibits Eg5 (a mitotic kinesin)-driven microtubule motility with an IC_{50} of 14 μM and has no effect on the localization and organization of the Golgi apparatus or lysosomes. Monastrol has gained acceptance as a biological tool for studying the mitotic function of Eg-5[11].

There are also several known small-molecule inhibitors of myosin. For example, blebbistatin is a known myosin II inhibitor discovered from a high-throughput screening assay[12]. It inhibits both the ATP and gliding activities of human platelet non-muscle myosin II without inhibiting myosin light chain kinase. It also rapidly disrupts directed cell migration and cytokinesis in vertebrate cells. Addition of blebbistatin to dividing cells blocks furrow ingression within 5 min and is reversible. It is also known that *N*-benzyl-*p*-toluene sulfonamide (BTS) inhibits the Ca^{2+}-stimulated rabbit muscle myosin

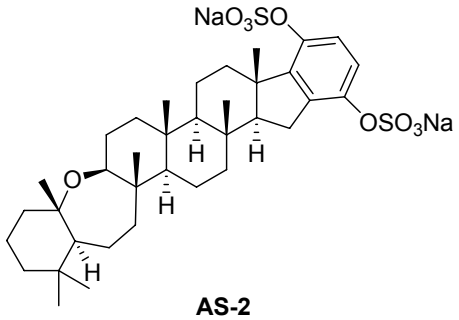

AS-2

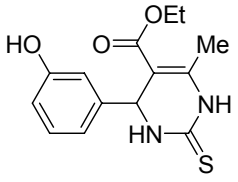

Monastrol

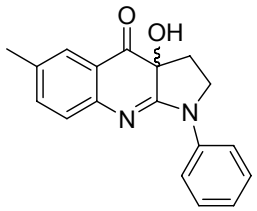

Blebbistatin

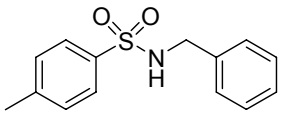

BTS

Figure 3. Chemical structures of the kinesin inhibitors AS-2 and monastrol, and the myosin inhibitors blebbistatin and BTS.

II S1 ATPase, and reversibly blocks gliding motility[12]. Although BTS does not compete for the nucleotide-binding site of myosin, it weakens myosin's interaction with F-actin. BTS reversibly suppresses force production in skeletal muscle fibres from rabbit and frog skin at micromolar

concentrations. The discovery of such motor protein inhibitors with high specificity and cell permeability suggests that motor proteins may be potential targets for therapeutic applications.

There are, however, few cell-permeable, dynein-specific inhibitors. At the time this work began, the only known dynein inhibitors included the ATP analogues *erythro*-9-(2-hydroxy-3-nonyl)adenine (EHNA) and 5'-adenylimidodiphosphate (AMP-PNP), the sulfhydryl-reactive agent *N*-ethylmaleimide (NEM) and the natural product purealin. Details on dynein inhibitors will be discussed in section 1.3.3.

1.3 Dynein as a molecular target

1.3.1 Cytoplasmic dynein

Dyneins are molecular motor complexes (dynein+dynactin) that generate force toward the minus ends of MTs[13]. There are approximately 15 forms of dynein found in vertebrates; most of them are "axonemal", referring to their role in ciliary and flagellar movement. Only two forms are "cytoplasmic": cytoplasmic dynein-1, initially discovered by Richard Vallee et al. as the microtubule-associated protein 1C (MAP1C)[13], which is widely expressed in cells and is responsible for a surprising range of functions; and cytoplasmic dynein-2, which has a restricted distribution and a narrow range of functions[14,15].

Cytoplasmic dynein is a multisubunit protein complex composed of a heavy chain (DyHC) polypeptide of >500 kDa, which is responsible for ATPase and motor activities, and several intermediate chains (ICs), light intermediate chains (LICs) and light chains (LCs) that are responsible for subcellular localization, and recognizing and binding the various forms of

"cargo" carried by dynein. The dynein motor domain is a hexamer of six tandemly linked ATPase-associated diverse cellular activities (AAA) modules[10,16,17]. The first four AAA modules are centrally located in dynein and are well conserved in all dynein sequences. It has been shown that the AAA1 module contains the site of ATP hydrolysis that leads to movement[18]. The next three modules, AAA2-AAA4, bind to nucleotides with lower affinity, but this binding is important for the regulation of dynein function[19]. AAAs 1-4 all contain well preserved P-loop elements that are important in removal of the γ-phosphate of ATP during hydrolysis. The P-loop elements within AAAs 5 and 6 are degenerate and less likely to be functional, but they must be intact with the other AAA modules for the proper dynein ATPase function[20]. A substantial projection called the 'stalk' emerges between AAAs 4 and 5 and has a microtubule-binding site at its tip (Figure 4).

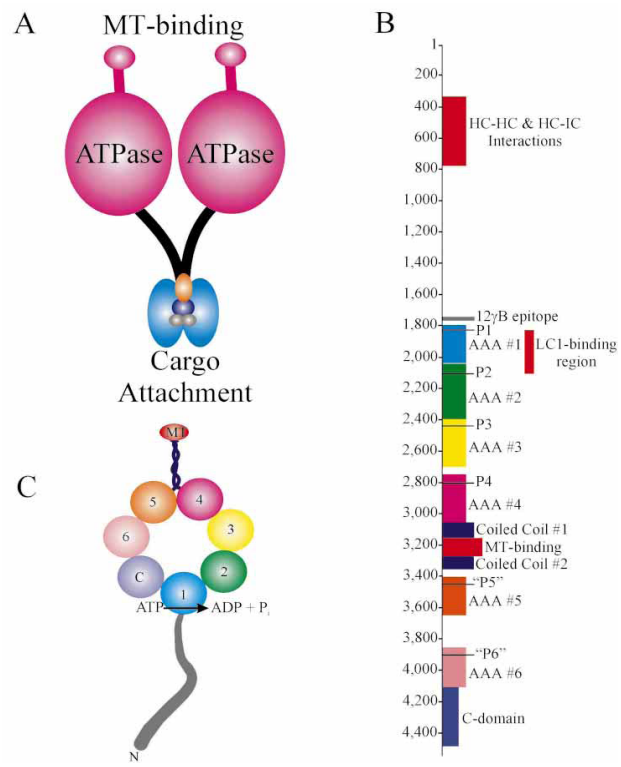

Figure 4. Organization of the dynein motor domain.
(A) Generic model of a dynein particle containing two heavy chains. (B) Map of the γ heavy chain (HC) from *Chlamydomonas* outer arm dynein indicating the six AAA domains (AAA1-AAA6), P-loops (P1-P6), the microtubule binding region and coiled-coil segments. Also illustrated is the section that in cytoplasmic dynein is involved in HC-HC and HC-IC interactions, the LC1-binding and the epitope recognized by conoclonal antibody 12γB. (C) Model for the organization of an individual HC illustrating the heptameric structure of the head. [From King, SM *J. Cell. Sci.* **2000**,113:2521, Ref.[10]]

A speculative model for the dynein cross-bridge cycle is shown in Figure 5[21]. In

the figure, the six AAA modules are depicted as spheres and are numbered. The stalk is the green projection at the top of the motor, and the stem connected to P1 is in blue at the bottom. The microtubule surface is at the top of the figure. These elements are not drawn to scale. Figure 5a shows the relaxed conformation. The dynein is not attached to the microtubule. Binding of nucleotides to P1–P4 (to all modules or to some subset of modules) causes inter-module reorientation and results in the tilting of the stalk (Figure 5b). Dynein remains unattached to the microtubule. Hydrolysis of ATP at P1 results in a 'cocking' of the stem and the subsequent binding of the stalk to the microtubule (Figure 5c). Release of the ATP hydrolysis products from P1 results in a force-generating swinging of the neck domain and the net movement of the microtubule towards the right (Figure 5d).

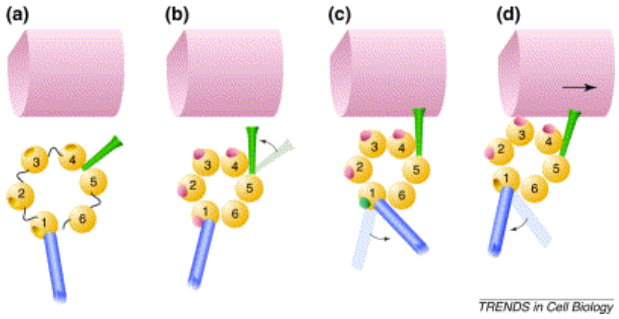

Figure 5. A speculative model for the dynein cross-bridge cycle.
[From Asai, DJ et al. *TRENDS in Cell Biol.* 2001, 11:196, Ref [21]]

Electron microscopy was used to reveal a new model for the structure and mechanism of dynein c, an isoform of flagellar dynein[22] (Figure 6). Six AAA domains and a C-terminal domain form a planar ring, with the stalk emerging between AAA4 and AAA5, and a hook-shaped stem joining AAA1. The conformation of stem and stalk in pre-power-stroke state (ADP·Vi) and post-power-stroke state (Apo) was compared to examine the magnitude of the power stroke (Figure

6a). Alignment of their stems suggests a mean displacement of 15nm of the tip of the stalk. A change in head orientation may also contribute to the apparent (projected) size of this displacement. A linker domain was also found to connect stem and head. In the typical ADP·Vi molecule (Figure 6b, left), the docked linker occludes the central channel and the stem emerges from the head far from the stalk. Rigid coupling between AAA1 and linker causes a rolling of the head towards the stem, which translates the microtubule by 15nm under zero load conditions. The resulting movement of AAA2–4 towards the linker increases the prominence of the central channel (Figure 6b, right). Movement between AAA4 and AAA5 increases stalk stiffness by changing the structure of its junction with them. This result suggests that a change in the head-linker orientation is fundamental in the power stroke of dynein.

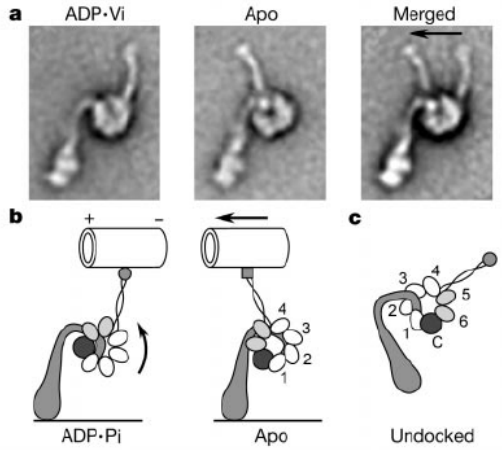

Figure 6. Structure and power stroke of dynein c.
a, Left views of dynein c showing the mean conformation of the stem and stalk relative to the head. Images were made by compositing class averages having the mean stem and stalk angles. Images are shown after alignment of their stems. The arrow indicates 15 nm. b, Speculative structure of the molecule suggesting an origin of the power stroke and how this might be converted into microtubule movement. The six AAA modules (1–6) and C-terminal sequence (C) are indicated. The microtubule track (not drawn to scale) is illustrated as moving under zero load with its plus end leading. c, Molecule showing the stem undocked from the head. [From Burgess, SA et al. Nature 421, 715, 2003. Ref[22]]

1.3.2 The dynein transportation system

Cytoplasmic dynein provides force towards the minus end of microtubules. It is involved in many fundamental cellular processes such as vesicular return to the MT organizing center, as well as the retention of the vesicles at this subcellular locale. Cytoplasmic dynein is intricately involved in the maintenance of the Golgi apparatus and the trafficking of membrane-encapsulated vesicles and proteins such as membrane-bound receptors. Cytoplasmic dynein is also involved in mitosis, including nuclear envelope breakdown at late prometaphase, several aspects of chromosome segregation and helping to form the mitotic spindle. It is known that p53 is associated with cellular microtubules and that dynein transports p53 to the nucleus[23]. P53 is a tumor-suppressor protein involved in cell-cycle control, apoptosis, differentiation, DNA repair and recombination, and centrosome duplication. Other examples of known cargoes and interaction proteins for the dynein include the proapoptotic Bcl-2 family member Bim[24], dynactin, which links dynein to its cargo, Cdc2 kinase, which phosphorylates a light intermediate chain of dynein during mitosis, and the mineralocorticoid receptor. It is also known that cytoplasmic dynein and its associated proteins are related to many diseases such as retinitis pigmentosa[25], lissencephaly[26], virus transport[27] and neurodegenerative diseases[28]. Several important known or potential drug targets interact with the cytosolic dynein complex at one or more points in their cellular lifetimes. Some examples include the tubulin deactylase HDAC6[29] and the heat shock protein Hsp90[30, 31]. The latter may well be an important partner in dynein's translocation of both hormone receptors and p53 protein to the microtubule organizing center at the nucleus. Galigniana et al.[30, 31] have presented data in recent reports describing compelling models for the interactions between p53 with dynein via linkages provided by Hsp90, in concert

with Hsp70, to immunophilins bound to region of the dynactin-associated portion of the dynein complex that binds the inhibitor dynamitin (Figure 7).

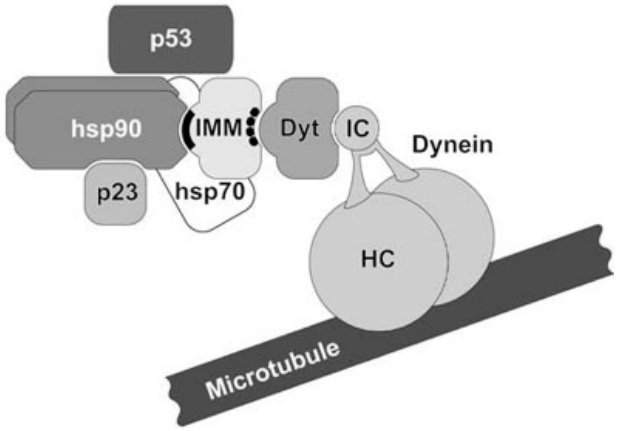

Figure 7. Model of links between cytosolic dynein heavy chain to p53.
An immunophilin (IMM) links to p53-bound HSP90 through its tetratricopeptide repeat (TPR) domain (solid line). The IMM in turn links to the dynamitin (Dyt)-binding region of the dynein-associated dynactin (Dyt) complex by means of its peptidyl-prolyl isomerase (PPIase) domain (dotted line). [From Galigniana et al., J.*Biol.Chem*. **2004**, 279:22483. ref. [30].]

Dynein also play roles in the transport of certain viruses into cells. By microinjecting function-blocking anti-dynein antibodies or overexpressing dynamitin, the role of dynein was established for the efficient nuclear targeting of herpes simplex virus (HSV)[32], adenovirus (Ad)[33,34] or canine parvovirus (CPV) capsids[35], HIV reverse transcription complexes[36] and influenza virus[37]. It is also known that incoming HSV capsids colocalize with dynein and dynactin[27,32], and also that Ad[38], in addition to CPV capsids[35], can interact with dynein and MT *in vitro*.

1.3.3 Known dynein inhibitors

Very little is known about dynein inhibitors (Figure 8). It is known that AMP-PNP, a ATP mimic, inhibits dynein's ATPase activity[39]. The sulfhydryl-reactive agent NEM has also been reported to interact with dynein ATPase[40]. EHNA inhibits axonemal dynein ATPase activity. It acts as a mixed inhibitor of both the axonemal dynein ATPase activity and of partially purified dynein 1 ATPase activity[41]. EHNA has little effect on either the myosin or the Na^+,K^+-ATPase. The only known non-ATP mimic, non-sulfhydryl reactive dynein inhibitor is the natural product purealin, which is be discussed in section 1.3.4. Purealin served as the starting point of this work in the search for dynein-specific, cell-permeable inhibitors. None of the dynein inhibitors known at the beginning of this work are specific for dynein motor.

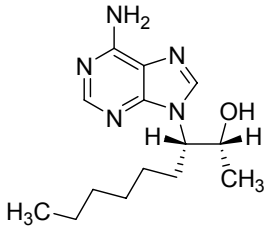

erythro-9-(2-hydroxy-3-nonyl)adenine (EHNA)

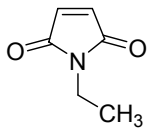

N-ethylmaleimide (NEM)

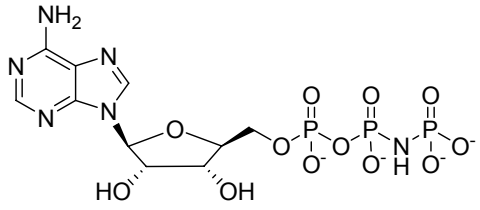

5'-adenylyimidodiphosphate (AMP-PNP)

Figure 8. Chemical structures of the known dynein inhibitors EHNA, AMP-PNP and NEM.

1.3.4 Purealin and purealin library

Purealin is a novel agent isolated from the sea sponge *Psammaplysilla purea*[42]. It selectively inhibits the ATPase activity of isolated dynein and myosin without competing for the ATP site on the motor proteins[43,44]. Other small molecules that can inhibit dynein includes vanadate anion, some ATP analogs, and thiol-perturbing agents since dynein has a thioredoxin-like domain including vicinal thiols[10]. The structure of the only known non-ATP-mimicking dynein inhibitor, purealin, and other related dibromotyrosine-derived natural products are shown in Figure 9. Many of the compounds consist of a center dibromotyrosine unit attached on the right to a side chain via an amide bond and attached to the left through a three-carbon spacer and another amide bond to a second dibromotyrosine ring.

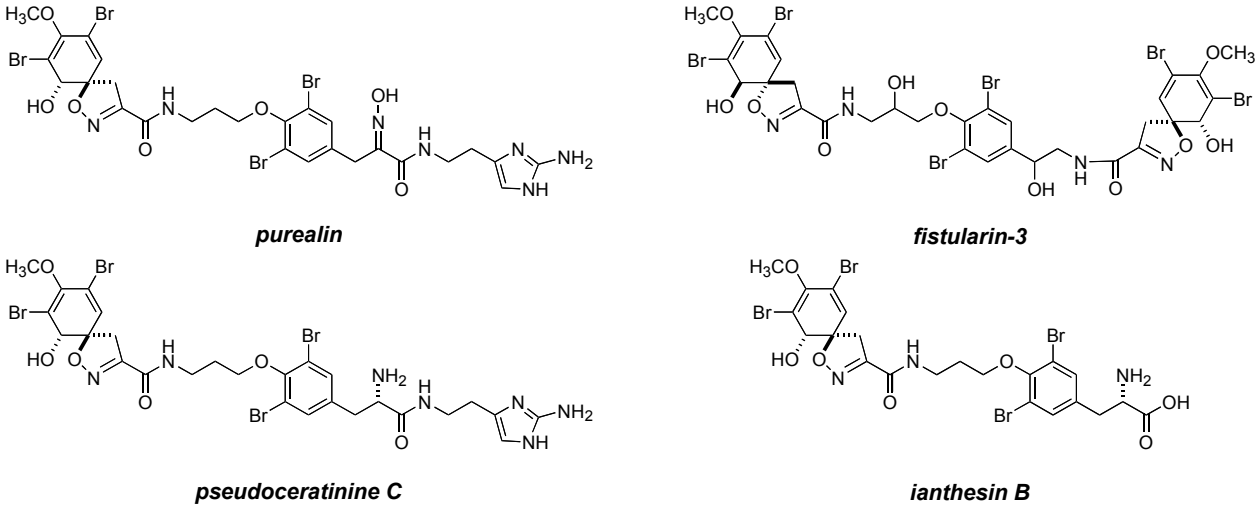

Figure 9. Structures of the only known non-ATP-mimicking dynein inhibitor, purealin, and other related dibromotyrosine-derived natural products.

In the last two decades, a series of publications report the isolation and structure elucidation of bromotyrosine-derived alkaloids, including purealin[45], purealidin A[26], lipopurealins A, B and C[46] (Figure 10). Common structures of these compounds include the bromotyrosine unit with the aminohistamine moiety. In purealin, the spiroisoxazoline as a side chain is coupled to the bromotyrosine amine; in lipopurealin A, B and C, fatty acids side chains are coupled with the bromotyrosine amine.

Purealidin A has weak inhibitory activity (22% inhibition at 100 μM) against Na^+,K^+-ATPase and exhibits some cytotoxicity against L1210 murine leukemia cells with a reported IC_{50} value of 1.1 μg/mL. Lipopurealins A, B and C exhibit inhibitory activities on Na^+,K^+-ATPase purified from porcine brain and dog kidney, with lipopurealin B being the most potent inhibitor[46].

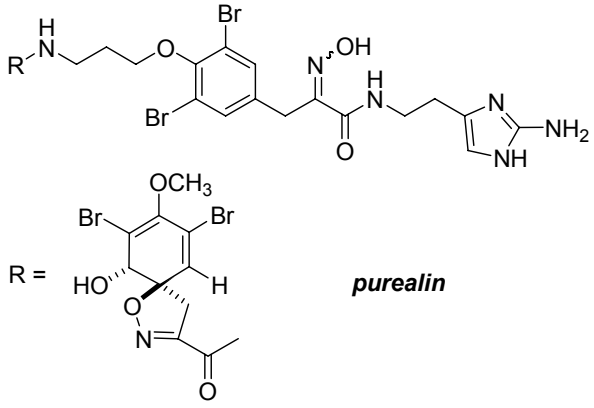

Figure 10. Bromotyrosine-derived alkaloids.

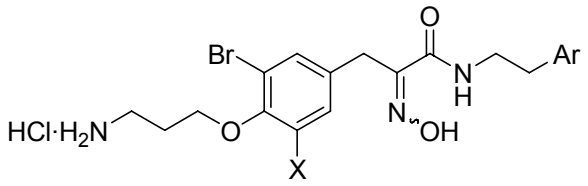

	Ar, X
***para*/phenyl/Br-purealidin A**	phenyl, Br
***para*/methoxyphenyl/Br-purealidin A**	4-methoxyphenyl, Br
***para*/chlorophenyl/Br-purealidin A**	4-chlorophenyl, Br
***para*/indolinyl/Br-purealidin A**	3-indolinyl, Br
***para*/phenyl/H-purealidin A**	phenyl, H
***para*/methoxyphenyl/H-purealidin A**	4-methoxyphenyl, H
***para*/chlorophenyl/H-purealidin A**	4-chlorophenyl, H
***para*/indolinyl/H-purealidin A**	3-indolinyl, H

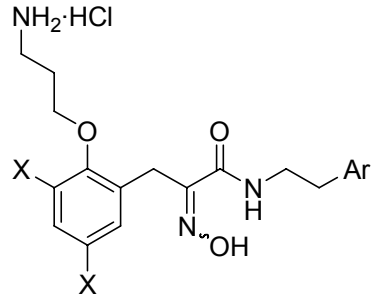

	Ar, X
***ortho*/phenyl/Br-purealidin A**	phenyl, Br
***ortho*/methoxyphenyl/Br-purealidin A**	4-methoxyphenyl, Br
***ortho*/chlorophenyl/Br-purealidin A**	4-chlorophenyl, Br
***ortho*/indolinyl/Br-purealidin A**	3-indolinyl, Br
***ortho*/phenyl/Cl-purealidin A**	phenyl, Cl
***ortho*/methoxyphenyl/Cl-purealidin A**	4-methoxyphenyl, Cl
***ortho*/chlorophenyl/Cl-purealidin A**	4-chlorophenyl, Cl
***ortho*/indolinyl/Cl-purealidin A**	3-indolinyl, Cl

Figure 11. Structures of 16 purealidin A analogues.

Since purealin is active against ATPase activity of axonamal dynein, the first hypothesis tested was that purealin, and perhaps its analogues, also inhibit cytoplasmic dynein ATPase activity, as well as cell proliferation. Therefore, purealin and the twenty synthetic purealidins

were prepared by Dr. Fanglong Yang in Prof. Curran's lab. These compounds (Figure 11) compose the first library examined in biological assays.

1.4 Hsp70 as a chemotherapeutic target

1.4.1 Hsp70 as a molecular chaperone

Molecular chaperones are a family of proteins which help a protein search for and anchor cellular partners, as well as provide force or anchoring points for the subsequent rearrangement or dissolution of muti-protein complexes. Molecular chaperones are generally up-regulated by heat shock or stress (e.g., glucose deprivation), and the heat shock proteins (Hsps) and glucose responsive proteins (Grps) uncovered from studies in mammalian cells were named based on the shock found to cause their upregulation, followed by their molecular masses. For example, Hsp70s are the heat shock proteins of molecular mass of ca. 70 kDa[13]. It is also known that several bacterial molecular chaperones, including DnaK and DnaJ, play essential roles in bacteriophagę DNA replication in *E. coli* and that Hsp70/DnaK and Hsp40/DnaJ are actually two highly conserved and abundant chaperone families. In addition, heat shock "cognate" proteins (Hscs) are Hsp homologues that play vital housekeeping roles by catalyzing protein folding, assembly, degradation, and transport. Hsc70 and Hsp70 generally exhibit identical biochemical activities and are highly conserved.

Hsp/Hsc70 chaperones contain three independent domains, a highly conserved 44-kDa N-terminal ATPase domain and an 18-kDa peptide binding domain and a 10-kDa C-terminal helical lid domain[47]. The helical lid gates the peptide substrates in an elongated channel and

ATP-binding to the ATPase domain opens the lid, resulting in a weaker affinity for peptide substrates[48]. Transient interactions with peptides stimulate Hsp70 ATP hydrolysis, resulting in a conformational change in the chaperone wherein the lid closes to capture peptide substrates. Hsp40s act as co-chaperones of Hsp70 and stimulate the ATPase activity of Hsp70s and stabilize the Hsp70-peptide complex. Hsp40 contains a ~70-amino acid "J domain" that interacts with the ATPase domain of Hsp70[49].

Hsp70 and Hsp40 co-chaperone are related to many human diseases. For example, they are a therapeutic target for the symptoms of cystic fibrosis caused by protein folding defects[50, 51]. Hsp70 and Hsp40 also contribute to tumorigenesis[52,53]. Several unique tumor types exhibit elevated expression of these chaperones, and overexpression of Hsp70 alone can lead to cellular transformation and tumorigenesis[54,55]. It is known that inhibition of Hsp70 synthesis by antisense (as) Hsp70 cDNA induces massive death of breast cancer cells[56]. The asHsp70-induced death is independent of known caspases and the p53 tumor suppressor protein. In addition, Bcl-2 and Bcl-X_L fail to rescue breast cancer cells from asHsp70-induced cell death. It is also known that some viral oncogenes recruit cellular Hsp70 to inactive growth control checkpoints[57]. The large T antigen (Tag) of the DNA tumor virus, simian virus 40 (SV40), contains a J domain that stimulates Hsp70 to rearrange multiprotein complexes involved in cell cycle regulation[57]. Therefore, Hsp70 modulators could serve as chemotherapeutic agents.

Hsp70 protects tumor cells from apoptosis (for a review, see ref.[58]) Although Hsp70 is induced upon cellular stress to prevent protein aggregation and facilitate protein refolding or disposal, it also protects cells from a wide range of apoptotic pathways. It is known that Hsp70 inhibits key effectors of the apoptotic machinery, including the apoptosome, the caspase activation complex, and apoptosis-inducing factor (AIF)[58]. Hsp70 facilitates the proteasome-

mediated degradation of apoptosis-regulatory proteins. Hsp70 also inhibits the stress-activated Jun N-terminal kinase (JNK), which is an apoptosis inducer though a caspase-independent pathway, the release of cytochrome (cyt) c and AIF from mitochondria, and the activation of Apaf-1 and caspase 3,9[59,60].

1.4.2 Compounds targeting Hsp70

Although Hsp70 plays very important roles and is related to human cancer and other diseases, very few Hsp70 modulators have been identified. One compound, 15-deoxyspergualin (DSG), binds specifically to Hsp70 with a Kd of ~ 4μM and stimulates its steady-state ATPase activity by 20~40%, but has no effect on peptide binding nor Hsp40 activation of Hsp70 ATPase activity[61-63]. It has been shown *in vitro* to modestly facilitate the trafficking of ΔF508-CFTR to the plasma membrane[64]. DSG has already been in Phase II trial as an immune-suppressant for kidney transplant patients[40]. However, DSG also binds Hsp90 with a Kd of ~ 5μM[62]. Therefore, DSG may function through its action on Hsp90 along with its binding to Hsp70.

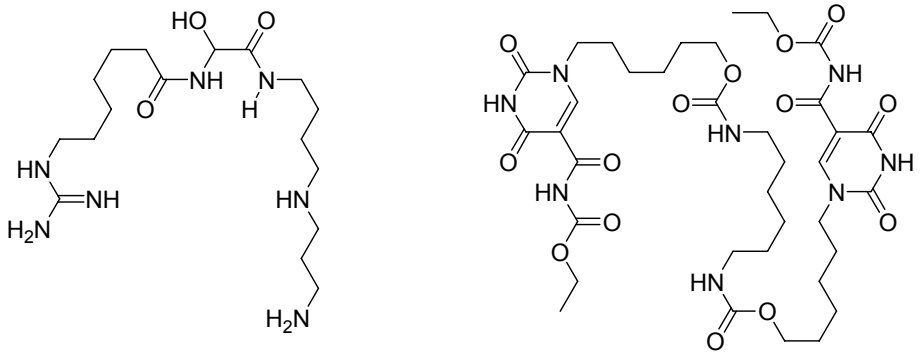

Figure 12. Chemical structures of DSG and NSC-630668-R/1.
Structures are drawn to maximize structural similarity.

Another class of Hsp/Hsc 70 modulator are the 3'-sulfogalactolipid (SGLs), including sulfogalactosylceramide (SGC), sulfogalactoglycerolipid (SGG) and adamantylSGC (adaSGC). SGLs bind to the ATPase domain of Hsc70 and inhibit its endogenous and Hsp40-stimulated steady-state ATPase cycle[65,66]. In addition, adaSGC inhibits Hsc70/SGL binding and behaves as a noncompetitive inhibitor of Hsc70 ATPase activity[66]. There is no report on the cellular actions of SGL compounds so far. However, I did work that showed adaSGC does not signifiantly alter the proliferation of the human breast cancer cell SK-BR3.

NSC-630668-R/1 (R/1) is another example of Hsp70 modulator. Its actions in this regard were discovered by the Day and Brodsky groups at the University of Pittsburgh[67]. It was selected from an *in silico* screen of DSG structural analogues in the National Cancer Institute's (NCI) Developmental Therapeutics Program. R/1 was found to inhibit the steady-state ATPase activity of yeast Hsc70 and to block the Hsc70-mediated translocation of a preprotein into yeast endoplasmic reticulum (ER)-derived microsomal vesicles. In their initial report, the Day/Brodsky collaborators also claimed that DSG and R/1 modulate Hsc70 activity by distinct mechanisms.

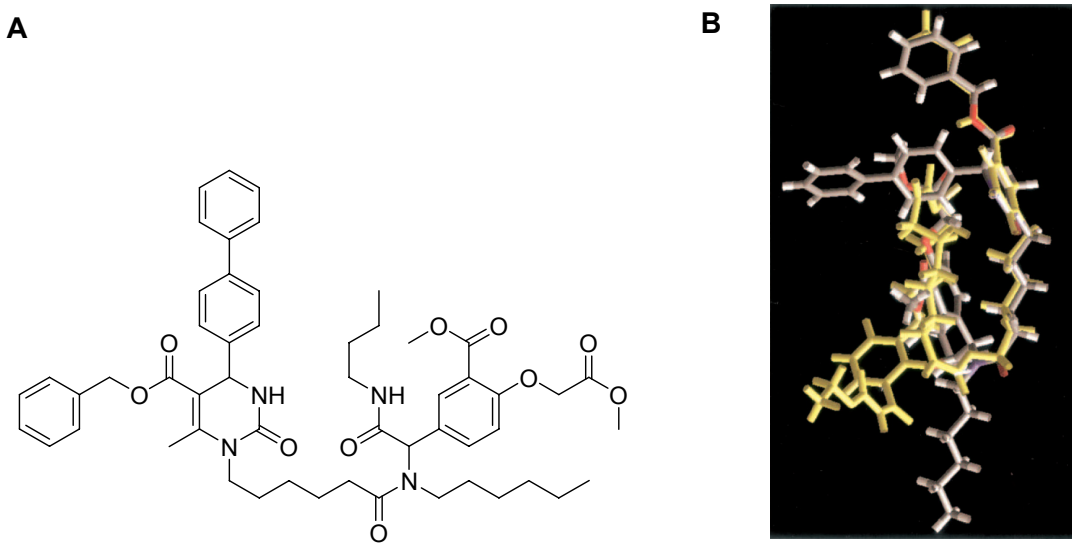

Figure 13. (A) Chemical structure of MAL3-101 and (B) superimposed molecular models of R/1 (yellow) and MAL3-101 (white).

Based on the initial findings, several dihydropyrimidines, synthesized from Biginelli and Ugi reactions by Prof. Wipf's group, were also found to interact with Hsp70. Computational conformational analysis showed one of the compounds, MAL3-101, can adopt a conformation very similar to that of R/1 compound (Figure 13). In a single turnover Hsp70 ATPase assay, MAL3-101 inhibits TAg-stimulated Hsp70 ATPase activity in a concentration-dependent way, without disturbing the ATPase activity of TAg. MAL3-101 served as the starting point for the search for more potent, Hsp70-specific inhibitors, with desired cellular properties.

2.0 MATERIALS AND EXPERIMENTAL PROCEDURES

2.1 Materials

RPMI 1640 medium, penicillin-streptomycin, L-glutamine, lipofectamine and trypsin-EDTA were obtained from Invitrogen Co., Carlsbad, CA. Fetal bovine serum (FBS) was obtained from Hyclone, Logan, UT. 4-(2-hydroxyethyl)-1-piperazineethanesulfonic acid (HEPES) and 37% formaldehyde were obtained from Fisher Co., Fairlawn, NJ. Piperazine-*N*,*N*′-bis(2-ethanesulfonic acid) (PIPES), adenosine triphosphate (ATP), guanosine triphosphate (GTP), 2-(morpholin-4-yl)ethanesulfonic acid (Mes), monosodium glutamate (MSG) and sucrose were obtained from USB Co., Cleveland, OH. $MgCl_2$, KCl, ethylenediaminetetraacetitic acid (EDTA), dimethylsulfoxide (DMSO), *erythro*-9-(2-hydroxy-3-nonyl)adenine (EHNA), sodium citrate, ethyleneglycoltetraacetic acid (EGTA), phenylmethylsufonyl fluoride (PMSF), trypan blue solution (0.4%), dulbecco's modified eagle's medium (DMEM), anti-dynein intermediate chain antibody, 2-Mercaptoethanol, α-cyano-4-hydroxycinnamic acid (CHCA), bovine collagen-I, Hoechst 33342, ammonium bicarbonate and formic acid were from Sigma Co., St.Louis, MO. Tris(hydroxymethyl)aminomethane (Tris), Coomassie G250 stain, Tween-20, polyvinylidene difluoride (PVDF) membrane, triton X-100, glycine and SDS were obtained from Bio-Rad Laboratories Inc., Hercules, CA. Dithiothreitol (DTT) was from Boehringer Ingelheim Inc., Ridgefield, CT. Paclitaxel was from the NIH Drug Synthesis Branch. ProtoGel 30% (w/v)

acrylamide:0.8%(w/v) bis-acrylamide stock solution was from National Diagnostics, Atlanta, GA. Malachite green and HCl were from J.T.Baker Co., Phillipsburg, NJ. Rabbit anti-dynein heavy chain polyclonal IgG was purchased from Santa Cruz Biotechnology Inc., Santa Cruz, CA. Acetonitrile was obtained from Fisher Co., Fairlawn NJ. Trypsin for in-gel tryptic digestions was sequencing grade modified trypsin from Promega Co., Madison, WI Mouse anti-α-tubulin antibody was from NeoMarkers/Lab Vision Inc. Fremont, CA. Sheep anti-p53 antibody was from Calbiochem Inc., Sandiego, CA. Cy5-labeled donkey anti-sheep and cy3-labeled donkey anti-mouse antibodies were from Jackson ImmunoResearch Laboratories Inc., West Grove, PA. Lipofectamine. Opti-MEM. etc. [^{32}P]ATP was from PerkinElmer Inc., Waltham, MA. Rabbit skeletal muscle myosin II was from Cytoskeleton Inc., Denver, CO. Dynein heavy chain siRNA and negative control siRNA were obtained from Ambion Inc, Austin, TX. Tubulin was purified in the Day lab by the method of Hamel, E. and Lin, C.M., ref [68].

2.2 Experimental procedures

2.2.1 Antiproliferative assay

Cells were grown in RPMI 1640 medium with 10% FBS. Human epithelial cancer cells (MDA-MB231 breast, PC-3 prostate, 2008 ovary and HT-29 colon) were trypsinized and plated into 96-well microtiter plates at 500-2000 cells/well (depending on the cell line) in 96-well plates, allowed to attach and grow for 72h, then treated with vehicle (DMSO) or test agent for an additional 72h. For the mouse leukemia L1210 line, cells were plated into 96-well plates at 7500 cells/well and treated with test agents, incubated for 48 h. In each case, one plate consisted

entirely of wells containing cells in medium and wells with medium alone to determine time zero time cell numbers. The other plates in a given determination contained eight wells of control cells, eight wells of medium, and each test agent concentration in quadruplicate. Cell viability was determined with the MTS assay and 50% growth inhibitory concentrations (GI_{50}) were determined. Discodermolide (DCD) was used as a positive control in all the assays.

2.2.2 Dynein purification from bovine brain

Extraction buffer (50mM HEPES + 50mM PIPES, pH 7.0, containing 2mM $MgCl_2$ and 1mM EDTA), Tris-KCl buffer (20mM Tris-KCl, pH 7.6, containing 50mM KCl, 5mM $MgCl_2$ and 0.5mM EDTA) were prepared. Fresh bovine brain (obtained free of charge from a local slaughterhouse) was homogenized in a blender at 4 ºC in one volume of extraction buffer. The mixture was centrifuged in a JA-18 rotor at 6,000rpm for 30min and kept at 4 ^{o}C. The supernatant was recovered and further centrifuged in a Ti45 rotor at 28,000rpm for 60min at 4 ^{o}C to obtain a clean cytosolic extract. Paclitaxel (20μM) was added to this extract and the mixture was incubated at 37 ^{o}C for 15min to polymerize tubulin. The mixture was centrifuged in a JA30.50 rotor at 18,600rpm for 30min in the presence of 7% sucrose in extraction buffer. The pellet was resuspended in extraction buffer and paclitaxel (5μM) was added. The mixture was incubated at 37 ^{o}C for 15min to form MTs. The mixture was centrifuged in a Ti70.1 rotor at 23,000rpm for 30min at 30 ^{o}C. The MT pellet was resuspends in extraction buffer and 3mM GTP along with 5μM paclitaxel were added. The mixture was incubated at 37 ^{o}C for 15min and spinned in a Ti70.1 rotor at 23,000rpm for 30min at 20 ^{o}C. The pellet was resuspended in extraction buffer and ATP (10mM) was added. The mixture was incubated at 37 ºC for 12min to release cytoplasmic dynein. The mixture was further centrifuged in a Ti70.1 rotor at 30,000rpm

at 20 ºC for 30. The supernatant was fractionated using 5-20% sucrose gradient (prepared in Tris-KCl buffer) in a SW41 rotor at 27,000rpm for 16h at 4 ºC. Protein content in the fractions was estimated with the Bio-Rad protein reagent. Aliquots of the sucrose gradient gradient fractions were analyzed on 6.5% polyacrylamide SDS-PAGE gels after staining with Coomassie blue.

2.2.3 Glycerol-based dynein purification

A homogenization buffer was prepared. Extraction buffer and Tris-KCl buffer were prepared as mentioned before. The fresh brain was homogenized in a blender at 4 ºC in one volume of extraction buffer (100mM PIPES, pH 6.9-7.2, containing 5mM $MgCl_2$, 1mM EGTA and 1mM PMSF), and the homogenate was centrifuged in a GSA rotor at 10,000rpm for 20min. The supernatant was obtained and adjusted to 1.0mM GTP. The mixture was centrifuged in a 45Ti rotor at 40,000rpm for 60min. Glycerol was added to the supernatant at a final concentration 2.74M. The mixture was incubated at 34-37 ^{o}C for 45min for the microtubule assembly, then was further centrifuged in 45Ti rotor at 40k rpm for 60min. The pellet was resuspended in the homogenization buffer in the presence of 0.5mM GTP and was incubated on ice for 30min. After another ultracentrifugation in a 70Ti rotor at 40,000rpm for 40min, the supernatant was adjusted to 2.74M glycerol and incubated again at 34-37 ^{o}C for 45min. The mixture was untracentrifuged, the pellet was resuspended, and 3mM GTP with 20uM paclitaxel were added to the solution, which incubated for 15min at 37 ^{o}C. After a centrifugation at 18k in a JA30.50 rotor for 20min, the pellets were resuspended in the extraction buffer and 20mM ATP was added to the solution for another incubation for 20min at 37 ^{o}C. After high speed centrifugation at 45k rpm, the mixture was fractionated using a 5-20% sucrose gradient (prepared

in Tris-KCl buffer) in a SW41 rotor at 27,000rpm for 16h. Aliquots of the sucrose gradient gradient fractions were analyzed on 6.5% polyacrylamide SDS-PAGE gels after staining with Coomassie blue.

2.2.4 Colorimetric ATPase assay

Malachite green (340 mg) was dissolved in 75 mL of water. Ammonium molybdate (10.5 g) was dissolved in a mixture of 83 mL of 37% HCl and 167 mL of water. The two solutions were mixed and water was added to give a final volume of 1 L. The solution was stored at 4^{o}C for no more than 1 month. A 1:250 volume of 10% Tween-20 was added just before using the malachite green solution. Paclitaxel-induced MTs, dynein heavy chain (20ug/mL final concentration) and the negative control (DMSO only) or the EHNA solution, were premixed in reaction buffer (the Tris-KCl buffer used in the dynein preparation work). The reaction mixture was incubated at 37ºC for 30min. Per 100µL of reaction mixture, 800 µL malachite green solution and 100 µL 34% aqueous sodium citrate were added and the absorbance at 655nm was determined in a 96-well microtiter plate reader. The amount of free phosphate released by dynein heavy chain was calculated from a sodium phosphate standard curve.

2.2.5 Western blotting

Proteins were transferred from SDS-PAGE gels to PVDF (Bio-Rad) membranes using a Bio-Rad Trans-Blot Semi-Dry transfer system for 1.5h in 25mM Tris, pH 7.0, containing 19mM glycine and 20% methanol. Membranes were washed in 50 mM Tris buffer, pH 7.4, containing

0.5M NaCl and 0.1% (v/v) Tween 20, and then blocked using the Amersham Western Blotting blocking agent. Rabbit anti-dynein heavy chain polyclonal IgG (1:500 dilution) was added to the blocking buffer and the membrane was incubated at 4^{o}C overnight. The membrane was washed, blocked once again, and anti-rabbit antibody (1:5000 dilution) was added. The Amersham ECL chemiluminescence system and Fuji film were used to detect the protein bands.

2.2.6 SDS-PAGE

Purified bovine cytoplasmic dynein (1.6 μg per well) was loaded into a 6.5% SDS-PAGE gel. A Tris-glycine buffer (Tris 6g/L, glycine 28.8 g/L, SDS 1 g/L) was used to run the gel. Gels were then washed in clean water and stained with Coomassie blue for 1 h.

2.2.7 In-gel digestion with trypsin

After visualization, the bands of interest were excised from the SDS-PAGE gels and soaked in 1:1 CH_3CN-25mM aq. NH_4HCO_3, pH 7.8, for 10 min with vortex mixing for full destaining. The supernatant was removed and the destaining process was repeated three times. The gel pieces were then completely dried in a SpeedVac lyophilizer. Enough aq. 25mM NH_4HCO_3, pH 7.8, containing 10mM dithiothreitol (DTT) was added to cover each individual gel piece and the mixtures were incubated at 56 ºC for 1 h to reduce disulfide bonds. The supernatant was removed and 25mM NH_4HCO_3, pH 7.8, containing 50 nM iodoacetamide was added to carbamidomethylate sulfhydryl groups. The mixture was incubated in the dark for 45 min at room temperature. The supernatant was removed and 25mM NH_4HCO_3, pH 7.8, was added. After 10 min of vortex mixing, the supernatant was removed and the gel plugs were

soaked in 1:1 CH_3CN-25mM aq. NH_4HCO_3, pH 7.8, for 5 min with vortex mixing. Subsequently, the gel pieces were completely dried in a SpeedVac.

Tryptic digestion was performed via the addition of 20 µL of 20 ng/µL trypsin in 20mM aq. NH_4HCO_3, pH 7.8, and incubation for 14h at 37 ºC without agitation. The digestion was stopped by the addition of 100 µL of H_2O. The peptides were extracted into 1:1 CH_3CN-H_2O containing 5% HCO_2H and the extract was taken to complete dryness in a SpeedVac.

2.2.8 Mass spectrometry

The dried samples were resuspended in 10 µL of 1:1 CH_3CN-H_2O containing 0.1% CF_3CO_2H. Then, 1 uL of the sample solution was mixed with 3 µL of 1:1 CH_3CN-H_2O containing 0.1% CF_3CO_2H and 6 uL of 1:1 CH_3CN-H_2O containing 0.1% CF_3CO_2H and saturated with α-cyano-4-hydroxycinnamic acid (CHCA). Subsequently, aliquots of 0.5 µL were applied to a stainless steel target and allowed to air dry. MALDI-TOF and MALDI-TOF/TOF mass spectra were recorded with an Applied Biosystem 4700 Proteomics Analyzer in the reflectron, positive ion detection mode.

2.2.9 Dynein ATPase inhibition assay

The ability of the purealin analogues to inhibit the ATPase activity of cytoplasmic dynein heavy chain was determined as follows. A colorimetric assay to measure inorganic phosphate release (malachite green assay) was used. With the malachite green detection system, paclitaxel-induced MTs (1mg/mL final concentration based on soluble tubulin incubated with 10µM pacitaxel), dynein heavy chain (20µg/mL final concentration) and the test agents (50, 10, 2, 0.4

and 0.08μM), as well as the positive control (EHNA, an adenosine analogue known to inhibit dynein ATPase activity, 5mM final concentration) and the negative control (DMSO only), were premixed in reaction buffer (20mM Tris-KCl, pH 7.6, containing 50 mM KCl, 5 mM $MgCl_2$ and 0.5mM EDTA). ATP (2mM) was added to initiate the reaction. The other controls, including a no enzyme control (all but dynein heavy chain), a no substrate control (all but ATP) and a no enzyme/substrate control (all but ATP and dynein heavy chain) were also prepared. The reaction mixture (100μL) was incubated at 37ºC for 30min. The malachite green solution (1mM malachite green, 8.5mM ammonium molybdate and 0.8M HCl, 100μL) and 34% aqueous sodium citrate solution (100μL) were added and the absorbance at 655nm was determined in a 96-well microtiter plate reader. The absorbance values determined from the controls were subtracted from the absorbance values of the full reaction. The amount of free phosphate released by dynein heavy chain was calculated from a sodium phosphate standard curve. The percentage of control was calculated from the ratio of the ATPase activity of dynein heavy chain with a specific concentration of an inhibitor and the ATPase activity of dynein heavy chain only (results are given in Figure 27 and Table 8).

2.2.10 P53 nuclear translocation assay

A549 lung cancer cells were cultured in RPMI 1640 medium plus 10% FBS and 0.1% penicillin/streptomycin. Slides/plates were first cleaned with 70% ethanol, allowed to air dry, and then coated with 0.25mg/mL bovine collagen-I in 0.1% acetic acid (freshly made) and dried in the hood overnight. Log phase growth cells were plated on the collagen-coated slides/plates and incubated for 48h at 37°C in a humidified, 5% CO_2 atmosphere. The cells were incubated in

the presence of compounds for 20h. At the end of an experiment, the solution was removed from the microplates/slides and immediately replaced with a solution of HBSS containing 4% formaldehyde and 10μg/mL Hoechst 33342 to fix the cells and fluorescently label their nuclei. After incubation at room temperature for 20 to 30 min, the solution was removed and replaced with Hank's balanced salts solution (HBSS) (100 μL/well). At this point, microplates could be sealed and stored at 4°C overnight. After removing the HBSS from each well, 0.5% (w/w) Triton X-100 was added and the plate was incubated for 5 min at room temperature to detergent-extract a fraction of the soluble cellular components, including soluble tubulin. The wells were then washed with HBSS (100 μL/well) followed by the addition of a primary antibody solution containing mouse anti-α-tubulin (NeoMarkers, 1:1000) and sheep anti-p53 (CALBIOCHEM, 1:500) in HBSS. After 1h of incubation at room temperature, the samples were washed with HBSS as above, followed by the addition of a secondary antibody solution containing Cy5-labeled donkey anti-sheep (Jackson ImmunoResearch, 1:500) and Cy3-labeled donkey anti-mouse (Jackson ImmunoResearch, 1:1000) antibodies diluted in HBSS. After a 1h incubation at room temperature, the samples were washed as above and HBSS was added (100 μL/well) before sealing the microplates/slides. Labeled microplates could be stored at 4 °C for up to 2 weeks before high-content analysis.

2.2.11 Dynein heavy chain siRNA experiment

Dynein heavy chain siRNA #1, 2, 3 were obtained from Ambion Inc (for sequences, see Table 6). A negative control siRNA was also obtained which is a 19bp scrambled sequence with 3' dT overhands and the sequence have no significant homology to any know gene sequences from mouse, rat or human.. Eight-well chamber slides were coated as described above with

0.25mg/mL collagen-I in 0.1% acetic acid (100μL/well) and dried in the hood for around 6 h. A549 cells were resuspended in RPMI 1640 medium with 10% FBS without antibiotics and plated in the 8-well chamber slides at 2,000 cells per well. Cells were allowed to attach for at least 24 h before transfection. On the day of transfection, for each well, 0.375 μL lipofectamine was gently mixed with 12.5 μL Opti-MEM and incubated at room temperature for 5min to obtain the lipofectamine mixture. A solution (50nM or 150nM) of the negative siRNA (0.375 μL) was gently mixed with 12.5 μL of Opti-MEM to give the negative siRNA mixture. 0.75 μL siRNA (1, 2, 3 or mixtures thereof) was gently mixed with 12.5 μL of Opti-MEM to give the siRNA mixture. The lipofectamine mixture was mixed with the negative siRNA mixture or siRNA mixture and incubated at room temperature for 15 min. Growth medium was removed from the culture well and cells were washed with Opti-MEM for three times. Lipofectamine-siRNA mixture was added to cell culture and incubated at 37 ºC for 4 h. Opti-MEM medium with 30% serum was added and incubated at 37 ºC. After 48 h, cells were detached by trypsinization, washed with HBSS, then lysed in 0.1M 2-(morpholin-4-yl)ethanesulfonic acid (Mes), pH 6.75, containing 0.1% Triton X-100, 1 mM $MgSO_4$, 2 mM EGTA and 4 M glycerol. The lysate was centrifuged at 14,000 rpm in an Eppendorf microcentrifuge. The supernatant was boiled in loading buffer, loaded onto 10% polyacrylamide gels, and separated by electrophoresis. Proteins were transferred to polyvinyldifluoride membranes (Biorad), using a Biorad Transblot Semidry system. After washing, blocking, and treating with appropriate antibodies, protein bands were detected using the Amersham ECL Western blotting system and Fuji film. Densitometric analyses were performed with ImageJ (v. 1.32j) software.

2.2.12 GFP-glucocorticoid receptor nuclear translocation assay

Mouse mammary adenocarcinoma cells 3617.4 (a kind gift from Prof. Gordon Hager, University of Michigan) stably expressing GFP-rat glucocorticoid receptor (GR)[69] under control of the "Tet-Off" inducible system were maintained in Dulbecco's modified Eagle's medium (DMEM) supplemented with 10% FBS and 10 μg/mL tetracycline at 37 ºC under a 5% CO_2, humidified atmosphere. Cells were plated at 6000 cells/well in a 96-well plate. At the time of transfer, the medium was replaced with DMEM without tetracycline to induce GFP-GR expression. Wells were then treated with the test agents (100μM), controls (*vide infra*), as well as vehicle (DMSO) only. To trigger GFP-GR translocation to the nucleus, cells were incubated for 15 min with 1 μM dexamethasone or its vehicle (ethanol – negative control). The medium was then removed and cells were washed three times with phosphate buffered saline (PBS). Cells were fixed and permeabilized by immersion in cold methanol (–20ºC) for 20 min. Hoechst 33342 (10 μg/mL) was added to fluorescently label nuclei. Mouse anti-α-tubulin (NeoMarkers, 1:1000) and Cy3 donkey anti-mouse (Jackson ImmunoResearch, 1:1000) antibodies were also used in some cases to fluorescently label microtubules. Cells were photographed with a Leica DC300F fluorescent microscope or an Olympus IX70 inverted microscope. Cells within images were then scored for GFP-GR nuclear translocation using a system published previously[70], wherein a score of 4 was given for nuclear fluorescence much greater than cytoplasmic fluorescence, 3 for nuclear fluorescence greater than cytoplasmic fluorescence, 2 for nuclear fluorescence equal to cytoplasmic fluorescence, 1 for nuclear fluorescence less than cytoplasmic fluorescence, and 0 for nuclear fluorescence much less than cytoplasmic fluorescence. The translocation scores reported represent the means ± S.E. from three different areas in an experiment, in which ≥ 30 cells/area were counted.

2.2.13 Glucocorticoid receptor ligand binding domain competitor assay

The GR competitor assay (Panvera) was performed according to manufacturer's recommendations with some modifications. Recombinant human GR was used at the recommended concentration of 16nM and the supplied fluorescently labeled glucocorticoid ligand (Fluormone^{TM} GS1) was used at 4nM in the final mixture. Recombinant human GR complexed with GS1 was distributed to all wells and then serial dilutions of test agents were added. DMSO content was kept at 1%. The required volumes of 4× concentration of GR and 4× concentration of GS1 were prepared on ice. GR and GS1 were then mixed together and distributed at 20 µL/well in square and black-bottom 384-well plates (Costar). Test agent dilutions, prepared in the screening buffer, were added at 20 µL/well. Dexamethasone was used as a standard. The plate was incubated at room temperature, protected from light, on a plate shaker for 2h. After incubation, the fluorescence polarization was measured using an Analyst^{TM} AD &HT Assay Detection Systems reader (Molecular Devices) equipped with 485 nm excitation and 530 nm emission interference filters with the appropriate FL505 dichroic mirror. The instrumental set up was validated using serial dilutions (100nM to 1pM) of methylfluorescein (Sigma) in the screening buffer. Data were analyzed using GraphPad Prism's one site competition method (Fig).

2.2.14 *In vitro* glucocorticoid receptor binding assay

3617.4 cells were plated in 100 mm culture dishes in DMEM high glucose supplemented with 10% charcoal-stripped FBS and 10 µg/mL tetracycline and grown to confluence. Cells were then harvested by scraping into Hank's buffered saline solution and centrifugation. The cell

pellet was resuspended in six volumes (compared to the packed cell volume) of lysis buffer (20 mM Tris-HCl, pH 7.5, containing 50 mM NaCl, 1 mM EDTA, 5 mM dithiothreitol, 20 mM sodium molybdate and 10% glycerol). Cells were lysed by three cycles of freeze-thawing. Cell lysates were first centrifuged at 20,000 × g at 4ºC for 20 min and then at 100,000×*g* at 4 ºC for 30 min. The supernatant, referred to as "cytosol", was collected and stored at –80 ºC. For cytosols to be assayed for hormone binding, 75 µL of cytosol was incubated at 4 ºC for 2 h with 25 nM [^{3}H]dexamethasone (75nCi, 40Ci/mmol) in the presence of 1% DMSO (positive control), test agents or a 5,000-fold excess of non-radioactive dexamethasone (background). Samples were mixed with a suspension of activated charcoal (100 mg/mL in lysis buffer) and incubated for 20 min on ice. Samples were centrifuged and radioactivity in metered aliquots of the supernatant was determined by liquid scintillation spectrometry. The percent specific binding was calculated from the ratio of the specific binding of a test agent and the specific binding of the positive control.

2.2.15 Recombinant cytoplasmic dynein motor domain expression and purification

The 380-kDa motor domain fragment was cloned from Gly1286–Glu4644 of rat cytoplasmic dynein into the baculovirus expression vector pVL1393 (BD Biosciences) with a C-terminal in-frame hexahistidine tag[71]. Hi5 cells were maintained at 26 ºC no CO_2 in Express Five SFM medium (GIBCO) supplemented with L-glutamine (GIBCO). Hi5 cells were infected with virus for 40 h. The cells were washed and resuspended in PBS, and the recombinant motor domain fragments were extracted from the cells by homogenization in lysis buffer (20mM Hepes, pH 7.0, containing 50mM NaCl, 2mM $MgSO_4$, 0.5 mM EGTA, 10mM imidazole and 1 mM DTT) supplemented with protease inhibitor (Sigma) and 1mM ATP. The cytosolic extract

was spun at 5000×*g* for 10 min at 4 ºC and 100,000×*g* for 30 min at 4 ºC. The supernatant was applied to a Ni^{2+}-affinity column (Ni^{2+}-nitrilotriacetic acid superflow; Qiagen) equilibrated in lysis buffer. Unbound material was removed by washing with 10 volumes of washing buffer (20mM Hepes, pH 7.0, containing 350mM NaCl, 2mM $MgSO_4$, 0.5mM EGTA and 30mM imidazole), and the protein was eluted in 6 volumes of elution buffer (20mM Hepes, pH 7.0, containing 50mM NaCl, 2mM $MgSO_4$, 0.5 mM EGTA and 250mM imidazole). Protein concentration was determined by the Bradford method, using albumin as a standard. A typical batch of six 15-cm dishes of confluent Hi5 cells produced 2–4 mg of recombinant protein that had no visible sign of contaminants or degradation. Peak fractions were pooled, flash-frozen in liquid nitrogen, and subsequently stored at –80 ºC.

2.2.16 Kinetics of cytoplasmic dynein heavy chain motor domain inhibition

Motor domain (21.25 μg/mL final concentration) was premixed with the test agents in 10 mM HEPES/10 mM PIPES, pH 7.0, containing 0.4 mM $MgSO_4$ and 0.2 mM EDTA. Different concentrations of ATP (250, 125, 62.5, 31.3 and 15.6 μM) were added to the system to initiate the reaction. The mixtures were incubated at 37 ^{o}C for 30 min. The reaction was stopped by the addition of the malachite green solution and 34% aqueous sodium citrate, and the absorbance at 650 nm was determined in a 96-well microtiter plate reader. In the microtubule-stimulated dynein motor domain ATPase kinetic study assay, paclitaxel (20 μM final concentration) was added to bovine tubulin. The mixture was incubated at 37ºC for 2 h to allow formation of microtubules, which were collected by centrifugation at 20,000 rpm in a Jouan MR23i microcentrifuge at 4ºC for 30 min. The pellet was then resuspended in the exchange buffer and adjusted to the desired final concentration.

2.2.17 Hsp70 and Hsp90 ATPase assays

Recombinant human Hsp70 was from Assay Designs, Inc. The yeast homolog of Hsp90, Hsc90 (Hsc82p), was isolated as described previously[72] from *Saccharomyces cerevisiae* yeast strain ECUpep4 with deletions in the chromosomal *HSC82* and *HSP82* genes and that encodes *HSC82* on a 2 μm plasmid. The effects of the compounds on steady-state Hsp70/Hsp90 ATPase activity were measured as follows. Test agent (100μM final concentration) or vehicle (DMSO) were preincubated with Hsp70/Hsp90 (3μg of Hsp70 or 6.25μg of Hsp90) on ice for 15 min. ATP hydrolysis was assayed at 30°C in ATPase reaction buffer (50mM Hepes, pH 7.4, containing 50mM NaCl, 2mM $MgCl_2$ and 10mM dithiothreitol) with 0.05mM ATP and 0.2μCi [^{32}P]ATP (3000 Ci/mmol; PerkinElmer, Inc.) in a final volume of 20 μL. At the specified time points, 2 μL aliquots were removed and added to 4 μL of stop solution (2 M LiCl, 4 M formic acid, 36 μM ATP) on ice to quench ATP hydrolysis. Aliquots of each reaction time point were spotted onto cellulose PEI thin layer chromatography plates (Selecto Scientific Inc.), which were developed with 0.5 M LiCl/1M formic acid solution and imaged with a PhosphorImager system (FUJIFILM Inc.) to determine the percentage of ATP hydrolyzed to ADP+Pi. MAL3-101[67] was used as the positive control in the Hsp70 assay and novobiocin[73] was used as the positive control in the Hsp90 ATPase assay.

2.2.18 Myosin Ca^{2+}-ATPase assay

The malachite green assay was used to determine the ability of the compounds to affect the Ca^{2+}-stimulated myosin ATPase activity. Rabbit skeletal muscle myosin II (Cytoskeleton Inc., (25 μg/mL final concentration) and the test agents (100μM final concentration), as well as the

positive control (purealin[42], a known myosin Ca^{2+}-ATPase inhibitor, 20μM final concentration) and the negative control (DMSO only), were premixed in the reaction buffer (50 mM Tris-HCl, pH 7.9, containing 0.23 M KCl and 2.5 mM $CaCl_2$). ATP (2.5 mM final concentration) was added to initiate the reaction. The reaction mixture was incubated at room temperature for 30 min. The malachite green assay was then performed as described above.

2.2.19 Cellular levels of soluble and polymerized tubulin

Soluble and polymerized tubulin levels in cells were determined with a Western blot procedure described previously[74, 75]. Briefly, cells were plated in 6-well plates and allowed to attach for 48 h, then treated with the indicated concentrations of the compounds. After 8 h, cells were detached by trypsinization, washed with HBSS, then lysed in 0.1M 2-(morpholin-4-yl)ethanesulfonic acid (Mes), pH 6.75, containing 0.1% Triton X-100, 1 mM $MgSO_4$, 2 mM EGTA and 4 M glycerol. The lysate was centrifuged at 14,000 rpm in an Eppendorf microcentrifuge. The supernatant (soluble tubulin fraction) and pellet (polymerized tubulin fraction) were dissolved in the in the cell lysis buffer. Protein samples were boiled in loading buffer, loaded onto 10% polyacrylamide gels, and separated by electrophoresis. Proteins were transferred to polyvinyldifluoride membranes (Biorad), using a Biorad Transblot Semidry system. After washing, blocking, and treating with appropriate antibodies, protein bands were detected using the Amersham ECL Western blotting system and Fuji film. Densitometric analyses were performed with ImageJ (v. 1.32j) software.

2.2.20 Tubulin polymerization assay

Tubulin assembly was monitored turbidimetrically at 350 nm in temperature controlled, multichannel Beckman DU4700 spectrophotometers as described previously[5]. Reaction mixtures without test compounds contained tubulin (10 μM, 1.0 mg/mL) in 1M monosodium glutamate, pH 6.9, containing GTP (400 μM if present). Baselines were established after addition of all reaction components except the test compounds to the cuvettes held at 0°C. Compounds predissolved in DMSO (1% final concentration) were added to give the indicated final concentrations, and the reaction mixtures (0.25 mL final volume) were subjected to the indicated sequential temperature changes.

3.0 BIOLOGICAL EVALUATION OF A PUREALIN LIBRARY

3.1 Introduction

Antiproliferative assays are widely used to evaluate the activity of new agents against carcinoma cells and are a requisite part of the drug discovery process. The 21 purealin and purealidins were assessed for antiproliferative and potential cytotoxic activity against a panel of human carcinoma cells, as well as against a mouse leukemia cell line. Four well-established human carcinoma cell lines were examined: MDA-MB231 (breast epithelium; mutant TP53), PC-3 (prostate epithelium; TP53 null), 2008 (ovarian epithelium) and HT-29 (colon; TP53 null). These cell lines were chosen in part because they are readily available, they can be used as xenotransplants in immunocompromised mice for antitumor studies, these cancer types represent a large percentage of new cancers reported, the cell lines have similar growth characteristics, are particularly sensitive to antimitotic agents, and represent a majority of the solid tumors found in humans. The L1210 mouse leukemia cell line was chosen for this assay to compare data obtained here against that reported in the literature for purealidin A[26].

The MTS [3-(4,5-dimethylthiazol-2-yl)-5-(3-carboxymethoxyphenyl)-2-(4-sulfophenyl)-2H-tetrazolium] assay was used here. It is a colorimetric method for determining the number of viable cells in proliferation or cytotoxicity assays. In this assay, the MTS tetrazolium compound is reduced by cells into a colored formazan product that is soluble in tissue culture medium[76].

This conversion is presumably accomplished by the NADPH or NADH produced by dehydrogenase enzymes in metabolically active cells[77]. Assays are performed by adding a small amount of the MTS reagent directly to culture wells, incubating for 1 h and then recording absorbance at 490nm minus that observed at 630nm with a plate reader. The quantity of formazan product as measured by the amount of 490nm absorbance is directly proportional to the number of living cells in culture[78]. The absorbance found at 630nm was used to remove any background contributed by excess cell debris, fingerprints and other nonspecific absorbance. The MTS assay is a convenient and fast way to determine the cell numbers and thus the antiproliferative activity of the compounds.

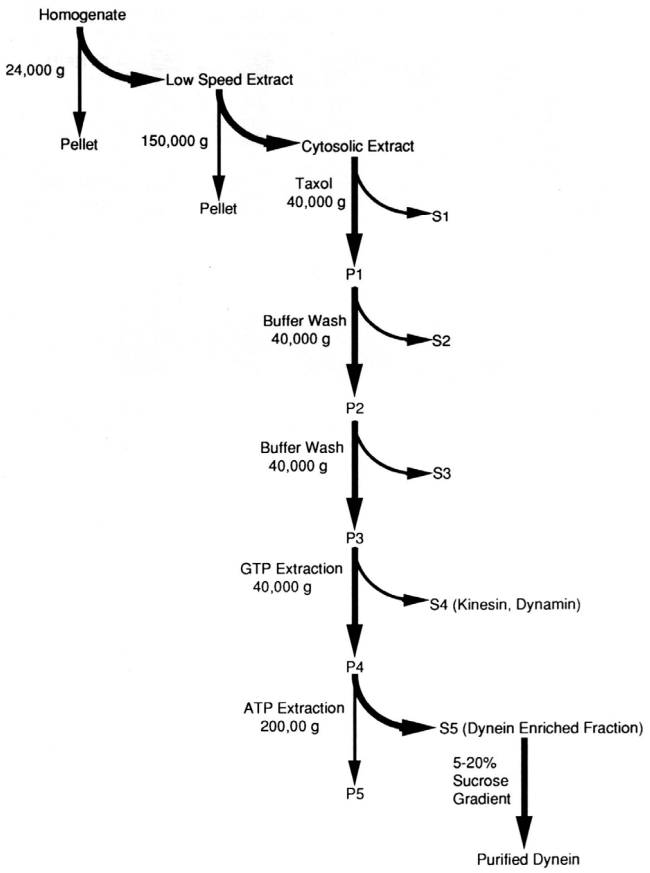

Figure 14. Flow diagram illustrating the preparation of brain cytoplasmic dynein. [From Paschal et al., Methods Enzymol, 1991. **196**:181 ref. [79]]

Cytoplasmic dynein was originally identified as MAP 1C and purified from calf brain by Prof. Vallee and colleagues[13,79]. Dynein produces forces along microtubules and hydrolyzes ATP to ADP and free phosphate. When microtubules are sedimented in the absence of ATP, most of the dynein will co-sediment. However, when microtubules are sedimented in the presence of ATP, only a trace amount of the dynein will sediment[79]. This is the basis for the dynein preparation. Also, GTP will extract kinesin and dynamin from microtubules[80,81], helping to eliminate these two proteins from the dynein preparation. A flow diagram illustrating the preparation of brain cytoplasmic dynein by Vallee's method is shown in Figure 14. Once dynein has been released from microtubules, it can be purified from trace contaminating polypeptides by sucrose density gradient centrifugation (Figure 15).

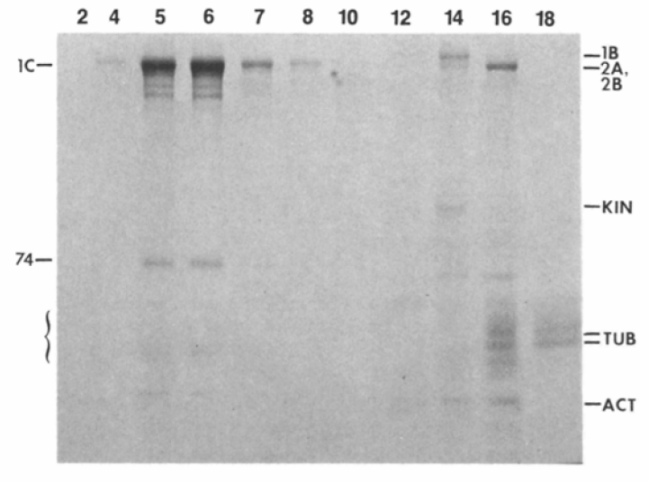

Figure 15. SDS-PAGE of bovine cytoplasmic dynein after sucrose gradient centrifugation.
[From Paschal et al., Methods Enzymol, 1991. **196**:181 ref. [79]]

Also, from the intermediate steps in the regular tubulin purification and isolation work in the Day lab, it should be possible to isolate cytoplasmic dynein, one of the MAPs, from tubulin preparations. Microtubules with MAPs were obtained following the regular steps in tubulin preparation. After additon of GTP to extract kinesin and dynamin from the microtubules, ATP

was added to release the dynein from the microtubules followed by sucrose density gradient centrifugation.

The dynein heavy chain and its related components must be characterized after the separation work. Sodium dodecyl sulfate-polyacrylamide gel electrophoresis (SDS-PAGE) was used to determine the relative purity of dynein heavy chain. Matrix-assisted laser desorption ionization-time of flight/time of flight- mass spectrometry/mass spectrometry (MALDI-TOF/TOF-MS/MS) was used to identify the cytoplasmic dynein heavy chain, any isotypes, and adapter proteins co-purified from bovine brain. The MS work is covered in chapter 3.3.2.

Since dynein heavy chain is an ATPase that can hydrolyze ATP to ADP and free phosphate, the ATPase activity of the purified sample can be measured by the free phosphate it released. The malachite green assay is a convenient way to measure free phosphate. Inorganic phosphate (Pi) forms complexes with ammonium molybdate, and the malachite green acts as additional ligand and colorimetric indicator for this reaction. Any instability of the signal was overcome by the addition of sodium citrate after the malachite green reagent. The absorbance maximum of the Pi-containing complex can be measured at ~650 nm[82].

It is reported that the ATPase activity of dynein heavy chain can be activated by the presence of microtubules[13], the ATPase activity of dynein heavy chain can be measutred as a function of microtubule concentration. The known dynein ATPase inhibitor EHNA was used as a positive control in the ATPase assay, as well as an indicator of the success of the purification work[41].

Western blotting is an immunochemical technique commonly used to positively identify the presence of a specific protein in a complex mixture and to obtain qualitative and semiqualitative data about the level of the protein. After electrophoresis, the separated proteins

are transferred onto a polyvinylidene fluoride (PVDF) or nitrocellulose membrane. The transferred proteins are exposed to a primary antibody for the protein, weak and nonspecific complexes are broken by washing steps, and the presence of highly retained antibody (i.e., specific binding) is detected by a variety of means. Here, an enzyme-labeled antibody was used as a probe. A substrate that reacts with that enzyme to form a chemiluminescent product is then added and resulting emitted light is quantified by either a chemiluminescence detector and/or by captured the light emitted through use of sensitive x-ray film.

Mass spectrometry has developed into a powerful tool to analyze proteins for information such as the protein sequence, some three dimentional structure information, as well as any post-translational modifications of the protein[83-85]. With the matrix-assisted laser desorption ionization (MALDI) method, nonvolatile molecules can be readily introduced into the gas phase and analyzed by mass spectrometry. The MALDI sample consists of a solid mixture of analyte and a crystalline matrix on a sample plate that is excited by laser light, resulting in soft ionization. Ions are guided by optics into the mass-to-charge ratio segregator (i.e., the mass spectrometer) (Figure 16A). The matrix is an organic acid with a chromophore absorbing at the laser wavelength, such as α-cyano-4-hydroxycinnamic acid (Figure 16B).

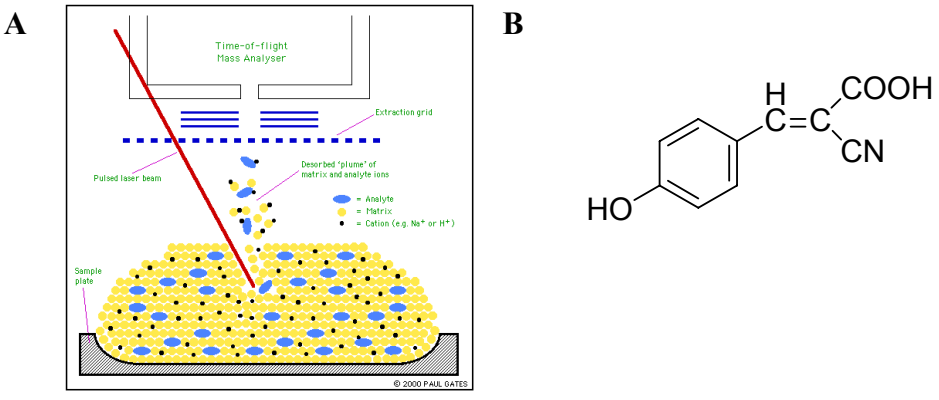

Figure 16. Schematic of MALDI (A) and structure of the matrix molecule α-cyano-4-hydroxycinnamic acid (B).

Typsin digestion has become a standard method in proteomic analysis. Trypsin hydrolyzes polypeptides on the carboxyl side of arginine and lysine residues. In-gel digestion of polyacrylamide gel electrophoresis (PAGE)-separated proteins has proved to be an efficient method to generate peptide fragment mixtures suitable for mass spectrometric analyses and comparison to theoretical peptides from in silico digests of the proteins coded by genes found in genomics databases. This process of matching experimentally measured peptide masses to the theoretical masses found by in silico manipulations of genomics databases is known as peptide mass fingerprinting.

3.2 Antiproliferative activities of purealin library components

The 21 purealidins and purealins were assessed for antiproliferative activity against a small panel of human carcinoma cells [MDA-MB231 (breast), PC-3 (prostate), 2008 (ovarian) and HT-29 (colon)] as well as against the mouse L1210 leukemia cell line. The L1210 cells were used to compare data obtained here against that reported in the literature for purealidin A[19]. The procedure is described in Chapter 2. In short, cells were plate in 96-well plate and allowed attach for 72 h. Cells were treated with compounds for another 72 h. The MTS assay was used to determine cell viability. The 50% growth inhibitory (GI_{50}) values obtained (Table 1) showed **purealin** and **purealidin A** to be inactive against the human cell lines. However, some of the purealidin A analogues, for example, ***ortho*/chlorophenyl/Cl-purealidin A** and ***ortho*/indolinyl/Cl-purealidin A**, showed low micromolar antiproliferative activity. The mouse leukemia cells, on the other hand, were uniformly sensitive to the individual library components.

Table 1. Antiproliferative activities of the purealin/purealidin library.

Compound	GI_{50} (μM)				
	2008	MDA-MB231	HT29	PC3	L1210
***para*/phenyl/Br-purealidin A**	29 ± 2	27 ± 0	31 ± 3	31 ± 3	6.4 ± 2.2
***para*/methoxyphenyl/Br-purealidin A**	24 ± 3	17 ± 2	20 ± 5	21 ± 5	2.8 ± 2.8
***para*/chlorophenyl/Br-purealidin A**	29 ± 1	27 ± 2	31 ± 1	30 ± 4	7.8 ± 2.5
***para*/indolinyl/Br-purealidin A**	27 ± 1	24 ± 2	26 ± 4	26 ± 9	5.8 ± 1.2
***para*/phenyl/H-purealidin A**	30 ± 5	>50	27 ± 4	31 ± 6	6.2 ± 0.9
***para*/methoxyphenyl/H-purealidin A**	31 ± 12	48 ± 14	30 ± 9	39 ± 4	9.9 ± 6.1
***para*/chlorophenyl/H-purealidin A**	27 ± 3	26 ± 1	27 ± 1	33 ± 4	6.5 ± 2.0
***para*/indolinyl/H-purealidin A**	26 ± 2	25 ± 1	30 ± 1	32 ± 6	7.6 ± 1.9
***ortho*/phenyl/Br-purealidin A**	19 ± 5	5.7 ± 0.8	5.3 ± 0.2	19 ± 6	6.3 ± 0.4
***ortho*/methoxyphenyl/Br-purealidin A**	25 ± 2	8.8 ± 0.6	4.9 ± 0.6	35 ± 15	6.2 ± 0.9
***ortho*/chlorophenyl/Br-purealidin A**	5.6 ± 0.9	5.6 ± 0.7	5.3 ± 0.2	15 ± 7	6.3 ± 0.8
***ortho*/indolinyl/Br-purealidin A**	7.5 ± 0.4	6.7 ± 1.0	6.0 ± 0.1	31 ± 6	5.4 ± 0.9
***ortho*/phenyl/Cl-purealidin A**	8.8 ± 2.7	7.6 ± 3.2	5.6 ± 0.2	31 ± 7	7.5 ± 0.9
***ortho*/methoxyphenyl/Cl-purealidin A**	29 ± 1	24 ± 2	6.2 ± 1.7	32 ± 11	6.9 ± 0.5
***ortho*/chlorophenyl/Cl-purealidin A**	5.4 ± 0.6	5.2 ± 0.9	5.5 ± 1.8	7.8 ± 0.9	5.9 ± 0.5
***ortho*/indolinyl/Cl-purealidin A**	5.7 ± 0.1	5.3 ± 0.0	6.0 ± 0.6	5.0 ± 1.1	5.8 ± 1.1
Lipopurealin A	28 ± 3	28 ± 1	29 ± 2	30 ± 4	9.0 ± 1.9
Lipopurealin B	29 ± 1	28 ± 3	30 ± 0	25 ± 9	12 ± 4
Lipopurealin C	5.7 ± 1.2	7.0 ± 0.4	20 ± 3	32 ± 3	9.7 ± 1.6
Purealidin A	>50	>50	>50	>50	4.7 ± 1.6
Purealin	>50	>50	>50	>50	3.2 $\pm$ 1.2
Discodermolide (nM)	2.7 ± 1.7	40 ± 7	28 ± 9	52 ± 8	9.2 $\pm$ 4.3

3.3 Dynein isolation and purification

3.3.1 Purification of bovine brain cytoplasmic dynein heavy chain

In order to test if the purealin library has any effect on dynein heavy chain ATPase activity, bovine cytoplasmic dynein heavy chain was purified from fresh bovine brain following the procedure described in Chapter 2. The Coomassie blue-stained SDS-PAGE of sucrose density gradient fractions in the standard purification of dynein heavy chain is shown in Figure 17A. It was similar to the standard SDS-PAGE of the sucrose gradient in Figure 15. The top bands are dynein heavy chain. Fractions 6 and 7 were well-seperated dynein-enriched fractions. The presence of dynein heavy chain was further verified by Wester blotting (Figure 17B). Using rabbit anti-dynein heavy chain polyclonal IgG, dynein heavy chain was found in fractions 6 and 7, but was unlikely to in fraction 5 even though there was a strongly-staining protein at the top of the SDS-PAGE gel in that fraction.

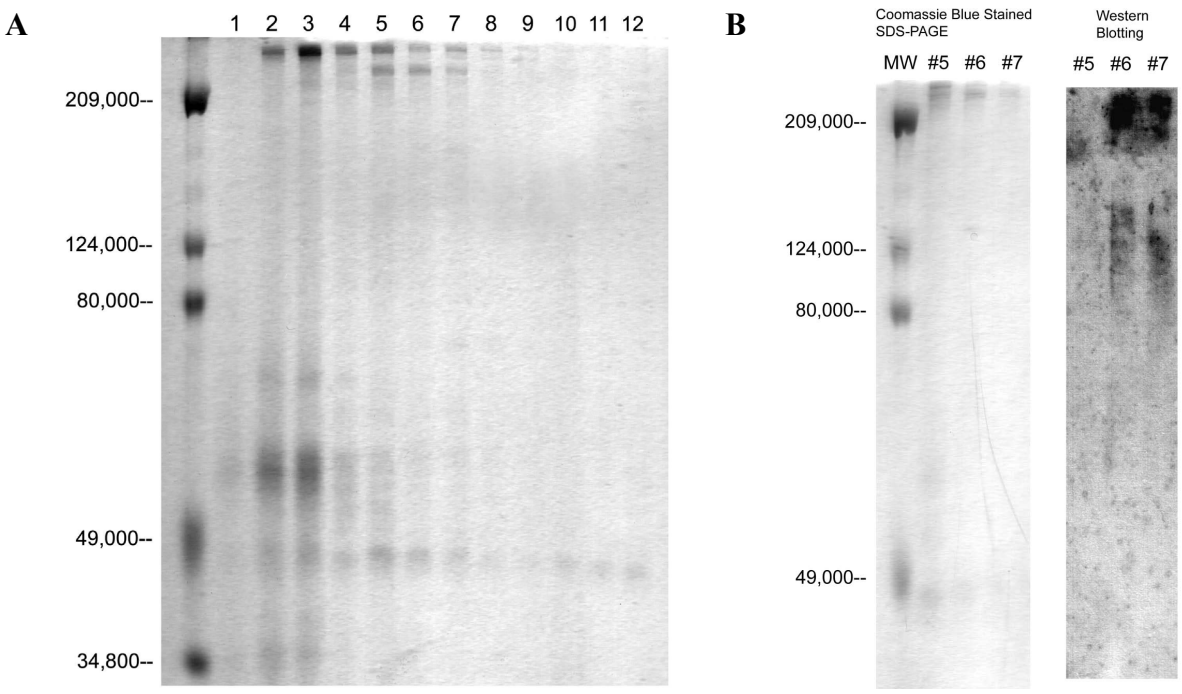

Figure 17. Coomassie blue-stained SDS-PAGE (A) and anti-dynein heavy chain Western blot (B) analysis of sucrose density gradient fractions in the standard purification of dynein heavy chain.

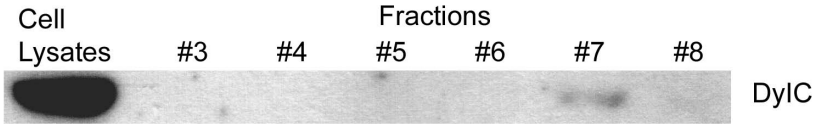

Figure 18. Anti-dynein intermediate chain Western blot analysis of sucrose density gradient fractions 3-8.

The protein concentration in fractions 5-7 was tested with the Bio-Rad protein reagent (Figure 19A). The ATPase activity of different dynein fractions was estimated with the malchite green-based ATPase assay (Figure 19B). From the results, the ATPase activity of dynein fraction 7 was found high, especially when the small amount of protein in the solution was taken into consideration. The ATPase activity of fraction 6 was reasonable, not much ATPase activity was observed in fraction 5. With this information in hand, fractions 6 and 7 were used for analysis of the potential cytoplasmic dynein heavy chain inhibitors.

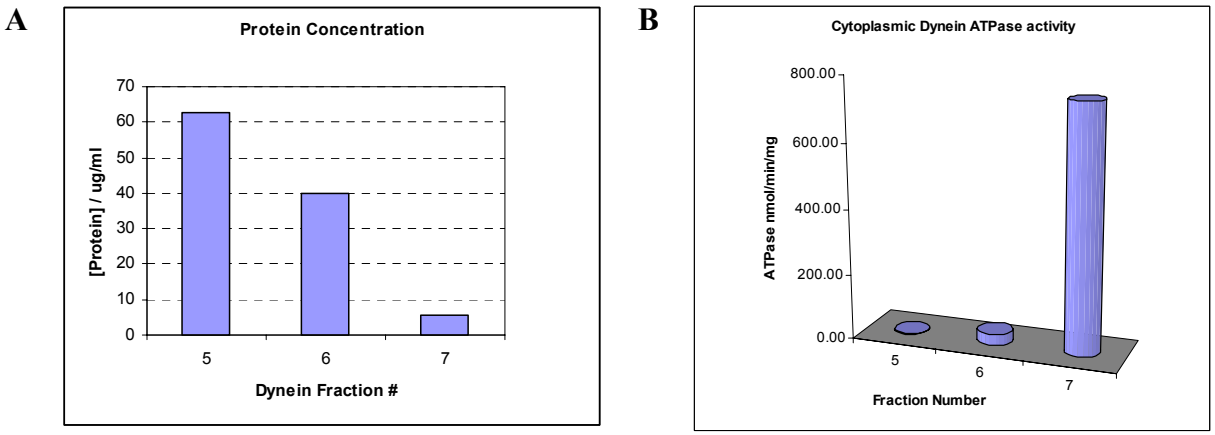

Figure 19. The protein concentration (A) and ATPase activity (B) of different dynein purification fractions 5-7.

Since dynein ATPase activity is dependent on the concentration of microtubules, the relationship between the concentration of tubulin and purified cytoplasmic dynein ATPase activity was tested (Figure 20). The result showed that microtubules behaved as a specific activator of the ATPase activity of the purified dynein, indicating the success of the purification work. The inhibitory effects of EHNA on cytoplasmic dynein ATPase activity is shown in Figure 21.

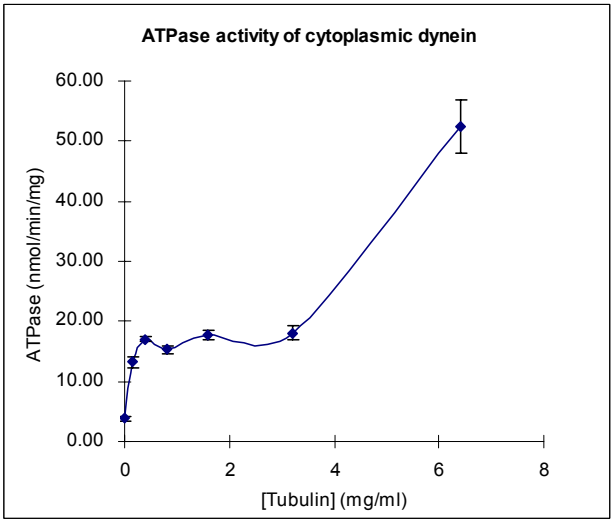

Figure 20. ATPase activity of brain cytoplasmic dynein as a function of microtubule concentration.

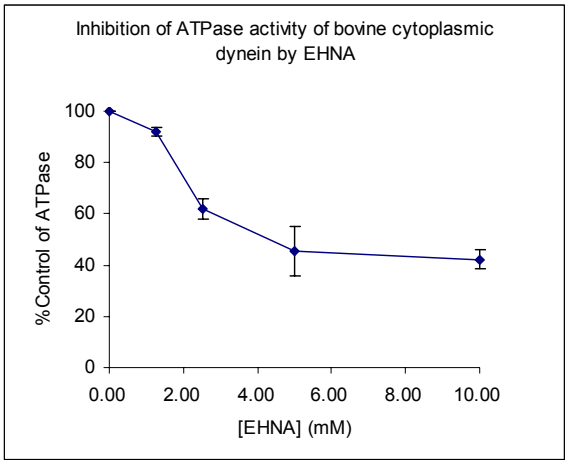

Figure 21. Inhibitory effect of EHNA on bovine cytoplasmic dynein ATPase activity.

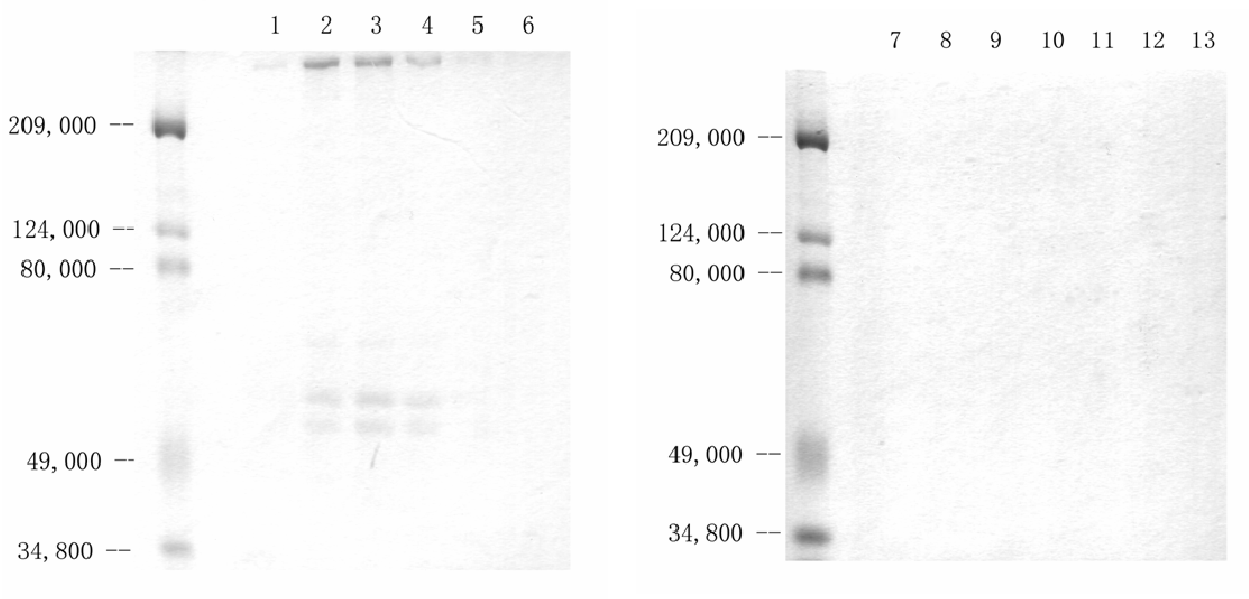

Figure 22. Coomassie blue-stained SDS-PAGE analysis of sucrose density gradient fractions in the glycerol-based dynein purification.

An attempt was also made to purify dynein heavy chain during the standard protocol of tubulin isolation from bovine brain, since dynein is actually one of the MAPs. The procedure was descried under section in Chapter 2. The resulting SDS-PAGE analysis after the sucrose density gradient centrifugation and staining of the developed gel with Coomassie blue is shown

in Figure 22. Fractions 2-4 were enriched in dynein, but the lower molecular radius bands around 50kDa were not as well separated as those in the standard dynein preparation (Figure 17).

3.3.2 Characterization of bovine cytoplasmic dynein by mass spectrometry

The intermediate prep during the glycerol-based dynein preparation procedure was segregated by SDS-PAGE stained with Coomassie blue (Figure 23). There were three major bands in the gel: one with an M_R of ca. 500kDa and two around 50kDa. These bands were excised from the gel, digested in-gel with trypsin and the released peptides were analyzed by MALDI-TOF-MS and MALDI-TOF/TOF-MS/MS.

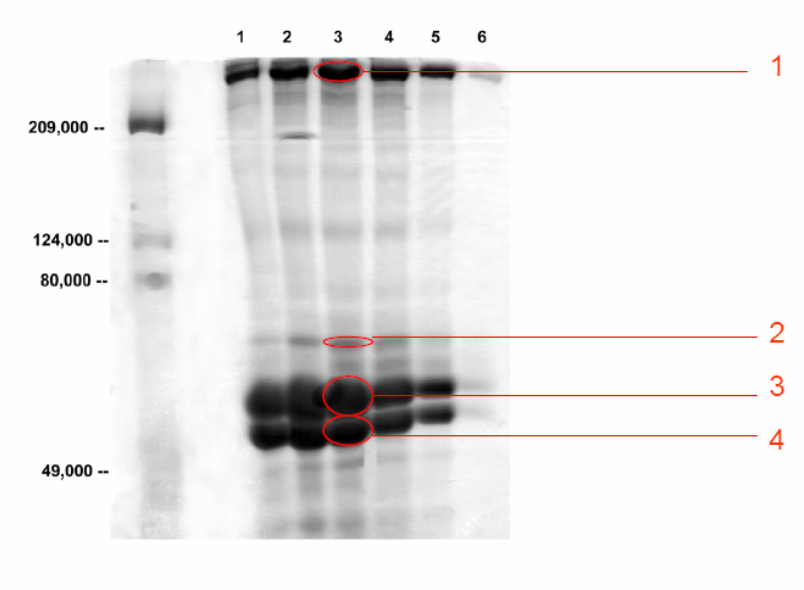

Figure 23. Coomassie blue-stained SDS-PAGE gel used in the mass spectrometric analysis of dynein fractions

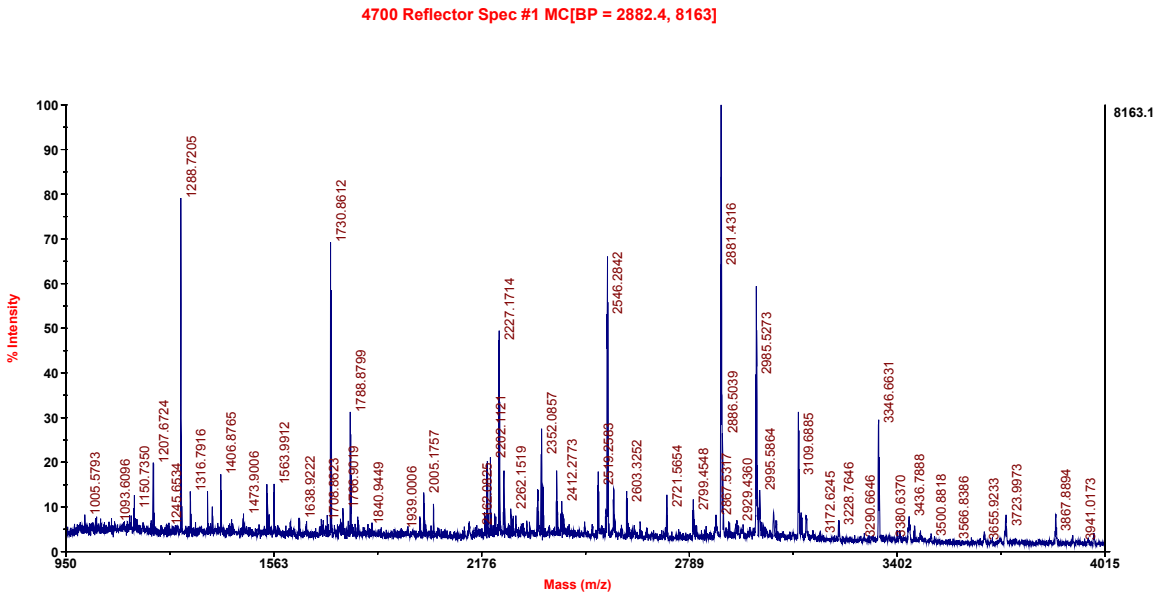

Figure 24. MALDI-TOF mass spectrum of spot 1

Table 2. Peak assignments of mass spectrum of spot 1

61/272 matches (22%).

Acc. #: P34036 Species: DICDI Name: Dynein heavy chain, cytosolic (DYHC)

Index: 142453 MW: 538824 Da pI: 6.2

m/z Submitted	MH^+ Matched	Delta Ppm	Modifications	Missed Cleavages	Database Sequence
1005.579	1005.5403	39	1Met-ox	1	(R)KMINDLQK(M)
1009.52	1009.5318	-11		1	(R) SDLREYVK (A)
1019.515	1019.5314	-16		0	(K) NPYYPIPR (Y)
1037.559	1037.509	49	pyroGlu	1	(R)QLDTYMKR(V)
1061.594	1061.5843	8.7		1	(R) KSLEDTLQK (L)
1063.538	1063.5536	-15		0	(R) SATSPALFNR (C)
1076.547	1076.5376	8.6		0	(K) LSSWEADLR (Y)
1137.65	1137.6268	20		0	(R) TILGSTIYGGR (I)
1178.593	1178.5404	45	1Met-ox	0	(K)TSFLDSSFMK(N)
1188.613	1188.6523	-33		1	(R) LATAKNAMNVR (V)
1201.636	1201.6078	23	pyroGlu	1	(R)QGRQNYVTPR(H)
1214.629	1214.6606	-26		1	(R) TGQDLLQRQR (F)
1302.722	1302.6905	24		1	(K) ENSKEVELLGGK (N)
1302.722	1302.7018	15		1	(K) ILQESKSINDR (I)
1332.673	1332.6946	-16		1	(K) EMKQSIGAVNQK (I)
1332.673	1332.7276	-41		1	(R) TTQNIKDPLFR (C)
1441.715	1441.7579	-30		0	(K) VTPEFSTLVASYK (R)
1441.715	1441.7763	-43		1	(K) DARELQVQLDVR (N)
1446.874	1446.8936	-14		0	(K) LTFALQLTIISVK (G)
1554.807	1554.7474	38		1	(K) SSDFDDDLRMLLK (R)
1579.992	1579.9423	31		0	(K) VSGAPLILEVLAIER (I)
1611.856	1611.907	-32		1	(R) KNATISEAIPQLQAK (I)
1658.873	1658.8616	7.1	1Met-ox	0	(R)FVAWMNGLSIYTIK(V)

1759.96	1759.8979	35		1	(R) GATHEYESQLIERVK (E)
1775.874	1775.9631	-50		1	(K) WLICLRQQVPSFSK (L)
1791.902	1791.903	-0.8		1	(R) VEGEWSAFNEILNRK (N)
1939.001	1939.0475	-24	1Met-ox	0	(R)LFMTSEIHPALPANLLR(M)
1958.078	1958.0751	1.3		0	(R) HYLDFINQVVLLINEK (R)
1958.942	1958.9751	-17		0	(R) FYFVGDEDLLEIIGNSK (D)
2027.136	2027.0523	41		1	(K) IMEPNFITSIINYDTKK (M)
2027.136	2027.0523	41		1	(K) KIMEPNFITSIINYDTK (K)
2120.11	2120.0732	17	1Met-ox	0	(R)ALLEAIQTMDGCTLEGLVR(L)
2138.13	2138.0657	30		0	(K) TTSWEVYLEAIEQVDNIK (S)
2177.179	2177.078	46		1	(K) LVDHIQQNSSDWKQFFGK (D)
2185.127	2185.1617	-16		0	(R) DAVVSSLVYIHQTIGEANIR (L)
2185.127	2185.1844	-26		1	(K) SVLSRFVAWMNGLSIYTIK (V)
2201.135	2201.1793	-20	1Met-ox	1	(K)SVLSRFVAWMNGLSIYTIK(V)
2223.125	2223.1985	-33		1	(R) IKPLREEVEQLENAANELK (L)
2232.148	2232.113	15		1	(R) YIPLGWTKFFEFNDADLR (G)
2238.18	2238.1328	21		1	(K) EVKSSSPLLLCSVPGYDASSK (V)
2244.15	2244.1229	12		0	(K) WYSVPETISLSVWISDFSK (R)
2252.076	2252.1147	-17		1	(R) RNLHVVFTMNPASPDFHNR (S)
2268.222	2268.1096	50	1Met-ox	1	(R)RNLHVVFTMNPASPDFHNR(S)
2278.18	2278.1607	8.4		1	(R) TYAQTSGKVTPEFSTLVASYK (R)
2298.323	2298.3033	8.7		1	(R) ILSAVSQQIQTIQVALKENSK (E)
2317.066	2317.0988	-14		1	(R) EAITKGYLEDPGFDYETVNR (A)
2351.104	2351.2043	-43		1	(K) IQFVGACNPPTDAGRVQLTHR (F)
2404.152	2404.2036	-21		1	(R) NGLILDSEEELYKYFTSQVR (R)
2428.266	2428.2652	0.19		1	(R) FYFVGDEDLLEIIGNSKDIIK (I)
2529.269	2529.3434	-29	1Met-ox	0	(K)ILQLHQILNINHGVMMVGPSGGGK(T)
2546.284	2546.1947	35	1Met-ox	0	(R)YPLVIDPSGQAMEFLMNQYADK(K)
2603.325	2603.3002	9.6	1Met-ox	1	(R)LLYSLMWGLGGSMGLVERENFSK(F)
2619.37	2619.2951	29	2Met-ox	1	(R)LLYSLMWGLGGSMGLVERENFSK(F)
2799.455	2799.4834	-10	pyroGlu	1	(R)QNYVTPRHYLDFINQVVLLINEK(R)
2907.435	2907.3201	39		1	(K) DFDWLYHMRYYYDATQENVLHK (L)
2926.412	2926.5103	-33		1	(R) WVYLQGIFSGSGDINQLLPAESTRFK (S)
2947.434	2947.4123	7.5		1	(R) FNRYPLVIDPSGQAMEFLMNQYADK (K)
2983.455	2983.4114	14		0	(R) HWIIFDGDVDPEWVENLNSLLDDNK (L)
3004.526	3004.4483	26		1	(K) ALGSQLGRFVLVFCCDEGFDLQAMSR (I)
3117.533	3117.6108	-25		1	(R) TIKPDDLGDKASSPEFLNLLQAGTTTWAK (N)
3119.532	3119.4223	35	2Met-ox	0	(K)VEETETVMQEISEVSALYNPMALSCSR(V)
3290.665	3290.6176	14		1	(K) MFAGLANLTLDDEKTTIIGMSSAEGETVTFK (K)
3344.7	3344.7248	-7.6	2Met-ox	1	(K)QEWVEKILQLHQILNINHGVMMVGPSGGGK(T)
3399.807	3399.7104	29		1	(K) RNENAQLQQQQQTTITSPILTSPPTTSSSSR (S)
3410.682	3410.7735	-27		1	(R) LVPVEEEIQDLKAVWVELSNTWQEIDSLK (E)
3655.923	3655.8965	7.3		1	(K) IQEQLQSIEQTTQMILNNLADSVLQDLSAQKR (K)

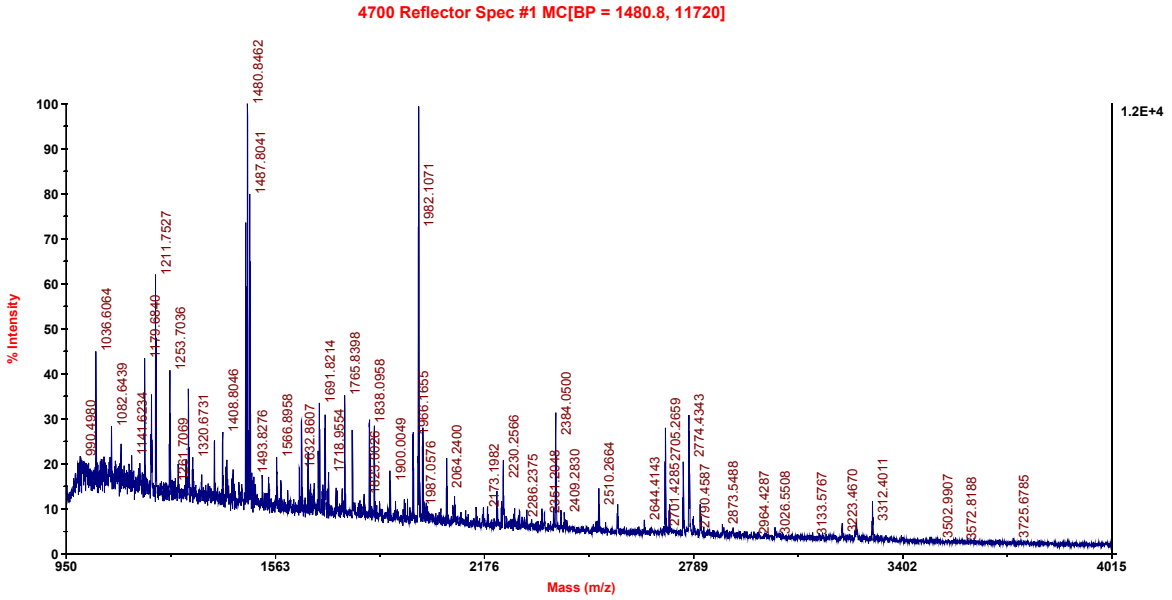

Figure 25. MALDI-TOF- mass spectrum of spot 2

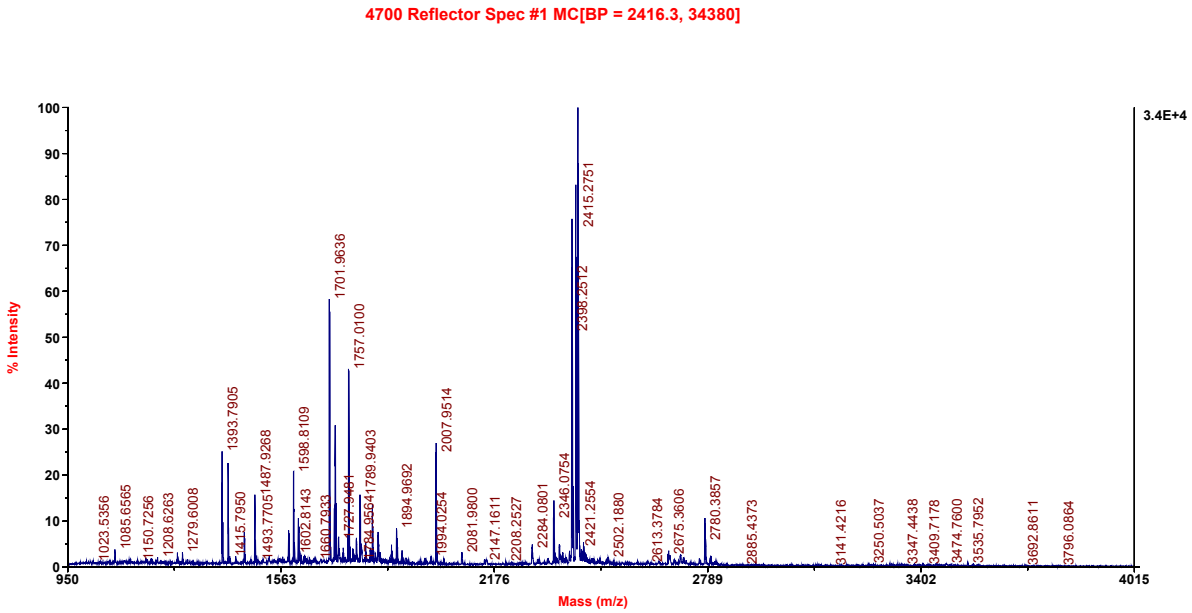

Figure 26. MALDI-TOF mass spectrum of spot 3

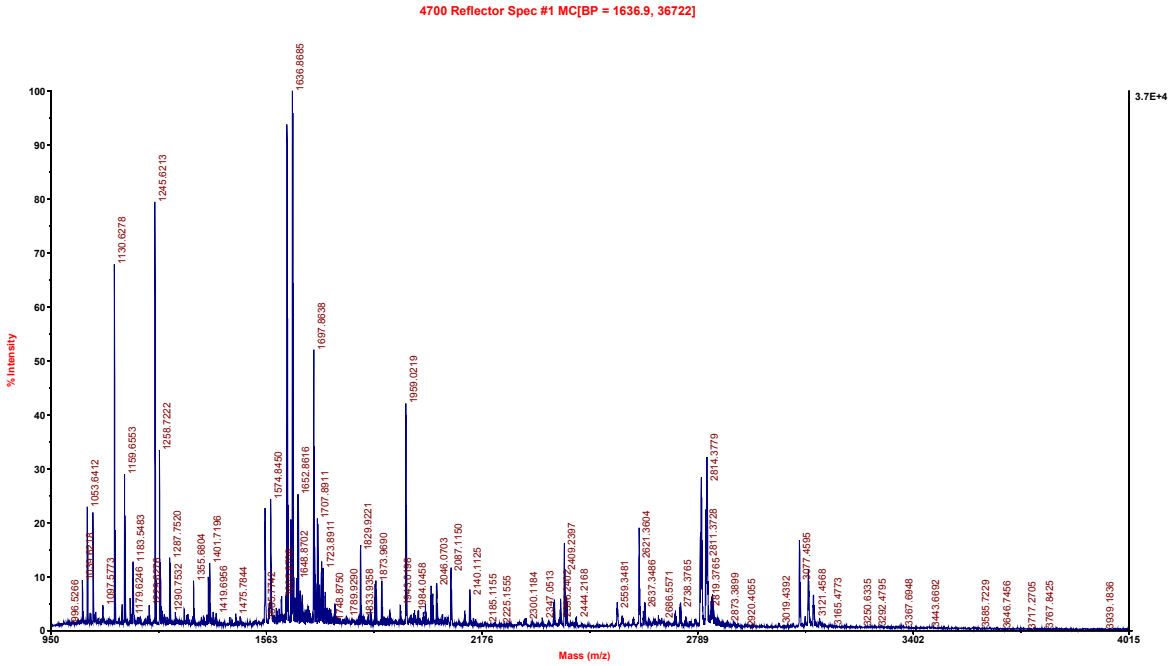

Figure 27. MALDI-TOF mass spectrum of spot 4.

Table 3. Protein identification results by MALDI-TOFMS.

Spot	MOWSE Score	# of (%) Masses Matched	% Cov	Mean Err ppm	Data Tol ppm	Protein MW (Da)/pI	Species	Protein Name
1	9.25E+12	61 (22)	20	2.91	54.5	538824/6.2	DICDI	Dynein heavy chain, cytosolic (DYHC)
2	5.08E+07	17 (5)	34	18.4	64.2	70872/5.4	MOUSE	Heat shock cognate 71 kDa protein
3	5.59E+14	29 (8)	62	27.6	12.5	50136/4.9	MOUSE	Tubulin alpha-1 chain
4	9.64E+14	40 (9)	66	16.4	31.7	50419/4.8	MOUSE	Tubulin beta-3

The mass spectra of spots 1-4 are shown in Figures 24-27. The ProteinProspector search engine from UCSF and SwissProt.2004.08.31 database were used for database searching. The protein identification results are shown in Table 3. From the results, the high molecular weight band in the SDS-PAGE matched well to *Dictyostelium* (slime mold) cytosolic dynein heavy chain. Since bovine cytosolic dynein heavy chain was not an entry in the database used, at the

moment, it can only be stated that the protein has a high probability of being bovine cytosolic cytosolic dynein heavy chain.

Moreover, the proteins co-purified with dynein heavy chain were also identified. The mass spectrum of the protein in spot 2 suggested it to be a kind of heat shock protein. Considering the MW of the band 2 is around 70 kDa and the known connection between dynein heavy chain and Hsp/Hsc70s, it is reasonable that the protein in spot 2 is one of the Hsp/Hsc70 family members. The mass spectra of proteins in spots 3 and 4 were consistent with alpha tubulin and beta tubulin, respectively. These results were the expected. The peak assignments of the mass spectra from spot 1 are listed in Table 2.

3.3.3 Expression and purification of dynein motor domain

In order to obtain more pure protein with higher enzymatic activity, a collaboration with Prof. Richard Vallee at Columbia University Medical Center, a pioneer of dynein research, was established. His group had very recetly expressed cytoplasmic dynein heavy chain motor domain via a baculovirus expression system and purified the protein. I repeated portions of the procedure, described in Chapter 2, in his lab, In short, the 380-kDa motor domain fragment was cloned from the coding region for Gly1286–Glu4644 of rat cytoplasmic dynein by insertion into the baculovirus expression vector pVL1393 (BD Biosciences) with a C-terminal in-frame hexahistidine tag. Hi5 cells were infected with virus for 40 h. The cells were washed and resuspended in PBS and the recombinant motor domain fragments were extracted from the cells by homogenization in lysis buffer supplemented with protease inhibitor and 1mM ATP. The cytosolic extract (CE) and cell pellet (CP) from the Hi5 cells were collected. The supernatant from the CE was applied to a Ni^{2+}-NTA affinity column equilibrated in lysis buffer, and the flow

through (FT) was collected. Unbound material removed by washing with 10 volumes of washing buffer and the elution (W) was colleted as well. The protein was eluted in 6 volumes of elution buffer and fractions 1~6 were collected. Protein concentrations of each fraction were determined by the Bradford method, using albumin as a standard. Protein samples (CE, CP, FT, W and fraction 1~6) were loaded onto a 3~8% Tris-acetate gel for electrophoresis analysis (Figure 28). From the SDS-PAGE analysis results, enrichment of the desired 380 kDa protein was evident in fractions 1 and 2. Therefore, fractions 1 and 2 were collected as purified cytoplasmic dynein heavy chain motor domain and flash frozen, with subsequent storage at –80 ºC. The protein obtained from baculovirus system was purer than that purified from bovine brain. Moreover, the ATPase activity of the expressed dynein motor domain was higher.

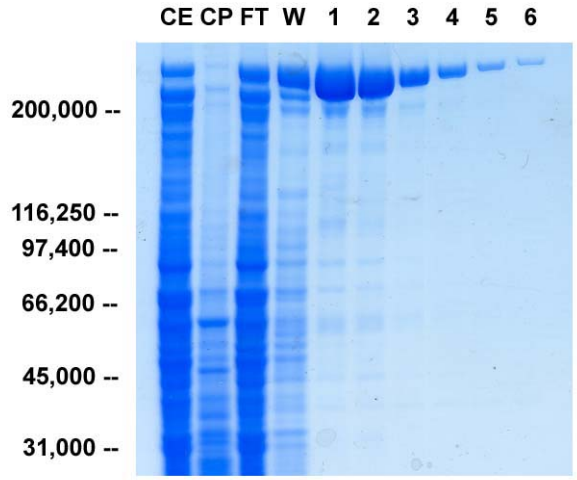

Figure 28. SDS-PAGE analysis of protein samples from the baculovirus/Hi5 cell cytoplasmic dynein heavy chain motor domain expression system.
CE, cytosolic extract; CP, cell pellet; FT, flow through; W, unbond materials; 1-6, elution fractions.

3.4 Biochemical evaluation of purealin library component

From the results of the antiproliferative assay discussed in section 3.2, it was apparent that some of the purealidin analogues had antiproliferative activity. Although purealin and purealidin A did not show antiproliferative activity in human carcinoma cell lines, the hope remained that they would bind to the proposed drug target, cytoplasmic dynein. Since the cytoplasmic dynein was isolated from bovine brain, its enzymaticic character was identified and the sequence was supported by mass spectrometry, the ATPase inhibition assay was then included as a characterization of the purealin library.

Fang et al. initially identified the inhibitory properties of purealin on dynein's ATPase activity[43] (Figure 29). The ATPase activity of 21S dynein was measured at 25 ºC. The sample was preincubated in the absence of purealin and ATP for 5 min, followed by the addition of purealin and further preincubation for 5 min. The reaction was started by the addition of 1mM ATP and stopped by adding one-third volume of cold 15% trichloroacetic acid. The amount of inorganic phosphate liberated at 0, 4, and 8 min after the addition of ATP was determined by the method of Martin and Doty[86]. The results of this experiment provided one basis for the hypothesis tested here, that purealins could inhibit cytoplasmic dynein.

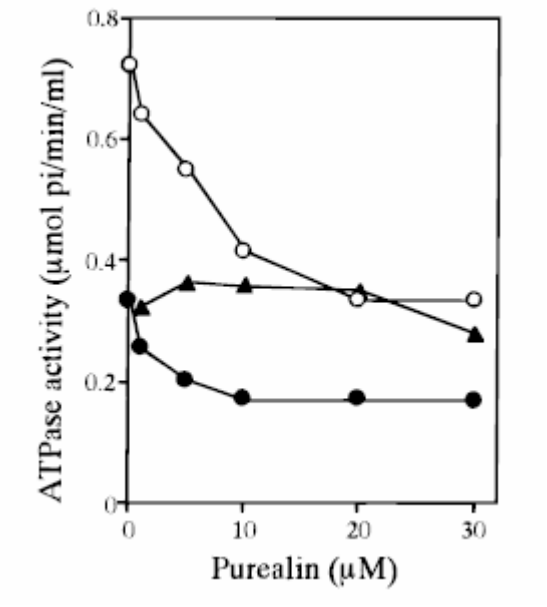

Figure 29. Inhibition by purealin of ATPase activity of axonemes and outer-arm-depleted axonemes.
Outer-arm-depleted axonemes were prepared by 0.6 M NaCl extraction of the axonemes as described in Materials and Methods. The ATPase activity of intact (open circles) and outer-arm-depleted (filled circles) axonemes was measured at 25 °C in the assay solution containing 1 mM ATP in the absence or presence of increasing concentrations of purealin. Effect of purealin on the ATPase activity of the

NaCl extract (filled triangles) was also measured as above and presented in this figure. [From Fang *et al*. *Biochemistry* **1997,** 36, (50), 15561-7, Ref. 42]

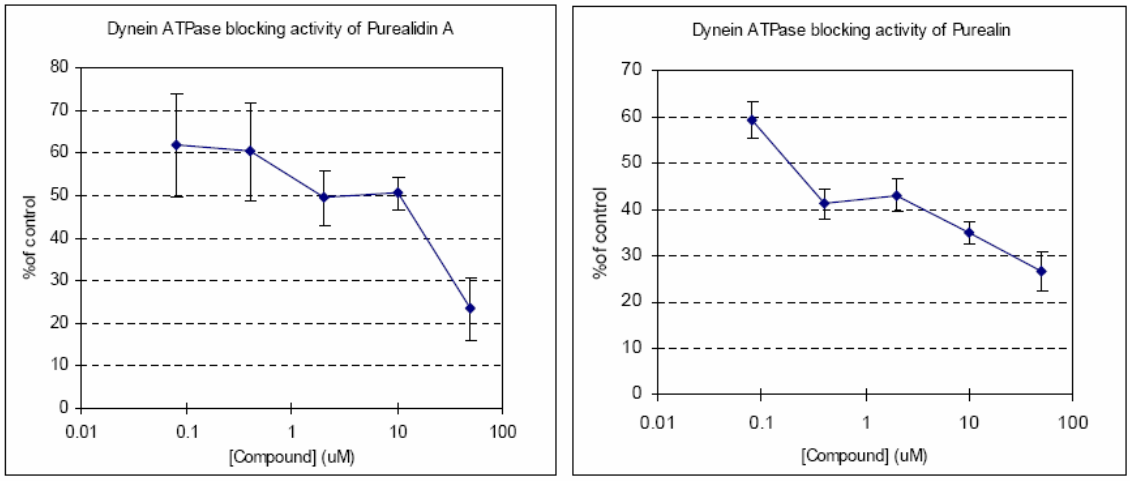

Figure 30. Inhibition of bovine brain dynein ATPase activity by purealin and purealidin A.

The ATPase inhibitory activities of purealin and purealidin A against purified bovine cytoplasmic dynein heavy chain is shown in Figure 30. The fifty percent dynein heavy chain ATPase inhibitory concentrations of the purealin library were calculated and are listed in Table 4. The results indicated that purealin and purealidin showed ATPase inhibitory activities against the target with the IC_{50}s of 0.24 μM and 10.9 μM, respectively. Most of the chemicals in the library did not show substantial inhibition. Nevertheless, the current library formed a basic platform for future work.

Table 4. Fifty percent dynein heavy chain ATPase inhibitory concentrations of the purealin library.

Compound	IC_{50} (μM)
***para*/phenyl/Br-purealidin A**	>50
***para*/methoxyphenyl/Br-purealidin A**	>50
***para*/chlorophenyl/Br-purealidin A**	>50
***para*/indolinyl/Br-purealidin A**	>50
***para*/phenyl/H-purealidin A**	>50
***para*/methoxyphenyl/H-purealidin A**	>50
***para*/chlorophenyl/H-purealidin A**	43 ± 36
***para*/indolinyl/H-purealidin A**	>50
***ortho*/phenyl/Br-purealidin A**	>50
***ortho*/methoxyphenyl/Br-purealidin A**	>50
***ortho*/chlorophenyl/Br-purealidin A**	>50
***ortho*/indolinyl/Br-purealidin A**	>50
***ortho*/phenyl/Cl-purealidin A**	>50
***ortho*/methoxyphenyl/Cl-purealidin A**	>50
***ortho*/chlorophenyl/Cl-purealidin A**	>50
***ortho*/indolinyl/Cl-purealidin A**	>50
Lipopurealin A	>50
Lipopurealin B	>50
Lipopurealin C	>50
Purealidin A	10.9 ± 5.9
Purealin	0.24 ± 0.06

The abilities of the library components to inhibit the MT-stimulated ATPase activity of recombinant dynein motor domain were also examined. First, the library components were screened against 50 μg/mL of rat cytoplasmic dynein motor domain in the presence of 5 mg/mL paclitaxel-induced tubulin polymer. **Purealin** and **purealidin A** gave IC_{50} values of 35μM and 42μM, respectively. The following compounds showed some inhibitory actions, but their IC_{50} values were > 50μM: ***para*/chlorophenyl/H-purealidin A**, ***para*/indolinyl/H-purealidin A**, ***para*/chlorophenyl/Br-purealidin A**, ***ortho*/indolinyl/Br-purealidin A** and ***ortho*/indolinyl/Cl-purealidin A**. The relationship of the concentrations of the inhibitors and the ratio of the dynein ATPase activity in the presence of compounds and without compounds was determined first. Purealin and purealidin A showed concentration-dependent inhibitory effects (Figure 31).

Recombinant dynein heavy chain (5 µg/ml) and 1 mg/ml paclitaxel-induced MTs were used in this assay. The reaction was induced by addition of 2mM ATP. The concentration-dependent dynein ATPase inhibition effect of purealin is shown in Figure 32.

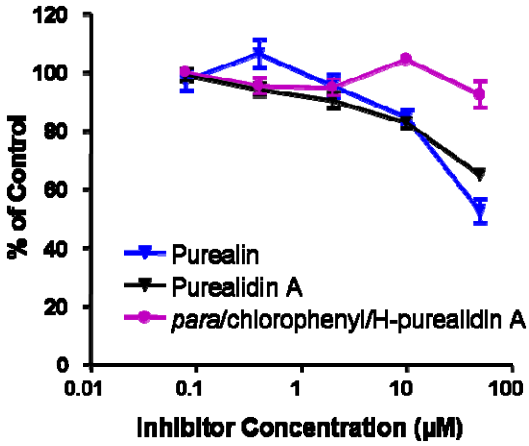

Figure 31. Dynein motor domain ATPase inhibitory activities of purealin, purealidin A and *para*/chlorophenyl/H-purealidin A**.**

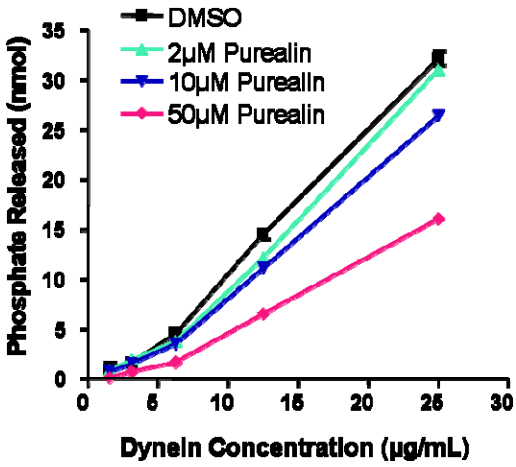

Figure 32. Inhibition by purealin of dynein ATPase activity.

To investigate the kinetics of dynein ATPase activity in the presence of different dynein inhibitors, 50 µM purealin, 50 µM purealidin A and 50 µM *para*/chlorophenyl/H-purealidin A

were added into the system with different concentration of the substrate, ATP, to determine the Michaelis-Menten parameters of dynein (Figure 33a). The calculated V^{app}_{max}, K^{app}_{M} and Ki values of dynein's ATPase activity with different inhibitors are shown in Table 5. The results further indicates the inhibitory effects of purealin and its analogues on dynein motor domain. The inhibitory effects of the three most potent compounds was in the order purealin > purealidin A > *para*/chlorophenyl/H-purealidin A. A Hanes-Woolf curve was generated and its pattern (Figure 33b) indicated the inhibitory effects of the purealins to be uncompetitive in nature.

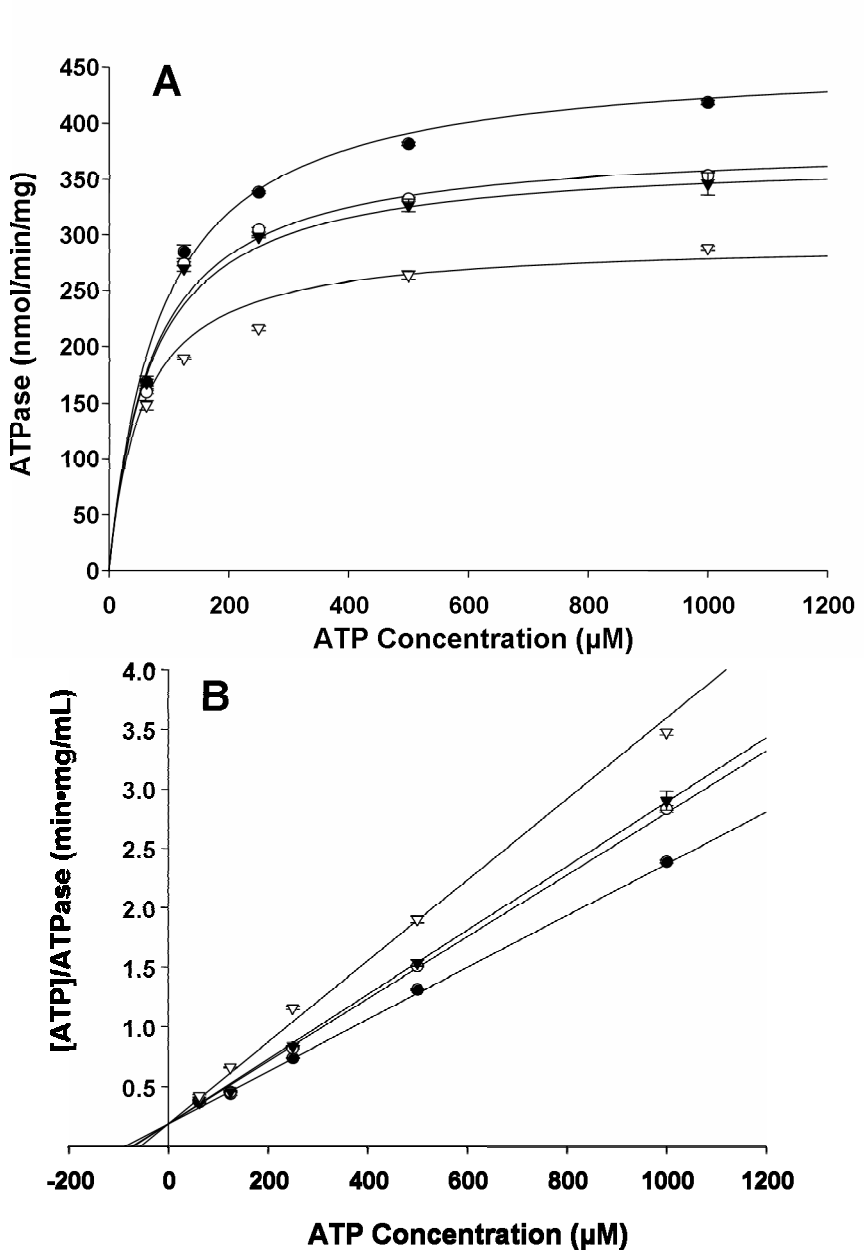

Figure 33. Michaelis-Menten curve (A) and Hanes-Woolf curve (B) of dynein in the presence of difference inhibitors: purealin, purealidin A and *para*/chlorophenyl/H-purealidin A.

The reaction was initiated with different concentrations of ATP in the presence of 12.5 μg/mL of recombinant dynein heavy chain and 1 mg/mL of paclitaxel-induced MTs. No inhibitor, filled circle; 50 μM *para*/chlorophenyl/H-purealidin A, open circle; 50 μM purealidin A, filled triangle; 50 μM purealin, open triagle.

Table 5. The V^{app}_{max}, K^{app}_{M} and Ki values of dynein ATPase with and without different inhibitors.

Inhibitor	V^{app}_{max} (nmol/min/mg)	K^{app}_{M} (M)	Ki (M)
No Inhibitor	4.57×10^{2}	9.06×10^{-8}	---
50 uM *para*/chlorophenyl/H-purealidin A	3.87×10^{2}	7.33×10^{-8}	2.95×10^{-4}
50 uM Purealidin A	3.78×10^{2}	7.01×10^{-8}	2.61×10^{-4}
50 uM Purealin	2.91×10^{2}	6.05×10^{-8}	8.49×10^{-5}

3.5 P53 nuclear translocation experiments

The 53 kDa tumor suppressor protein p53 (aka TP53 in humans) is a transcription factor involved in cell-cycle regulation, the initiation of apoptotic cell death, and of DNA repair[87]. Previous results from others have indicated that cytoplasmic dynein is responsible for the transportation of both wild-type and mutant p53 from the cytoplasm to the nucleus[23,30]. For example, Galigniana et al. have shown that the overexpressed, temperature-sensitive, mutant mouse p53 in HT29-tsp53 cells undergoes dynein-dependent movement to the nucleus. p53 movement was examined in HT29-tsp53 cells expressing *myc*-labeled dynamitin. Dynamitin is a 50-kDa subunit of the dynein-associated dynactin complex, and its overexpression blocks dynein function by dissociating the motor from its cargoes[88,89]. In HT29-tsp53 cells overexpressing dynamitin (Figure 34A), there was very little movement of p53 compared with surrounding nontransfected cells, where p53 accumulated in the nucleus after the switch to the permissive temperature.

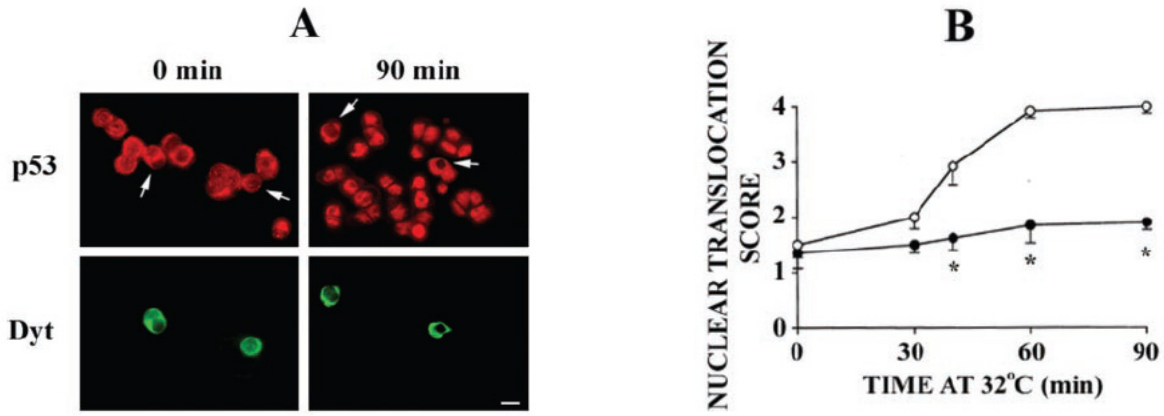

Figure 34. Overexpression of dynamitin inhibits p53 movement to the nucleus.
A, HT29-tsp53 cells were transfected with pCMVH50m plasmid encoding for *myc*-tagged dynamitin (*Dyt*). p53 nuclear translocation was triggered by shifting the temperature from 39 to 32 °C. The cells were double-stained for p53 (*red*) and dynamitin (*green*). *Arrows*, transfected cells. *Bar*, 10 μm. *B*, rate of nuclear translocation of p53 (mean ± S.E., $n = 3$) in cells transfected with empty vector (○) or with dynamitin (●). *, $p \leq 0.005$, significant difference. Adapted from Galigniana MD, et al, *J. Biol. Chem.* 279, 21, 22483 (2004), ref. [30].

Cell-based immunofluoresence assays are another powerful tool to evaluate dynein-inhibiting compounds. The Day lab and its collaborators have developed a working cell-based assay system useful for the evaluation of various chemical libraries[75]. Nuclear morphology and chromatin density, microtubule architecture, p53 levels and their subcellular locale, etc., can be used to compare changes in cell structure and function induced by novel chemical agents. The system allows for simultaneous analysis of multiple parameters in populations of cells when treated with test agents. When an antibody to wild type p53 with a fluorescently-labeled secondary antibody is employed, the induction and nuclear translocation of the protein after minor DNA damage, by e.g., low concentrations of the topoisomerase I inhibitor camptothecin, can be visualized and analyzed (Figure 35).

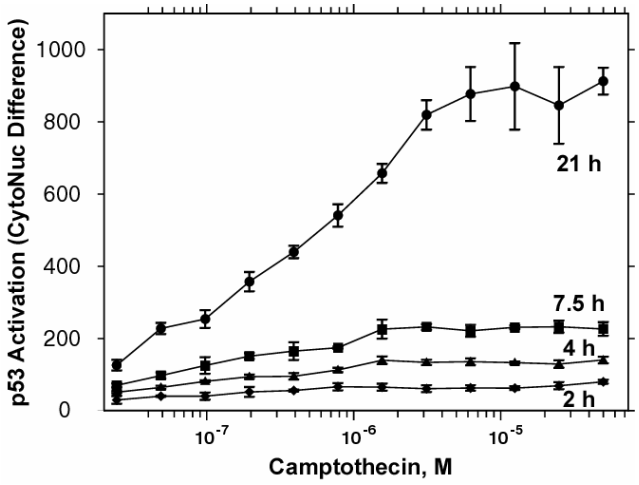

Figure 35. Dynein-driven nuclear uptake of wild type p53 in A549 cells treated with camptothecin (data courtesy of Dr. Kenneth Giuliano).

Using fluorescent protein biosensors, the inhibition of dynein-driven cargo transport when cells are treated with dynein-perturbing library components can be determined. The assay that determines the nuclear localization of wt p53 by dynein after slight DNA damage with a sub-lethal concentration of the DNA-damaging agent camptothecin, by use of fluorescent labels in human lung cancer cells was developed. A549 lung cancer cells were cultured in RPMI 1640 medium plus 10% FBS. Log phase growing cells were plated on collagen-coated slides/plates and incubated for 48h at 37 °C in a humidified 5% CO_2 atmosphere. The cells were incubated in the presence of compounds for 20h. At the end of the experiment, the solution was removed from the microplates and immediately replaced with a solution of HBSS containing 4% formaldehyde and 10 μg/mL Hoechst 33342 to fix the cells and fluorescently label their nuclei. After incubation at room temperature for 20 to 30 min, the solution was removed from each well and replaced with HBSS. At this point, microplates could be sealed and stored at 4 °C overnight. After removing the HBSS from each well, 0.5% (w/w) Triton X-100 was added and the plate incubated for 5 min at room temperature to detergent-extract a fraction of the soluble cellular

components, including soluble tubulin heterodimers. The wells were then washed with HBSS (100 µL/well) followed by the addition of a primary antibody solution containing mouse anti-α-tubulin (1:1000) and sheep anti-p53 (1:500) in HBSS. After incubation at room temperature for 1h, the microplate wells were washed with HBSS as above, followed by the addition of a secondary antibody solution containing Cy5-labeled donkey anti-sheep (1:500) and Cy3-labeled donkey anti-mouse (1:1000) antibodies diluted in HBSS. After a 1h incubation at room temperature, the microplate wells were washed as above and HBSS was added (100 µL/well) before sealing the microplates. Labeled microplates could be stored at 4 °C for up to 2 weeks before high-content analysis.

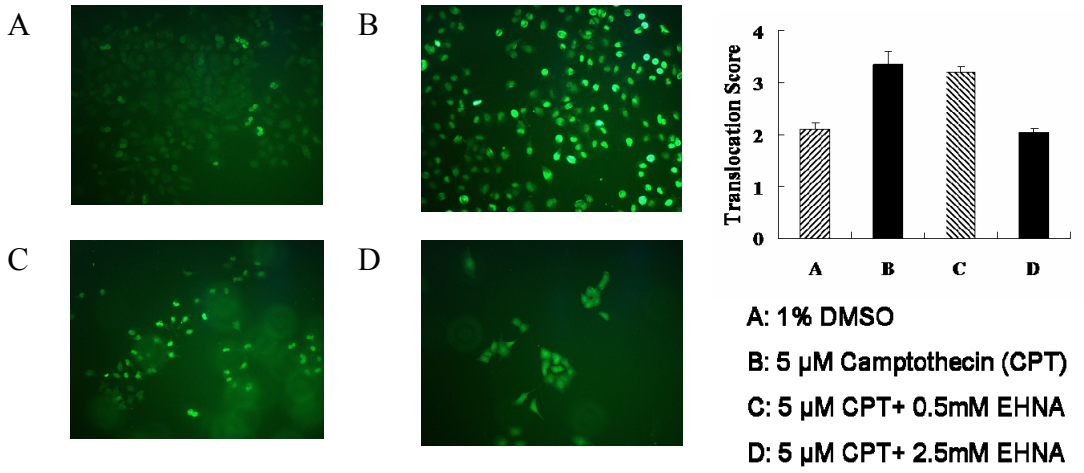

Figure 36. EHNA blocks p53 translocation into the nucleus after DNA damage.

EHNA was the first compound tested in the p53 nuclear translocation assay. A549 cells were treated vehicle only (DMSO, Figure 36A), 5 µM camptothecin (Figure 36B), or 5 µM camptothecin with different concentration of EHNA (Figure 36C, D) for 24h. The cells were fixed and stained with fluorescent markers. The translocation score was obtained as described in the following way: a score of 4 was given for nuclear fluorescence much greater than

cytoplasmic fluorescence, 3 for nuclear fluorescence greater than cytoplasmic fluorescence, 2 for nuclear fluorescence equal to cytoplasmic fluorescence, 1 for nuclear fluorescence less than cytoplasmic fluorescence, and 0 for nuclear fluorescence much less than cytoplasmic fluorescence. The translocation scores reported represent the means ± S.E. from three different areas in an experiment, in which ≥ 30 cells/area were counted. Without camptothecin, the p53 distributed evenly in cytoplasm and nucleus to give a translocation score of around 2. However, after treatment with 5μM camptothecin for 24 h, most of the p53 entered into the nucleus. A lower concentration (0.5mM) of EHNA has very little inhibitory effect on the p53 nuclear translocation. However, with the treatment of 2.5mM EHNA, p53 failed to enter into the nucleus after DNA damage by camptothecin. This result further supports the hypothesis that chemical inhibition of dynein's ATPase activity will also block the transportation of its cargo into the nucleus.

The activity of purealin and its analogues were examined in the p53 nuclear translocation assay (Figure 37). Purealin at 50 μM showed weak inhibition of p53 nuclear translocation after DNA damage. One of the purealin analogues, *para*/chlorophenyl/H-purealidin A, also showed an inhibitory effect, but at a lower concentration of 5 μM. Purealin and *para*/chlorophenyl/H-purealidin A both showed inhibitory effects against dynein motor domain ATPase activity *in vitro* (Chapter 3.4). However, purealin was not antiproliferative in human cancer cells, whereas *para*/chlorophenyl/H-purealidin A gave GI_{50} values in the low micromolar range (Chapter 3.2). One of the explanations for the lack of agreement between the cell-based and *in vitro* activity of the compounds is that they may be hitting cellular targets other than dynein. However, about a simpler explanation is that the cell-permeability of purealin, based on its action *in vitro* and in

cell-based antiproliferative as well as p53 nuclear translocation assays, simply does not enter cells as well as *para*/chlorophenyl/H-purealidin A.

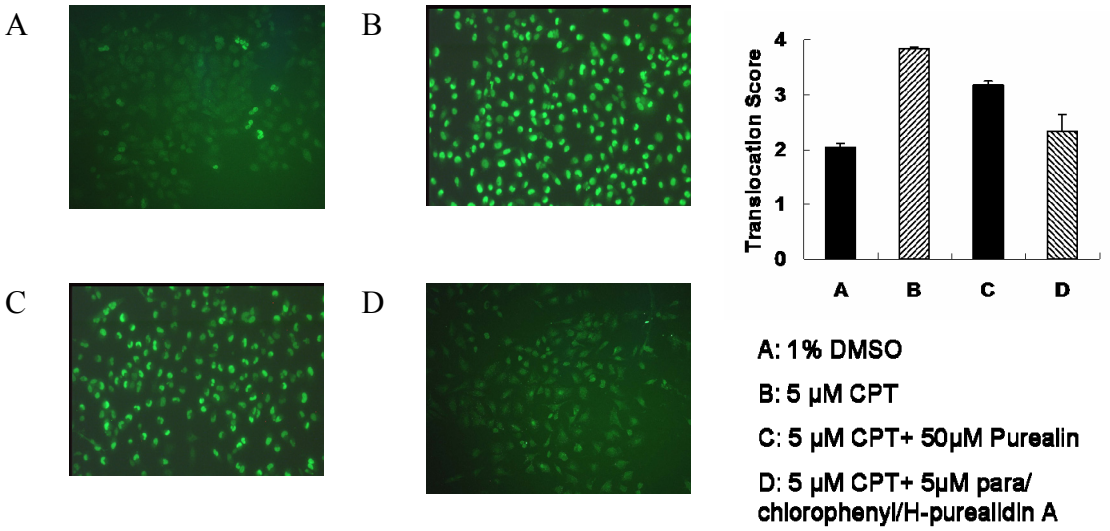

Figure 37. Inhibitory activity of purealin and *para*/chlorophenyl/H-purealidin A on p53 translocation into the nucleus after DNA damage

A high-throughout and high-content screening (HTS and HCS) system was further developed to study the p53 nuclear accumulation upon treatment of dynein inhibitors. HCS defines the effects that test agents have on the temporal and spatial regulation of multiple cell functions, and has been adopted by the pharmaceutical industry as a standard platform for compound screening [75]. The procedure used here is described in Chapter 2. Briefly, A549 cells were plated on collagen-coated 384-well microtiter plates, allowed to attach, and then treated for 24 h with DMSO or test agents. After the treatment period, the cells were fixed with formalin and their chromatin stained with Hoechst 33342. Cells were permeabilized and treated with primary antibodies for α-tubulin with fluorophore-labeled secondary antibodies. The three fluorescent channels were then examined on an ArrayScan II®, an automated fluorescence microscope system, after scanning the plates using either target activation or compartmental

analysis bioapplications, which give quantitative pixel distribution and density information in each channel on a per cell basis. An Omega XF93 filter set at excitation/emission wavelengths of 350/461 nm (Hoechst), 494/519 nm (Cy5), and 556/573 nm (Cy3) was used for scanning and 1000 cells/well were imaged at these wavelengths. The bioapplications portion of the software was used to perform automated image acquisition, characterization and classification of the cell population according to response relative to controls.

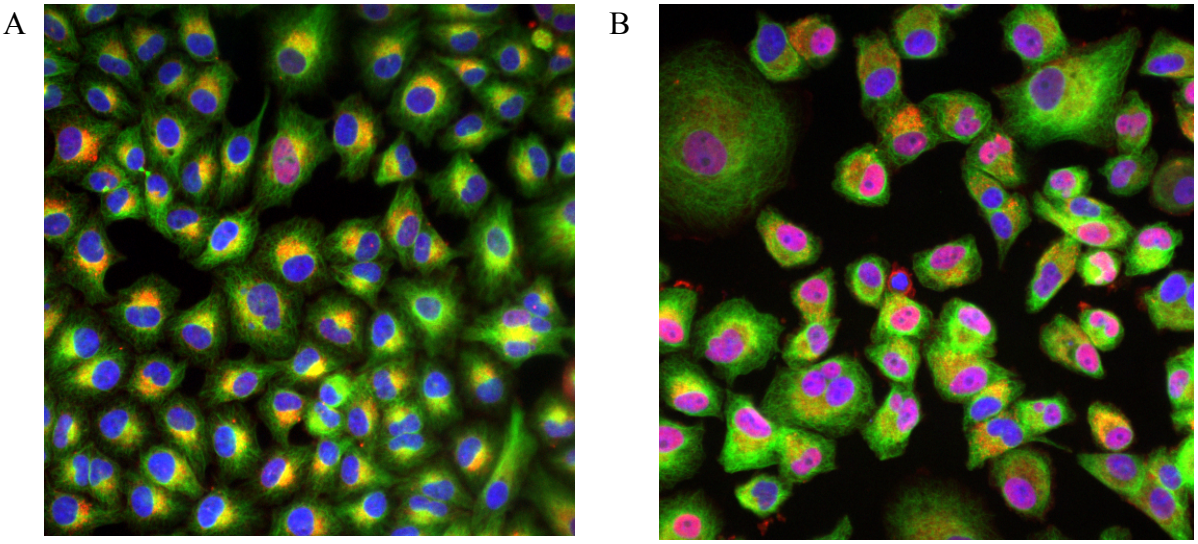

Figure 38. Representative composite immunofluorescent images from p53 nuclear translocation high content screening experiments.
A, DMSO (1%). B, Camptothecin (2 µM). Each image represents tubulin polymer (Cy5, green), nuclear chromatin (Hoechst 33342: blue), and p53 (Cy3: red) fluorescence.

Representative immunofluorescent images from ArrayScan depicting tubulin polymer (Cy5: green), nuclear chromatin (Hoechst 33342: blue), and p53 (Cy3: red) intensities are shown in Figure 38A-B. Upon the treatment of A549 cells with 2µM camptothecin, most of p53 accumulated in the nucleus, as the image obtained (Figure 38B) showed clearly the expected phenotype, accumulation of red fluorescence in the nucleus.

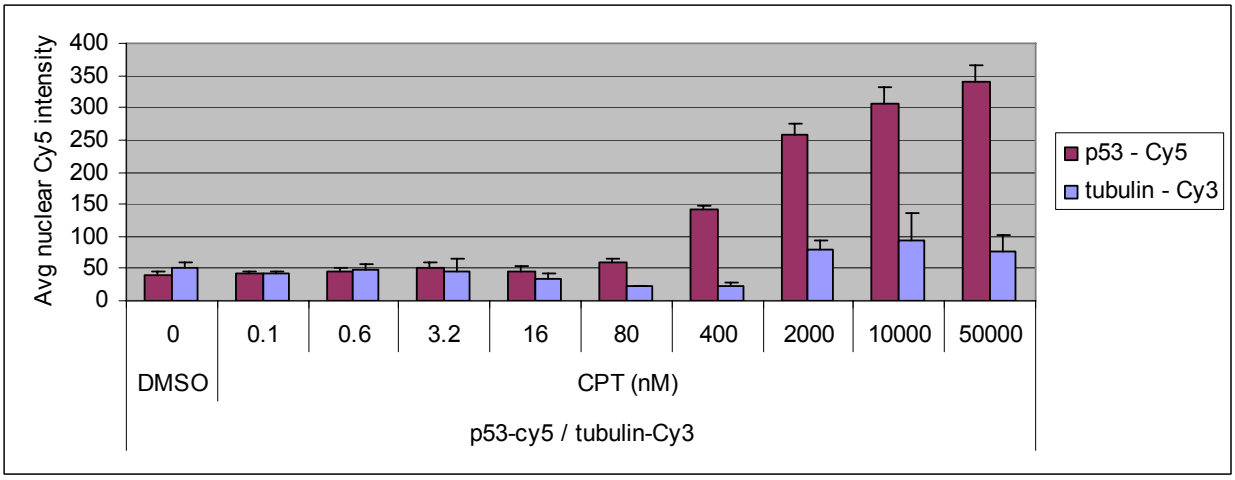

Figure 39. Average florescent intensity in A549 cells after treatment with camptothecin (CPT).
Red bars, the average florescent intensity of Cy5-labled p53 in nucleus; Blue bars, the average florescent intensity of Cy-3 labled tubulin in cells.

The concentration of camptothecin needed to trigger nuclear translocation was first optimized using the ArrayScan system. Different concentrations of camptothecin were added to A549 cells for 24 h and cells were fixed and fluorescently labeled. The ArrayScan was utilized to scan the plate and quantify the p53 nuclear translocation. In this case, the average nuclear Cy5 intensity represents the extent of p53 nuclear accumulation (Figure 39). The results clearly showed that with increasing concentration of camptothecin, more p53 accumulated in the nucleus.

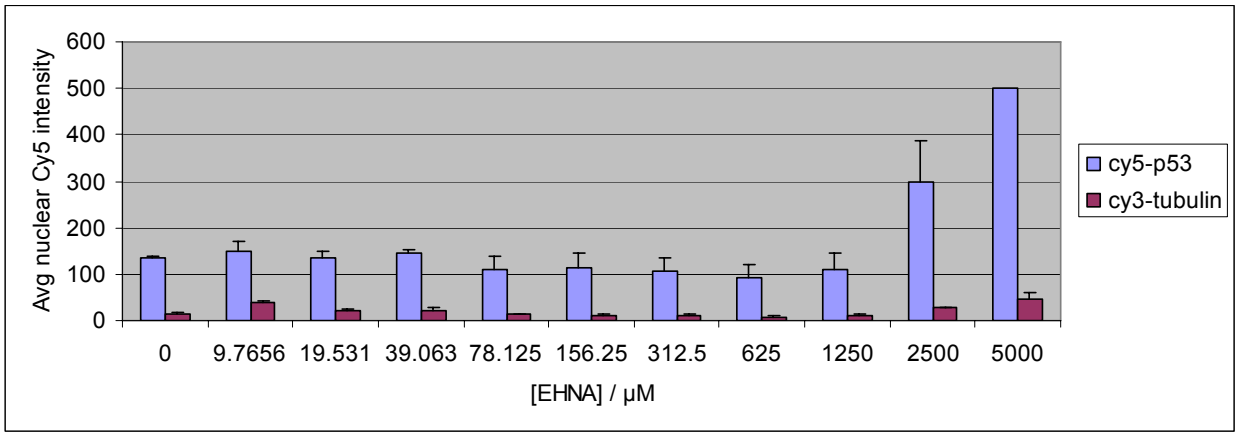

Figure 40. Average florescent intensity in A549 cell upon the treatment of EHNA.

Red bars, the average florescent intensity of Cy5-labled p53 in nucleus; Blue bars, the average florescent intensity of Cy-3 labled tubulin in cells.

EHNA was included in the next experiments to investigate its inhibitory effects on p53 nuclear translocation. Different concentrations of EHNA (starting from 5mM) were added to A549 cells for 24 h (Figure 40). There was a slight decrease of p53 nuclear intensity when the concentration of EHNA was present in the range of 9.77μM to 1.25mM. However, the p53 nuclear intensities were significantly higher when the EHNA concentrations were 2.5mM and 5mM. Part of the reason for this is the toxicity of EHNA. At the higher concentrations of EHNA, most of cells rounded up and went into apoptosis, which could cause the increase of nuclear fluorescence intensity. This is supported in part by the very lower number of cells that ArrayScan captured for analysis in these cases (i.e., the cell number decreased).

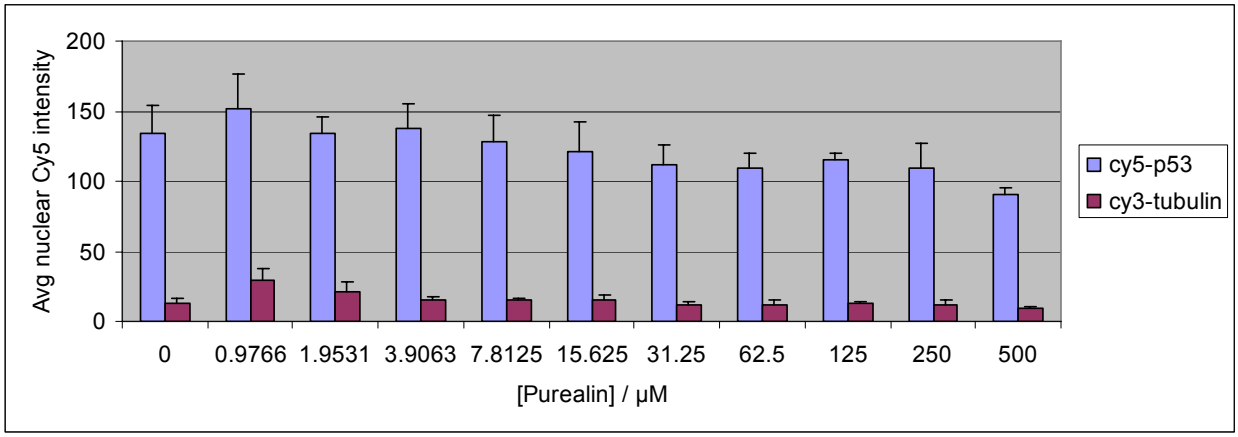

Figure 41. Average florescent intensity in A549 cells after treatment with purealin.
Red bars, the average florescent intensity of Cy5-labled p53 in nucleus; Blue bars, the average florescent intensity of Cy-3 labled tubulin in cells.

Finally, the effect of purealin on camptothecin-induced p53 nuclear translocation was studied. Different concentrations of purealin (from 0.98μM to 500μM) along with 2μM camptothecin were added to A549 cells before fixing and immunostaining (Figure 41). Purealin

showed a weak concentration-dependent inhibitory effect on camptothecin-stimulated p53 nuclear translocation. This ArrayScan-determined result obtained was consistent with the previous one in which the manual immunostaining and human-based fluorescence scoring was used (Figure 37).

3.6 siRNA-based knockdown of dynein heavy chain

RNA interference (RNAi) is the process of using specific sequences of double stranded RNA (dsRNA) to knock down the expression levels of complementary genes. RNAi technology has become a modern tool for the cell biological study of specific protein functions. The RNAi pioneers, Andrew Z. Fire and Craig C. Mello, were awarded the Nobel Prize in Physiology or Medicine in 2006 "for their discovery of RNA interference - gene silencing by double-stranded RNA"[90]. Here the intention was to use dynein heavy chain siRNA to knock down dynein heavy chain levels, which could potentially serve as a positive control in the evaluation of dynein inhibitors.

Table 6. Dynein heavy chain siRNA sequences.

	Sense (5'->3')	**Antisense (5'->3')**
siRNA 1	CGUACUCCCGUGAUUGAUGtt	CAUCAAUCACGGGAGUACGtt
siRNA 2	GCAAAAUAUUGAAAUUCCGtt	CGGAAUUUCAAUAUUUUGCtg
siRNA 3	GCCAAAAGUUACAGACUUUtt	AAAGUCUGUAACUUUUGGCtt

Dynein heavy chain siRNAs 1, 2, 3 were obtained from Ambion, Inc (Table 6). A negative control siRNA was also obtained, which was a 19 base pair (bp) scrambled sequence with 3' dT overhangs and a sequence with no significant homology to any known gene sequences from mouse, rat or human. The transfection procedure used is described in Chapter 2. In short, A549 lung cancer cells were plated in RPMI 1640 medium without antibiotics in 6-well plates. Oligonucleotide-Oligofectamine^{TM} complex in Opti-MEM I reduced serum medium were prepared according to the manufacturer's instructions. The complex was added to cells and incubated at 37 ºC for 4 h. Opti-MEM medium with three times the normal concentration of serum and without antibiotics was added, and the cells were incubated for 48 h. Cells were then detached with trypsin, pelleted by centrifugation and resuspended in a lysing buffer. Cell extracts were separated by 6.5% SDS-PAGE in Tris-glycine-SDS buffer for 8 h. Western blotting analysis was performed with rabbit anti-dynein heavy chain antibody and mouse anti-dynein intermediate chain antibody. Band intensities were measured with ImageJ software.

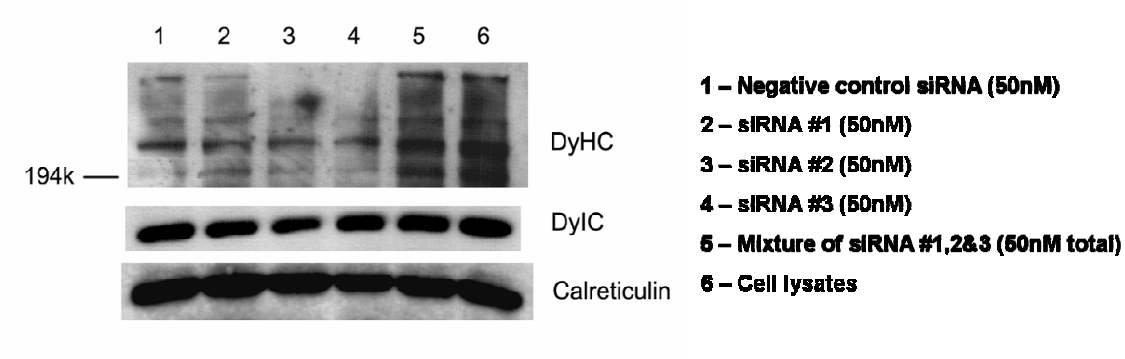

	Band Intensity			Ratio		% of Inhibition	
Intensity	DyHC	DyIC	Calreticulin	DyHC/Cal	DyIC/Cal	DyHC	DyIC
Negetive Control	3822	14136	20187	0.27	0.70	0.00	0.00
siRNA #1	2524	10929	19403	0.23	0.56	14.58	19.56
siRNA #2	2234	9162	18842	0.24	0.49	9.82	30.56
siRNA #3	1721	10229	15061	0.17	0.68	37.77	3.01
Mixture	1639	11092	16224	0.15	0.68	45.35	2.37

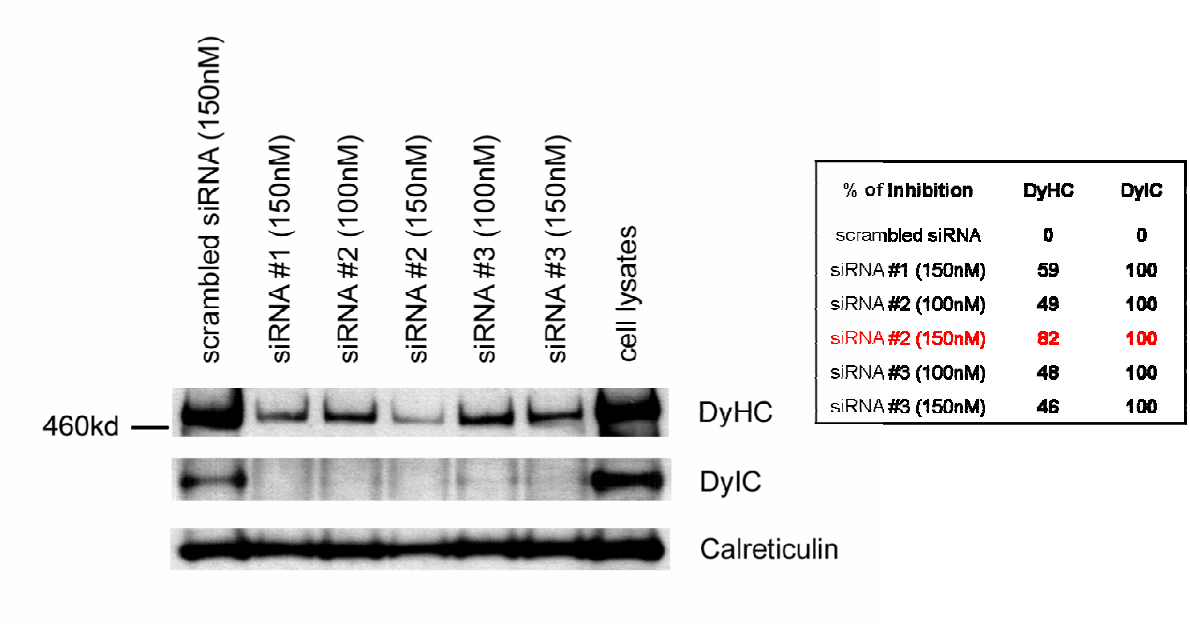

% of Inhibition	DyHC	DyIC
scrambled siRNA	0	0
siRNA #1 (150nM)	59	100
siRNA #2 (100nM)	49	100
siRNA #2 (150nM)	82	100
siRNA #3 (100nM)	48	100
siRNA #3 (150nM)	46	100

Figure 42. siRNA knockdown of dynein heavy chain.

A final concentration of 50nM negative siRNA or siRNAs 1, 2 or 3, as well as the 1:1:1 mixture of siRNA 1, 2 and 3 giving a sum of 50nM, were transfected into A549 cells for 48 h. The results showed that 50nM of the individual siRNAs 1, 2, 3, as well as the mixture of the

three inhibited the dynein heavy chain expression level by 15%, 10%, 38% and 45%, respectively (Figure 42). It seemed that 50nM siRNA with 48 h of transfection time was not enough to totally knock down the dynein heavy chain level. Therefore, higher amounts of siRNA with longer transfection times were tried. siRNA 1 (150nM), 100nM and 150nM siRNA 2, and 100nM and 150nM siRNA 3 were examined with a transfection time of 72 h. The results illustrated that these concentrations of siRNAs after the prolonged time of exposure dramatically knocked down the level of dynein intermediate chain. siRNA 2 at 150nM generated an 82% decrease of the level of dynein heavy chain (Figure 42). Thus, siRNA 2 was used at 150nM for 72 h as a potential positive control in the cell-based p53 nuclear translocation assay.

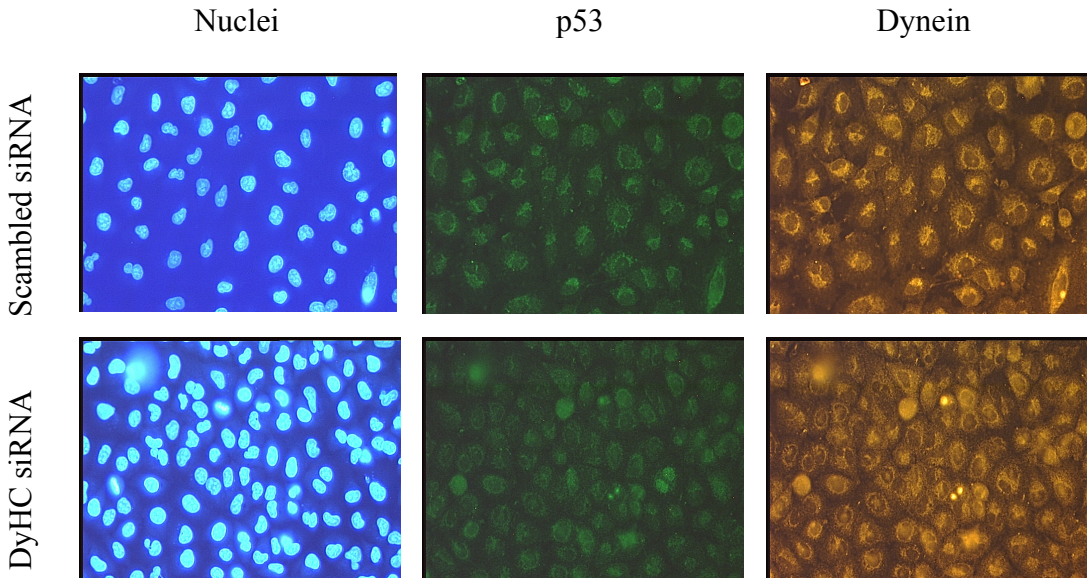

Figure 43. Immunostaining of nuclei, p53 and dynein heavy chain in A549 cells uppn treatment of scrambled siRNA or DyHC siRNA.
A549 cells were transfected with a final concentration of 150nM scrambled siRNA or 150nM DyHC siRNA 2 for 72 hrs. Rabbit DyHC antibody and Alexa 555 anti-rabbit antibody were used for immonustaining of dynein heavy chain. Mouse p53 and Alexa 488 anti-mouse antibody were used for immonustaining of p53.

However, it seems that siRNA did not knock down the dynein activity in cells (Figure 43). Therefore, it seems likely that the lifetime of cytoplasmic dynein in cells is too long for the siRNA approach to be useful in a screening protocol.

3.7 Discussion

Dynein plays an important role in variety of cellular processes. Recent work is beginning to uncover the mechanism of dynein movement and its power stroke[22, 71, 91]. A variety of molecules involved in cell growth control, including p53, Bim, cdc2 kinase, HDAC6, Hsp70 and Hsp90 have also been reported to interact with or be under control of cytoplasmic dynein[23, 24, 29, 30, 92]. Motor activity and motor-cargo interactions in dynein and other motor proteins, such as kinesin and myosin, might represent attractive drug targets and are certainly of interest in the development of chemical biology tools. Recently, RNA interference technology has been applied against dynein as well as its regulatory polypeptides[16, 93-96], showing that lowering the level of the cytoplasmic dynein heavy chain (and therefore its activity in bulk) leads to a block in mitosis[16]. Effective small molecule dynein inhibitors could therefore be useful for further investigation of the cellular function of dynein *in vivo*.

Very little is known, however, about the structural requirements needed for small molecules to inhibit dynein. Agents that competitively inhibit the binding of ATP to the protein are the most studied, and redox active agents will also inhibit the protein. Neither of these seems appropriate for finding a selective agent, as ATP and redox balance are cell-wide requirements. The only non-ATP, non-inorganic and non-redox active agent known to inhibit the axonemal isoform of cytoplasmic dynein is the natural product purealin, which acted as the seminal lead in these studies. The results showed that synthetic purealin and two of its analogues inhibit MT-

stimulated cytosolic dynein heavy chain's ability to hydrolyze ATP. Thus, the purealins might be useful for further physiological investigation of dynein function.

Kon and coworkers[97] showed that ATP binding and its hydrolysis only at the P1 site of dynein heavy chain are essential for the motor activities of cytoplasmic dynein, and suggested that the motor activities are also regulated by the other nucleotide-binding/hydrolysis sites. For example, nucleotide binding at the P3 site is also critical for MT-activated ATPase and motility activities of cytoplasmic dynein. It is known that purealin inhibits the ATPase activity of axonemal dynein but does not compete for the ATP binding site, whereas little is known about the kinetic properties of cytoplasmic dynein inhibitors. The kinetics of inhibitors in the cytoplasmic dynein motor domain ATPase assay were examined here. Plotting of the data in the Hanes-Woolf format showed no significant change in the y-intercept, which represents the value of K_m/V_{max}, in the presence of purealin, purealidin A and *para*/chlorophenyl/H-purealidin A**.** This indicates that the binding pattern of the purealins is uncompetitive, meaning the inhibitors bind to a site that becomes available only after the ATP has bound to the P1 site, giving rise to the conclusion that purealins do not compete for the binding of ATP nor with its hydrolysis at the P1 site. The binding site of purealins is still unknown.

Although purealin and purealidin A were inactive as human cancer cell antiproliferative agents, their inhibition of cytoplasmic dynein ATPase activity supports the hypothesis that purealin/purealidin and analogs are good leads for finding small molecules to inhibit this target. *para*/chlorophenyl/H-purealidin A showed reasonable antiproliferative activity against human carcinoma cell lines as well as against a mouse leukemia cell line, and inhibited dynein motor domain ATPase activity, providing correlative support of the hypothesis that small molecule inhibitors of the molecular motor can have antiproliferative effects. Compared to the effects on human cancer cell lines, the growth of the mouse leukemia L1210 cell line was uniformly sensitive to low micromolar concentrations of the purealin/purealidin library components. Since purealin has very weak inhibitory effects against p53 nuclear translocation assay and failed the

antiproliferation assay, there remained a need to search for more potent, cell-permeable and dynein-specific inhibitors.

4.0 DISCOVERY OF NEW SMALL-MOLECULE INHIBITORS OF CYTOPLASMIC DYNEIN BY A PHENOTYPIC SCREEN

4.1 Introduction

In Chapter 3, the biological evaluation of the cytoplasmic dynein ATPase inhibitor purealin and its analogues was given in detail. Although purealin and some of its analogues showed inhibitory effects against the ATPase activity of both bovine cytoplasmic dynein heavy chain and recombinant rat cytoplasmic dynein heavy chain motor domain, purealin showed only weak effect in cellular assays. Therefore, the search for new dynein inhibitors shifted to a chemical biology approach. Since it is known that the overexpression of dynamitin inhibits ligand-dependent movement of the glucocorticoid receptor (GR) to the nucleus, chemical inhibition of dynein movement will also lead to inhibition of GR translocation into the nucleus. Therefore, a phenotypic cell-based assay was established to screen compounds that block the hormone-stimulated GR nuclear uptake as putative dynein inhibitors.

4.2 Chemical Libraries for screening

A small (110-member) but structurally rich library synthetic library of compounds was obtained from University of Pittsburgh Center for Methodologies and Library Development

(UPCMLD). The compounds were chosen as a representative of a larger library with considerable scaffold and physicochemical property variability. The library members included tricyclic pyrroles, cyclopropyl(phenyl)alkylamides, cyclopentapyridines, quinolines/naphthoquinones, pyrimidinones and dihydropyrroles whose syntheses have been reported before[27, 67, 98-101] (Figure 44).

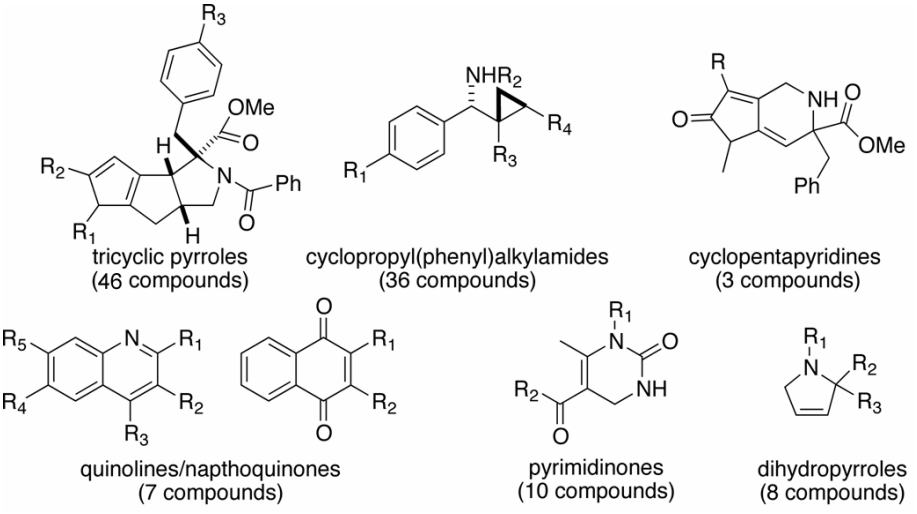

Figure 44. Structural classes within the UPCMLD initial discovery library.

4.3 GFP-GR nuclear translocation screening results

4.3.1 Inhibitory effect of EHNA on GFP-GR nuclear translocation

In the GFP-GR nuclear translocation assay, a mouse mammary adenocarcinoma cell line (3617.4) stably expressing GFP-rat GR[69] was used to illustrate the inhibition of nuclear translocation by dynein inhibitors. Treatment with a high concentration of EHNA blocked GFP-GR nunclear translocation (Figure 3). GFP-GR expression in this cell line is under control of the "Tet-Off" inducible system. Cells were grown in DMEM supplemented with 10% FBS and 10

μg/mL tetracycline. Cells were routinely maintained in an incubator at 37 ºC, 5% CO_2. At the time of transfer to test slides or 96-well plates, the medium was replaced with DMEM with 10% FCS without tetracycline to induce GFP-GR. Cells were then treated with test agents for 24 h. Receptor translocation was induced by adding 1μM dexamethasone (vehicle was ethanol) for 15 min. The medium

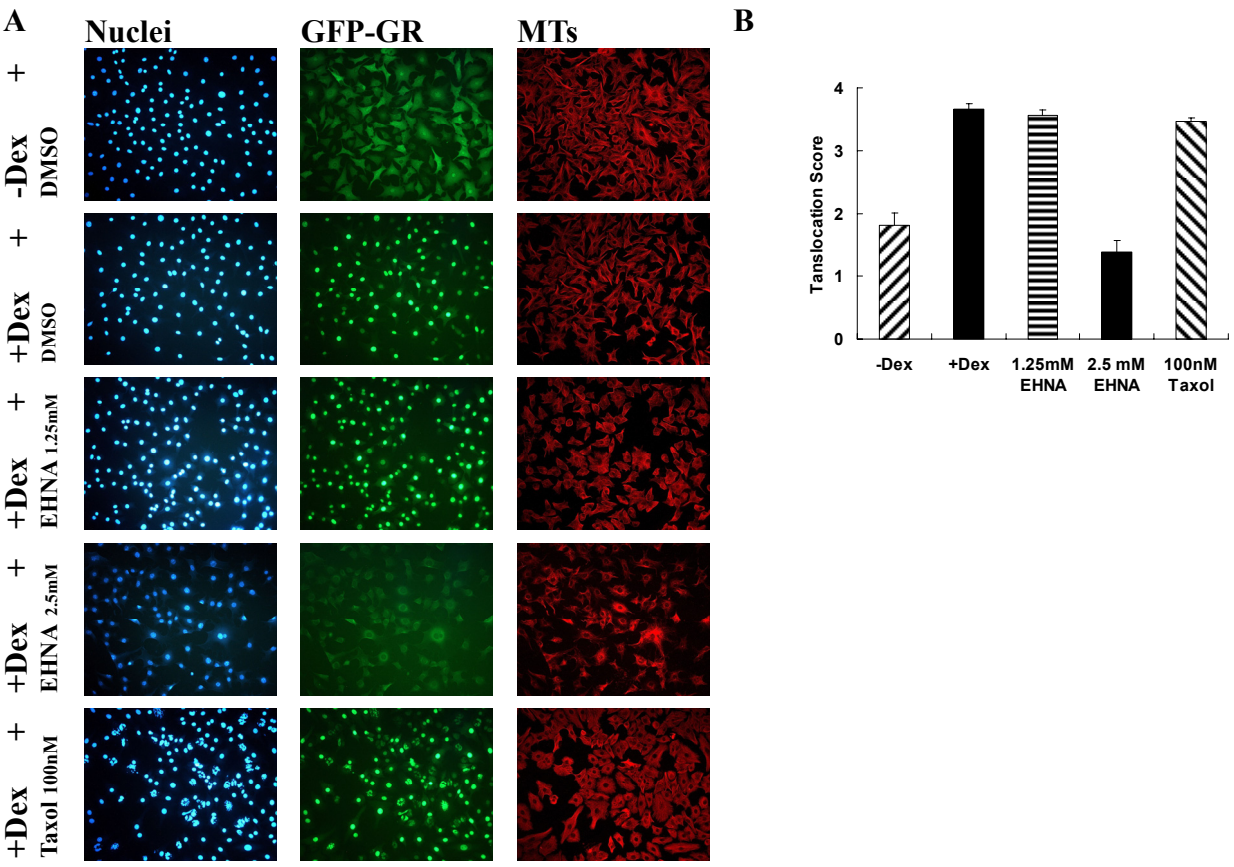

Figure 45. EHNA blocks GFP-GR nuclear translocation.
(A) Mouse mammary adenocarcinoma cells (3617.4) stably expressing GFP-rat GR were incubated with vehicle (DMSO) or drugs for 24 h. Cells were then treated for 15 min in the absence (-Dex) of presence (+Dex) of dexamethasone. (B) The bar graph presents the nuclear translocation scores in each condition.

was then removed and cells were washed three times with phosphate buffered saline (PBS). Cells were fixed and permeabilized by immersion in cold methanol (–20 ºC) for 20 min. Mouse anti-α-

tubulin (NeoMarkers), Cy3 donkey anti-mouse (Jackson ImmunoResearch) and Hoechst 33342 were then used to fluorescently label microtubules and the nucleus. Cells were photographed with a Leica DC300F fluorescent microscope and scored for GFP-GR translocation as described above. After treatment with 2.5mM EHNA for 24h, hormone-stimulated GFP-GR nuclear translocation was significantly blocked (Figure 45). EHNA also showed a time-dependent inhibitory effect on the GFP-GR nuclear translocation (Figure 46).

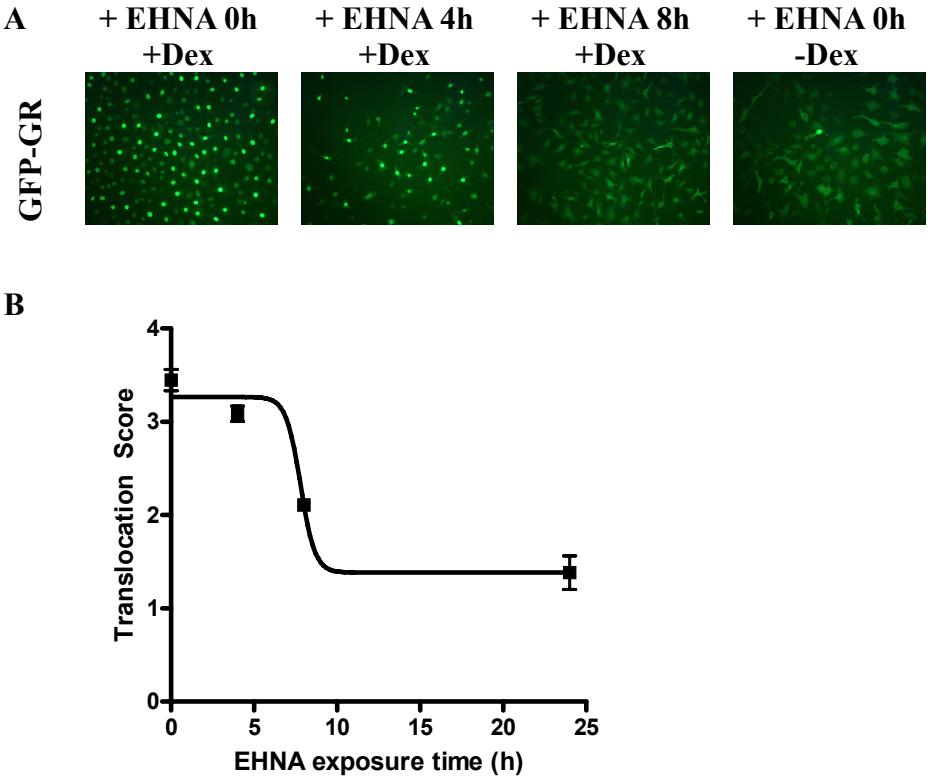

Figure 46. Time-dependent inhibitory effect of 2.5mM EHNA against GFP-GR nuclear translocation.
(A) Mouse mammary adenocarcinoma cells (3617.4) stably expressing GFP-rat GR were incubated with vehicle (DMSO) or EHNA for 0, 4 or 8 h. Cells were then treated for 15 min in the absence (-Dex) of presence (+Dex) of dexamethasone. (B) The graph presents the nuclear translocation scores in each condition.

4.3.2 Inhibition by purealin of GFP-GR nuclear translocation

Purealin was also tested in the GFP-GR nuclear translocation assay. It showed a weak inhibitory effect against GFP-GR nuclear translocation (Figure 47).

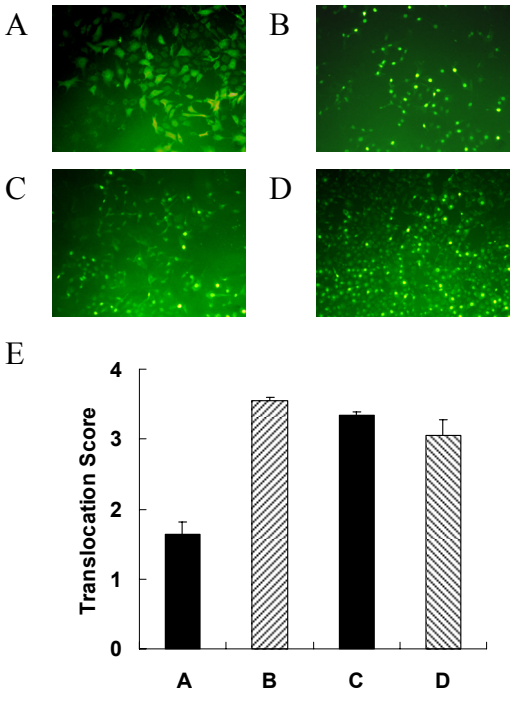

Figure 47. Purealin inhibition effect of GFP-GR nuclear translocation.
Mouse mammary adenocarcinoma cells (3617.4) stably expressing GFR-rat GR were incubated with 1% DMSO (A, B) , 100 μM purealin (C) or 10 μM geldanamycin (D) for 24 h. Cells were then treated for 15 min in the absence (A) of presence (B-D) of dexamethasone. The bar graph (E) presents the nuclear translocation scores in each condition.

4.3.3 Inhibitory effect of the UPCMLD library compounds on GFP-GR nuclear translocation

The UPCMLD library described above was screened to identify any compounds that might block GFP-GR nuclear translocation. Cells were pretreated with library compounds or vehicle (DMSO) for 8 h or 24 h prior to dexamethasone (DEX) addition. After incubation with DEX, the cells were fixed and stained with Hoechst 33342. Cells were then photographed with a Leica DC300F fluorescent microscope or an Olympus IX70 inverted microscope. Cells within images were then scored for GFP-GR nuclear translocation as described in Chapter 2.

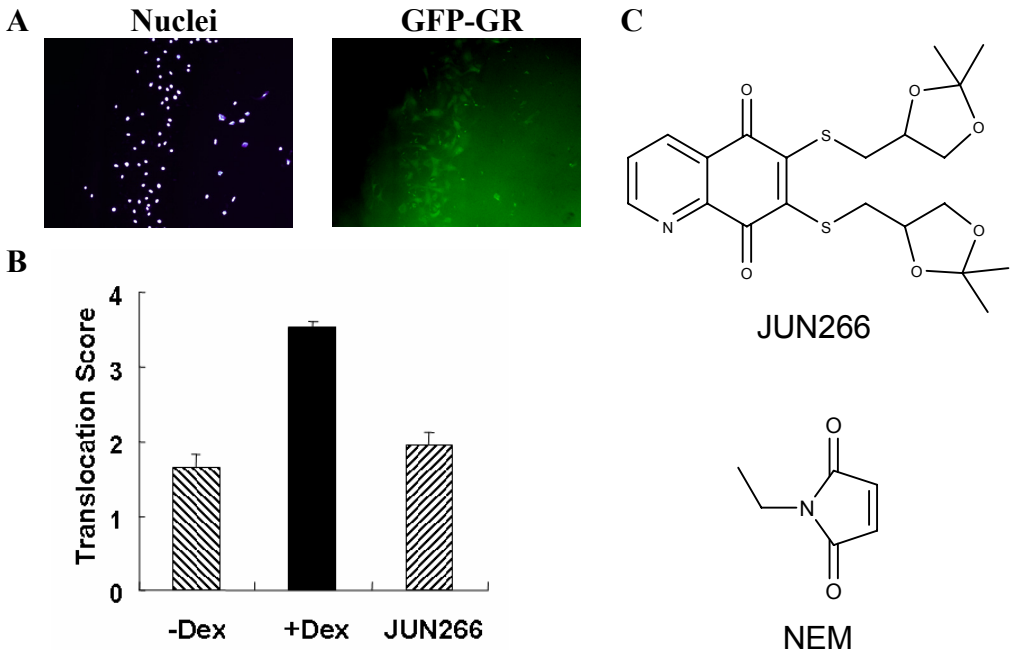

Figure 48. GFP-GR nuclear translocation inhibitory effect of JUN266.
(A) Example picture of Hoechst-stained nuclei and GFP-GR in 3617.4 cells upon the treatment of JUN266; (B) Translocation score of the negative control (-DEX), positive control (+DEX) as well as JUN266; (C) Chemical structure of JUN266 and its analogue, NEM.

One of the compounds within the UPCMLD library, JUN266, showed an inhibitory effect against GFP-GR nuclear translocation (Figure 48). However, the structure of the compound provided some reasons to avoid pursuit of this hit. One is the toxicity of the compound. Upon the treatment of JUN266, it seemed that the cells failed to respond to hormone stimulation due to the fact that the cells seemed to have entered into JUN266-induced apoptosis, as could be seen from the morphology their nuclei presented (Figure 48A). Most of the nuclei shrank in response to JUN266. Another reason not to pursue this compound is the questionable specificity it might provide. JUN266 is a quinone and, like *N*-ethylmaleimide (NEM), is likely a sulfhydryl-reactive reagent. JUN266 could therefore block the GFP-GR nuclear translocation by some some non-

specific redox reactions with, e.g., other ATPases or kinases. Therefore, JUN266 was not pursued in this context.

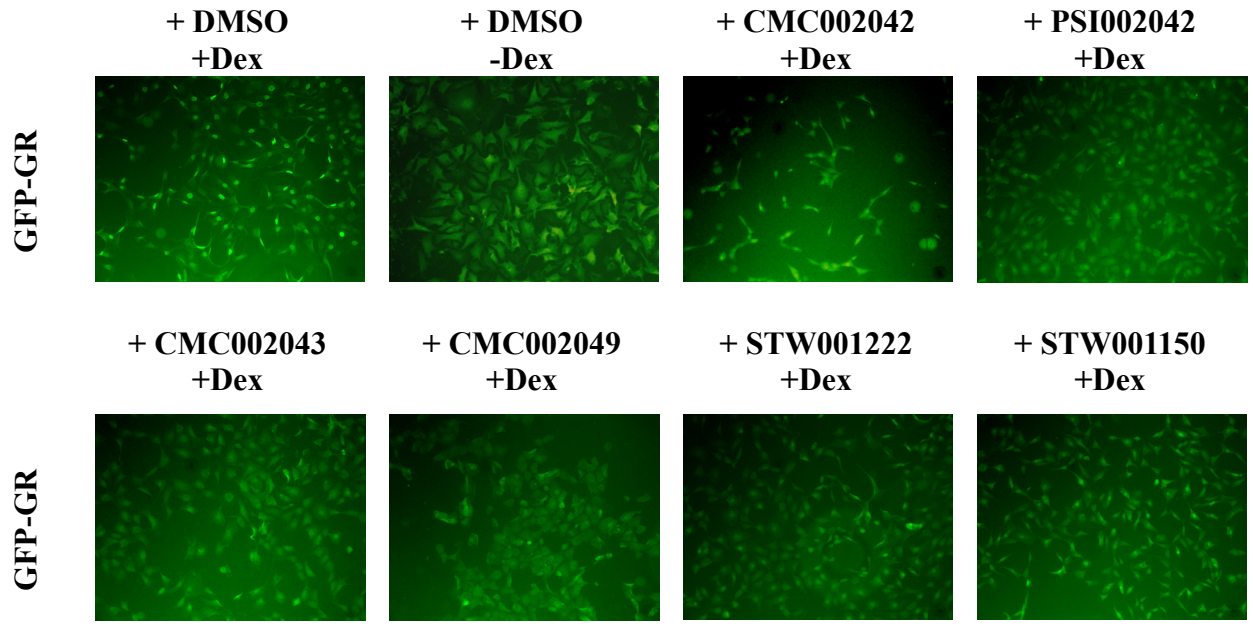

Figure 49. GFP-GR nuclear translocation inhibitory activity of the UPCMLD compounds. GFP-GR nuclear translocation inhibitory activity of library compounds CMC002042, PSI002042, PSI002043, PSI002049, STW001222 and STW001150. Mouse adenocarcinoma 3617.4 cells expressing GFP-GR were pretreated with different compounds or vehicle (DMSO) and then incubated with dexamethasone (+DEX) or vehicle (ethanol, –DEX).

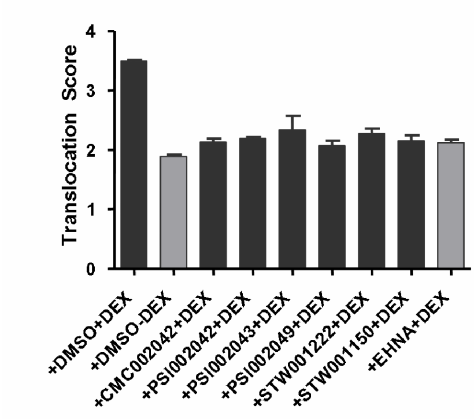

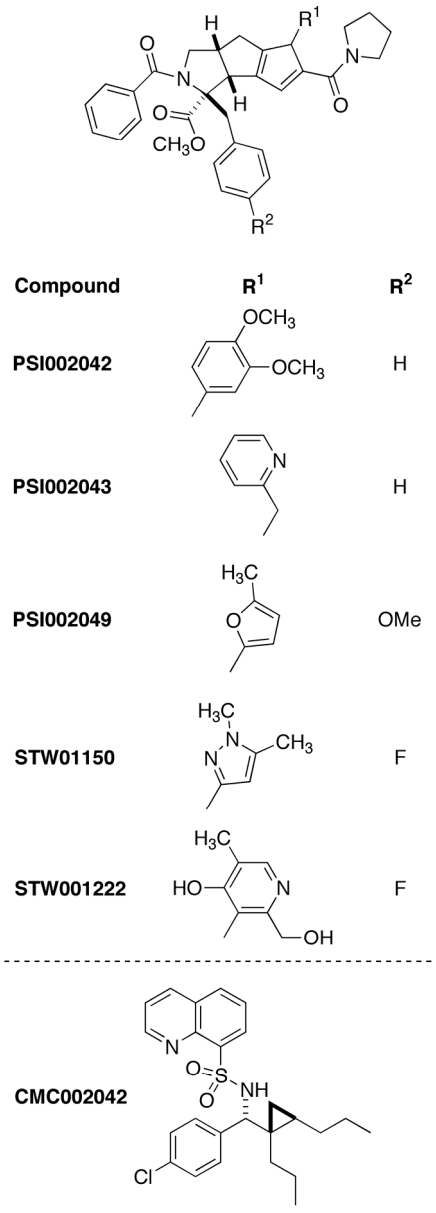

Figure 50. The nuclear translocation scores of the active UPCMLD compounds (left) and chemical structures of the compounds (right).

Six of the library compounds inhibited dexamethasone-stimulated GFP-GR nuclear translocation (Figure 49) without perturbing cellular microtubule arrays. Results of quantitative analysis of the GFP-GR nuclear translocation and the chemical structures of the compounds that inhibited GFP-GR nuclear translocation are shown in Figures 50. EHNA was used as a positive

control and it blocked GFP-GR nuclear translocation when present at 2.5mM (Figure 45). Geldanamycin (GA), a known Hsp90 inhibitor, also served as a positive control (Figure 47D), giving results similiar with an earlier report[102].

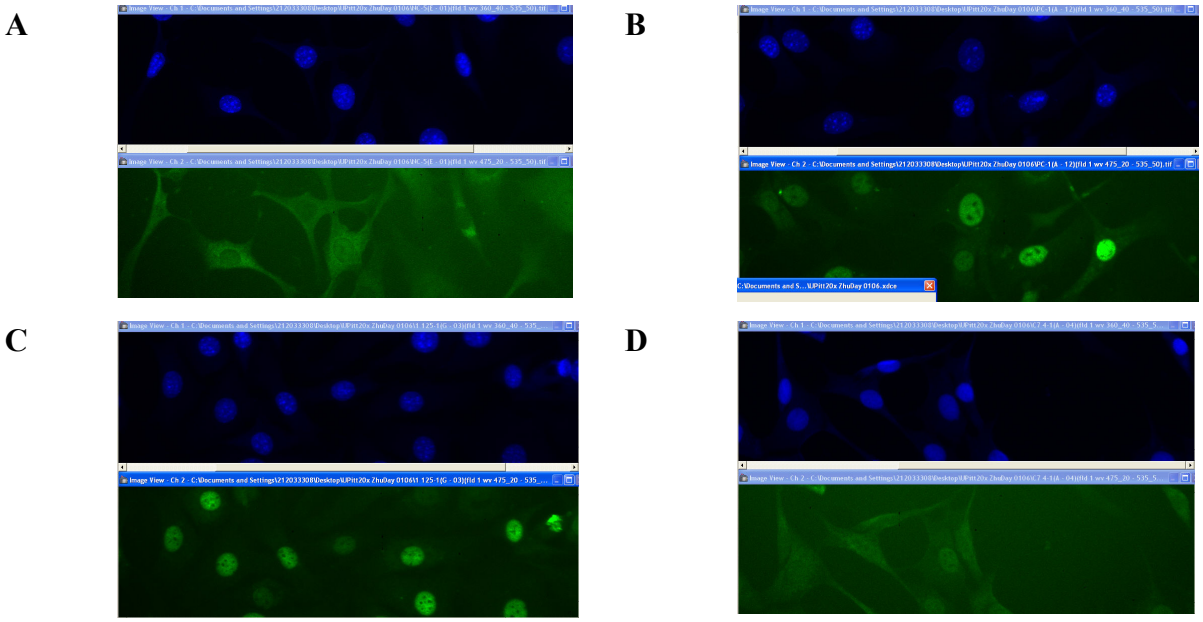

Figure 51. Representative images of GFP-GR nuclear translocation assay by IN Cell Analyzer 1000 system.
3617.4 cells expressing GFP-GR (green, lower panel in each figure) and stained with Hoechst 33342 (blue, upper panel in each figure). (A) –DEX (negative control); (B) +DEX (positive control); (C) 125μM purealin + DEX; (D) 4μM CMC002042 + DEX.

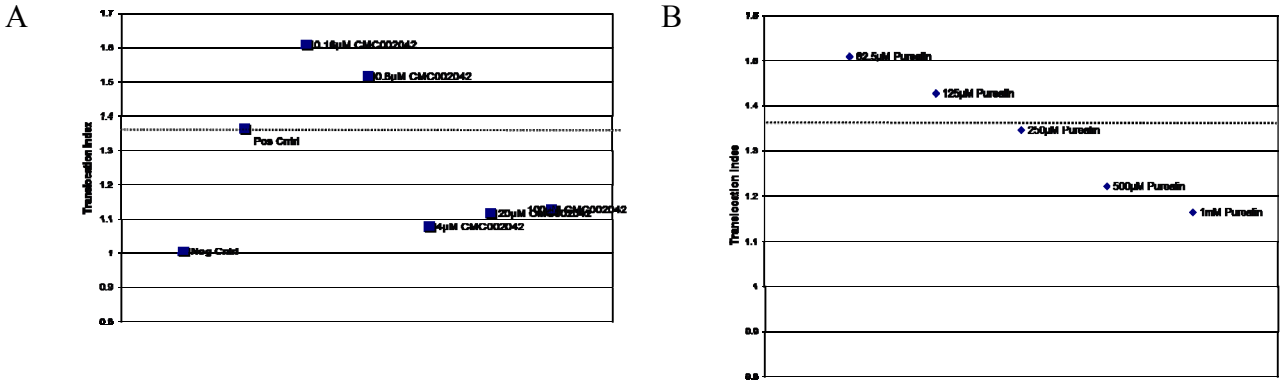

C

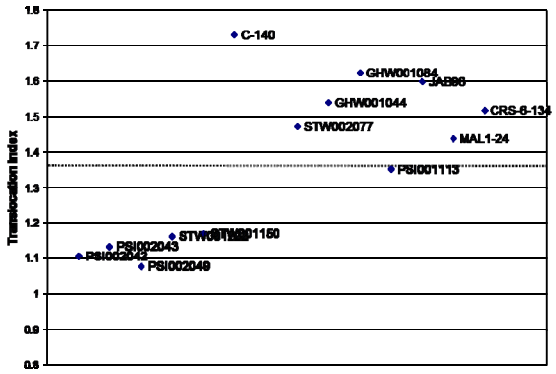

Figure 52. Quantification of GFP-GR nuclear translocation assay by IN Cell Analyzer 1000. (A) Concentration dependent inhibitory effect of 0.16, 0.8, 4, 20, 100μM CMC002042 (C7) on 3617.4 GFP-GR nuclear translocation; (B) Concentration dependent inhibitory effect of 62.5, 125, 250, 500 and 1000μM purealin (CMPD 1) on 3617.4 GFP-GR nuclear translocation; (C) Inhibitory effects of compounds PSI002042, PSI002043, PSI002049, STW001222 and STW001150.

With the help of Drs. Dwayne W. Dexter and Ann del Campo at GE Healthcare Inc., the GFP-GR nuclear translocation assay results were further analyzed by the IN Cell Analyzer 1000 system. A translocation index was automatically obtained for quantification of GFP-GR nuclear accumulation. Figure 51 shows representative images obtained from the IN Cell Analyzer 1000 system. Compound CMC002042 showed a concentration-dependent inhibitory effect against DEX-stimulated GFP-GR nuclear translocation (Figure 52A). Purealin also showed a weak inhibitory effect against GFP-GR nuclear translocation in a concentration-dependent pattern (Figure 52B). The IN Cell Analyzer 1000 system also helped to further confirm earlier findings that compounds PSI002042, PSI002043, PSI002049, STW001222 and STW001150 inhibit hormone-stimulated GFP-GR nuclear translocation in 3617.4 cells (Figure 52C).

4.4 *in vitro* GR binding assay results

The possibility that the compounds active as inhibitors of GFP-GR nuclear translocation were targeting GR directly needed to be ruled out. For example, hormone-dependent GFP-GR nuclear uptake would be prevented if hormone binding to GR was being inhibited. A GR competitor assay was therefore performed in which the compounds were tested for their ability to displace a glucocorticoid agonist from the ligand binding domain of the GR. Recombinant human GR was bound with fluorescently-labeled dexamethasone and then treated with test agents. After 2h, fluorescence polarization (FP) was measured. The fluorescent analogue of dexamethasone when bound to GR protein generates high FP values. The presence of a displacing ligand causes a decrease in the FP. Concentration-dependence curves were constructed. The one-site competition method in GraphPad Prism 4 software was used for constructing concentration–response curves and for calculating IC_{50}'s. Dexamethasone gave an IC_{50} of 0.65 ± 0.01nM, while the test compounds had IC_{50} values above the highest concentration tested (200 μM). Thus, the compounds that blocked GFP-GR nuclear transport are unlikely to affect GR hormone binding (Figure 53).

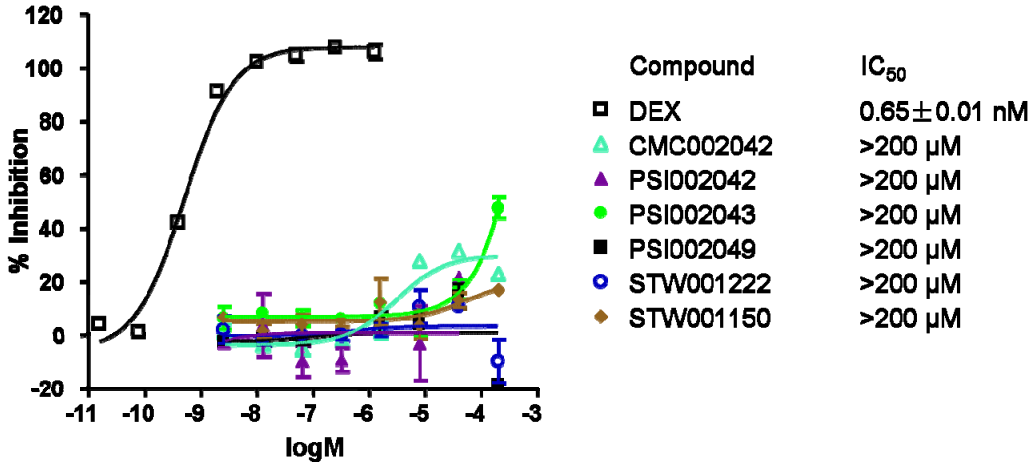

Figure 53. Low potency of the GFP-GR translocation-inhibitory compounds in an *in vitro* GR competition assay as compared to DEX (mean ± SD, N = 4).

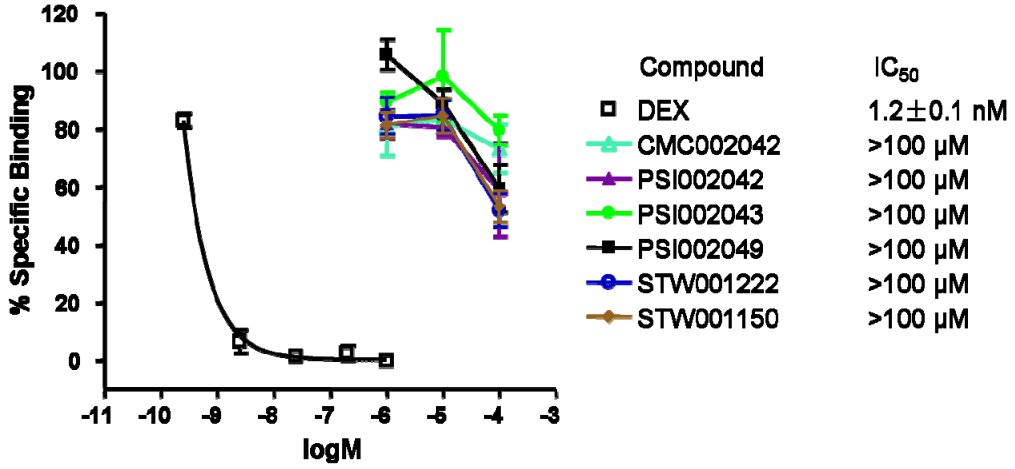

Figure 54. Low potency of the compounds in affecting hormone-specific GR binding as compared to DEX (mean ± SD, N = 2).

Molecular chaperones play an important role in the nuclear translocation of GR. Specifically, a dynein-immunophilin-Hsp90-Hsp70-GR heterocomplex appears to be required for GR nuclear transport[103]. The GR competitor assay does not directly test the GR chaperone complex. If GR binds hormone, the chaperone complex is intact. Therefore, experiments were

performed to determine if the compounds altered the Hsp90-Hsp70-GR heterocomplex. For example, the known Hsp90 ATPase inhibitor geldanamycin (GA) blocks nuclear translocation of the GR by breaking the dynamic cycle of heterocomplex assembly/disassembly, which leads to Hsp90 degradation via the ubiquitin/proteasome pathway[73]. In order to corroborate the GR competitor assay, an *in vitro* hormone binding assay with [^{3}H]dexamethasone was performed using cytosol isolated from untreated 3617.4 cells. A GR ligand in this assay will displace [^{3}H]dexamethasone and decrease the specific binding. Dexamethasone gave an IC_{50} of 1.2 ± 0.1nM, which is in the same range as found in the GR competitor assay. The GFP-GR translocation-inhibitory library compounds registered IC_{50} values greater than the highest concentration used (100μM) (Figure 54). This result further indicated that the compounds were neither GR ligands nor affected GR hormone binding. Furthermore, the results suggest that the compounds do not disrupt the GR heterocomplex containing various chaperones and co-chaperones.

4.5 Inhibition of dynein motor domain ATPase

In order to ascertain if the compounds directly affected the desired target, a recombinant form of the full motor domain of rat cytoplasmic dynein heavy chain[71] was used to test whether the compounds inhibit the protein's basal ATPase activity. The compounds that inhibited the GFP-GR nuclear translocation were first mixed with recombinant rat cytoplasmic dynein motor domain and the protein's basal ATPase activity was assessed. Concentration-dependent experiments showed PSI002049 to have an IC_{50} value of 2.0±0.2μM. Four other compounds, PSI002043, STW001222, PSI002042 and CMC002042, had weaker concentration-dependent

inhibitory effects on the basal ATPase activity of dynein motor domain (Figure 55).

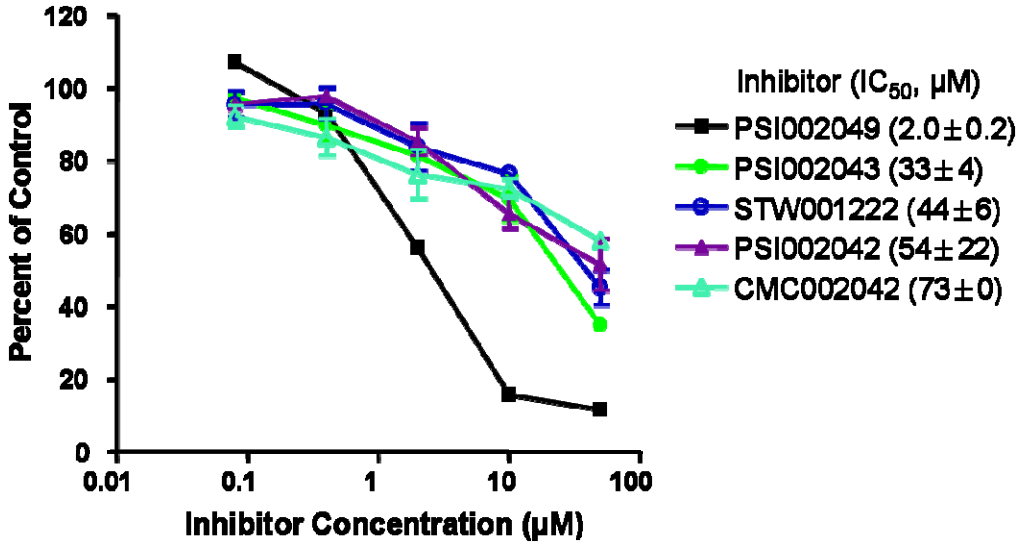

Figure 55. Inhibitory activities of UMCMLD compounds against recombinant dynein heavy chain motor domain.
The reaction was initiated by addition of 2 mM ATP in the presence of the indicated concentration of the compounds (mean±SD, N=4).

4.6 Kinetics study on the new dynein inhibitors

The inhibitory ability of the new dynein inhibitors was further studied. First, different concentrations of cytoplasmic dynein motor domain were used to determine the concentration-dependent inhibition by PSI002049 of phosphate release (Figure 56). To investigate the inhibitor's effects on enzyme kinetics, different concentrations of PSI002049 (0, 2, 10, 50 μM) were each incubated with different concentrations of the substrate, ATP, to determine the Michaelis-Menten parameters of the dynein motor domain (Figure 57; calculated V^{app}_{max}, K^{app}_{M} and K_i values are given in Table 7). These results further show the inhibitory effects of compound PSI002049 on the dynein motor domain ATPase activity. An examination of the kinetics in the Hanes-Woolf format (Figure 57, right), wherein no significant change in the y-

intercept was noted, indicated that the compound displayed uncompetitive inhibition, giving rise to the conclusion that the PSI002049 does not bind to the ATP site. The kinetics of inhibition by CMC002042, PSI002042, STW001222 and PSI002043 were also examined (Figure 58; Table 8) and revealed the uncompetitive inhibition of basal ATPase activity of the dynein motor domain. Finally, STW001222, PSI002043 and PSI002049 inhibited microtubule-stimulated dynein motor domain ATPase in an uncompetitive pattern (Figure 59; Table 9).

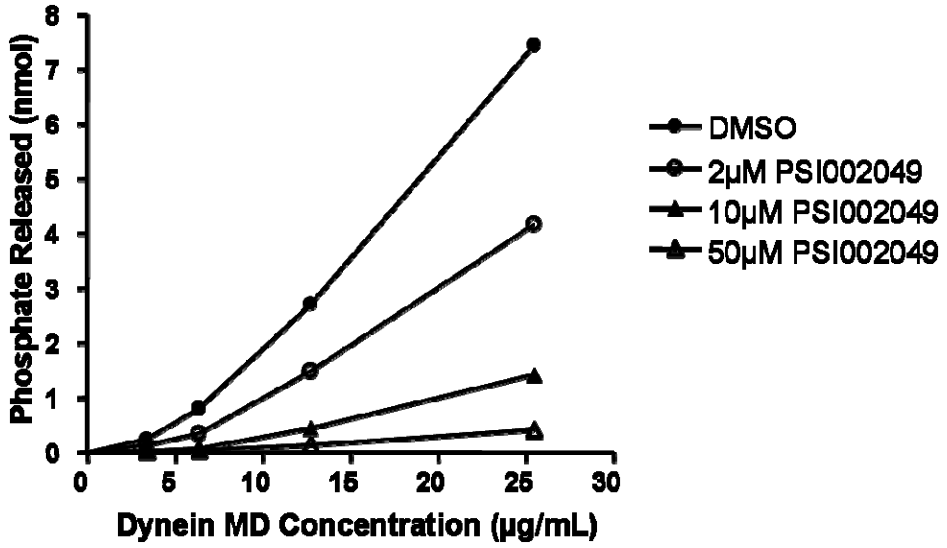

Figure 56. Inhibition by PSI002049 of recombinant rat cytoplasmic dynein heavy chain motor domain-catalyzed release of free phosphate from ATP.
Dynein motor domain was mixed with the test agent. ATP (2 mM) was added to initiate the reaction and the concentration of free phosphate was determined after incubation at 37 ^{o}C for 0.5 h. Each point is the mean of four determinations ± SD (some of the error bars are smaller than the symbols used).

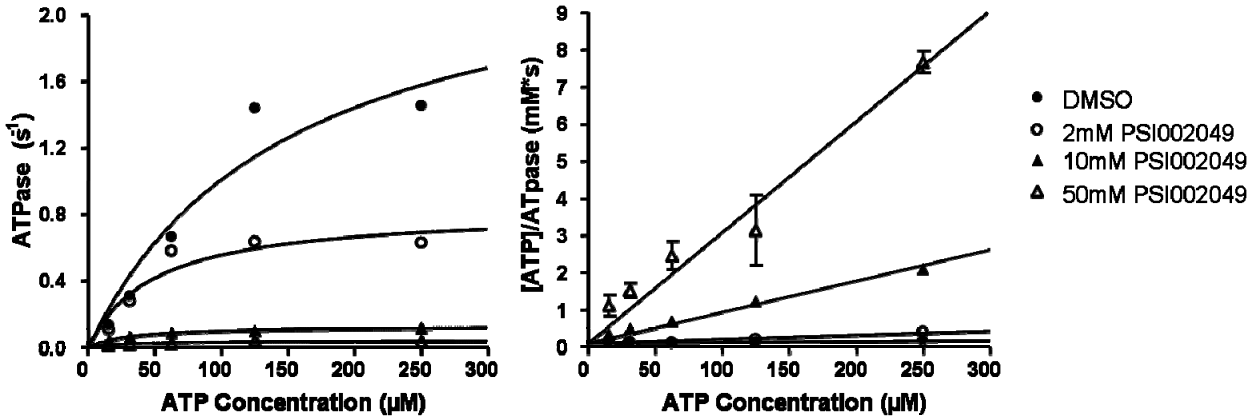

Figure 57. Michaelis-Menten (*left*) and Hanes-Woolf (*right*) plots of basal dynein motor domain ATPase activity in the presence of different concentrations of PSI002049. The reaction was initiated with different concentrations of ATP in the presence of 21.25 μg/mL recombinant dynein heavy chain.

Table 7. The V^{app}_{max}, K^{app}_{M} and K_i values of the ATPase activity of recombinant cytoplasmic dynein heavy chain motor domain in the presence of 2, 10 and 50 μM PSI002049.

[PSI002049] (μM)	V^{app}_{max} (s^{-1})	K^{app}_{M} (μM)	K_i (μM)
0	2.52	150	0.82
2	0.83	49	
10	0.13	32	
50	0.04	29	

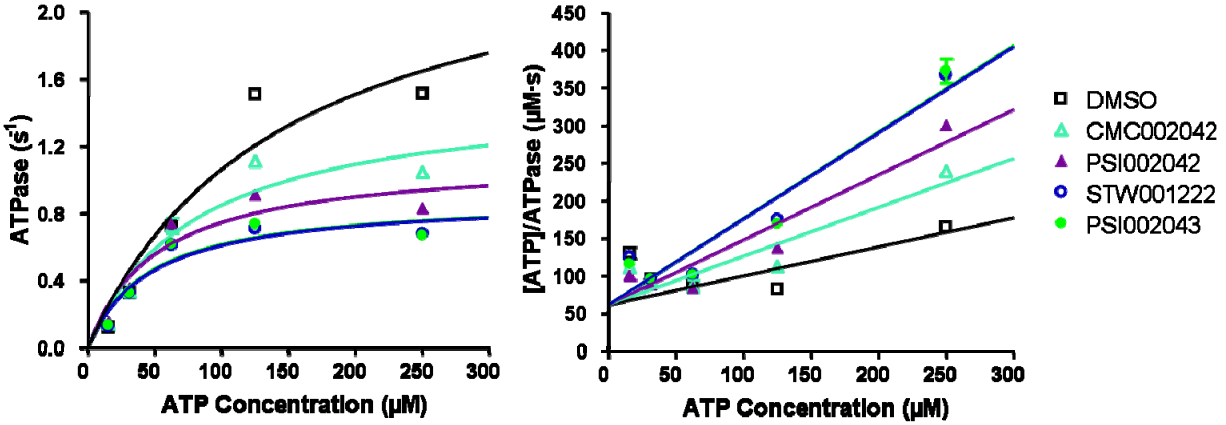

Figure 58. Michaelis-Menten (left) and Hane-Woolf (right) plots of basal dynein motor domain ATPase activity in the presence of 50µM CMC002042, PSI002042, STW001222 and PSI002043.
The reaction was initiated with different concentrations of ATP in the presence of 21.25 µg/mL recombinant dynein heavy chain.

Table 8. The V^{app}_{max}, K^{app}_{M} and K_i values of the ATPase activity of recombinant cytoplasmic dynein heavy chain motor domain in the presence of 50µM CMC002042, PSI002042, STW001222 and PSI002043.

Compound	V^{app}_{max} (s^{-1})	K^{app}_{M} (µM)	K_i (µM)
No inhibitor	2.60	145	---
CMC002042	1.53	80	62
PSI002042	1.13	52	28
STW001222	0.90	47	24
PSI002043	0.90	45	23

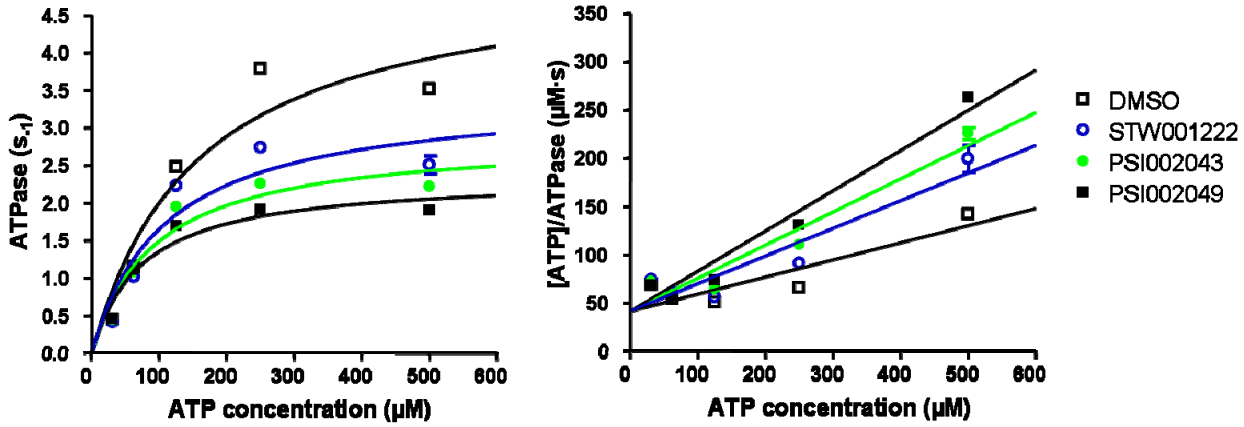

Figure 59. Michaelis-Menten (left) and Hane-Woolf (right) plots of microtubule-stimulated dynein motor domain ATPase activity in the presence of 50μM STW001222, PSI002049 and PSI002049.

The reaction was initiated with different concentrations of ATP in the presence of 12.75 μg/mL recombinant cytoplasmic dynein heavy chain and 1 mg/mL of paclitaxel-induced tubulin polymer.

Table 9. The V^{app}_{max}, K^{app}_{M} and K_i values of the microtubule-stimulated ATPase activity of recombinant cytoplasmic dynein heavy chain motor domain in the presence of 50μM STW001222, PSI002049 and PSI002049.

Compound	V^{app}_{max} (s^{-1})	K^{app}_{M} (μM)	K_i (μM)
No inhibitor	5.16	157	---
STW001222	3.45	108	101
PSI002043	2.88	93	63
PSI002049	2.36	74	42

4.7 Specificity studies

4.7.1 Hsp70 and Hsp90 ATPase assay results

Compounds that inhibit GFP-GR nuclear translocation may do so by inhibiting the activities of receptor-associated chaperones, such as Hsp90 and/or Hsp70. Therefore, the effects of the compounds on the steady state ATPase activities of recombinant human Hsp70 and a close homologue of human Hsp90, yeast Hsc82p, were examined. Mixtures containing [^{32}P]ATP and either Hsp70 or Hsc82p were incubated at 30 ºC in the presence of the compounds, established inhibitors (for Hsc82p, novobiocin[73]; for Hsp70, MAL3-101[67]) or vehicle (DMSO). The conversion of Hsp70/90-bound ATP to ADP•Pi was monitored by thin layer chromatography and phosphor image analysis. Whereas novobiocin and MAL3-101 inhibited the rate of ATP hydrolysis by their respective target chaperone proteins, none of the new dynein inhibitors at up to 100 μM had any significant inhibitory effect (Table 10, 11).

Table 10. Effects of the compounds on the rate of Hsp70 ATP hydrolysis.
Steady state Hsp70 ATPase assays were carried out at 30 ºC in the presence of 100 μM test agent. The rates of ATP hydrolysis were converted from the free phosphate released at the 5 min timepoint and determined from two independent experiments (± S.D.). The relative "Fold change" of each compound compared to the rate of ATP hydrolysis in the presence of DMSO is indicated.

Compound	Hsp70 ATPase × 10^4 (s^{-1})	Fold change
DMSO	21 ± 6	--
CMC002042	22 ± 1	1.0
PSI002042	18 ± 0	–1.2
PSI002043	17 ± 5	–1.2
PSI002049	14 ± 1	–1.5
STW001222	16 ± 8	–1.3
STW001150	15 ± 1	–1.4

Table 11. Effects of the compounds on the rate of Hsp90 ATP hydrolysis.
Steady state Hsp90 ATPase assays were carried out at 30 ºC in the presence of 100 μM test agent. The rate of ATP hydrolysis were converted from the free phosphate released at the 30 min timepoint and determined from at least two independent experiments (± S.D.). The relative "Fold change" of each compound compared to the rate of ATP hydrolysis in the presence of DMSO is indicated.

Compound	Hsp90 ATPase × 10^4 (s^{-1})	Fold change
DMSO	7.1 ± 1.1	--
CMC002042	7.3 ± 0.9	1.0
PSI002042	6.8 ± 2.0	1.0
PSI002043	6.8 ± 0.9	1.0
PSI002049	7.6 ± 1.4	1.1
STW001222	7.3 ± 0	1.0
STW001150	7.1 ± 0.1	1.0

4.7.2 Myosin ATPase assay results

The natural product purealin inhibits myosin's Ca^{2+}-stimulated ATPase activity with a concentration for half inhibition of 4 μM[42]. The new dynein inhibitors were therefore tested against the ATPase activity of rabbit skeletal muscle myosin II. Synthetic, racemic purealin[75] was tested as a positive control in the assay and an IC_{50} value of 36 ± 2 μM was obtained for it. In contrast, none of the new dynein inhibitors at up to 100 μM altered the myosin Ca^{2+}-ATPase activity significantly (Table 12).

Table 12. Effects of the compounds (100 μM) on the rate of myosin Ca^{2+}-stimulated ATPase activity of rabbit muscle myosin II (25 μg/mL).
The reaction was initiated with 2.5 mM ATP in the presence of myosin and the compounds. The rate of ATP hydrolysis was calculated from the free phosphate released (mean ± S.D., N = 4), and the relative "Fold change" caused by each compound as compared to the rate of ATP hydrolysis in the presence of DMSO is indicated.

Compound	Myosin Ca^{2+}-ATPase (s^{-1})	Fold change
DMSO	0.17 ± 0	---
CMC002042	0.16 ± 0.01	-1.1
PSI002042	0.20 ± 0.01	1.1
PSI002043	0.19 ± 0.01	1.1
PSI002049	0.17 ± 0.01	1.0
STW001222	0.20 ± 0	1.2
STW001150	0.18 ± 0	1.0

4.7.3 Microtubule polymerization assay results

Compounds active in the GFP-GR nuclear translocation assay may act so by perturbing the cellular microtubule network. One example is the tubulin assembly inhibitor colcemid. It has been shown to block corticosterone-stimulated GFP-GR nuclear translocation in 3T3 cells. Therefore, it was important to determine if the new dynein inhibitors had any effect on the microtubule network. The cellular levels of soluble and polymerized tubulin was determined cells were treated with the compounds. The 3617.4 cells were plated in 6-well plates and allowed to attach for 48 h, then treated with the indicated concentrations of different compounds. After 8 h, cells were detached by trypsinization, washed with Hanks' balanced salt solution (HBSS), then lysed in lysis buffer (see Chapter 2). The lysate was centrifuged at 14,000 rpm in an Eppendorf microcentrifuge. The supernatant (containing soluble tubulin fraction) and pellet (containing polymerized tubulin fraction) were dissolved in lysis buffer. Protein samples were analyzed by SDS-PAGE and Western blotting. Densitometric analyses were performed with ImageJ (v. 1.32j) software. Two controls were first included in this assay. A series dilutions of colchicine, a known tubulin assembly inhibitor, and paclitaxel, a known microtubule stabilizer, were used to treat cells for 8. Western blot analysis of polymerized (p) and soluble (s) tubulin fractions of 3617.4 cells showed that colchicine lowers the polymerized tubulin fraction in cells (Figure 60, upper). With the treatment of 320 nM colchicine, only 7% of the tubulin was in the polymerized form. However, treatment with paclitaxel increased the polymerized tubulin fraction (Figure 60, lower). The control results matched with the known roles of colchicine and paclitaxel in cells, providing the rationale for using this assay to check if the new dynein inhibitors perturb cellular microtubule networks.

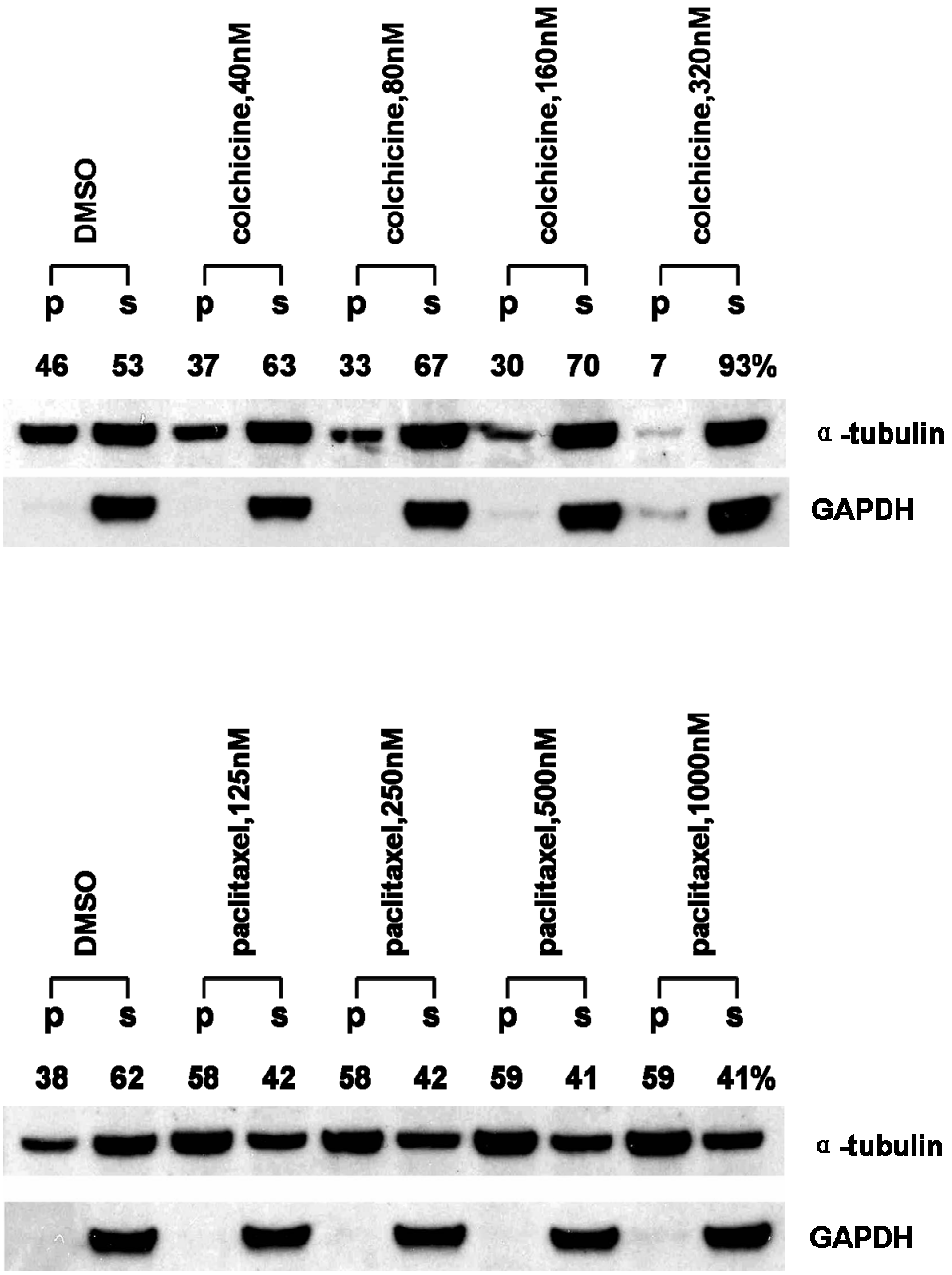

Figure 60. Western blot analysis of polymerized (p) and soluble (s) tubulin fractions of 3617.4 cells with treatment of colchicine or paclitaxel.

The dynein inhibitors were examined with this assay. The compounds at 100μM, as well as 1000nM paclitaxel and 320nM colchicine, were used (Figure 61). The results showed that the relative intensity of polymerized tubulin fraction in the presence of DMSO ranged from 0.9-1.6.

The dynein inhibitors caused the same. However, treatment with paclitaxel and colchicine gave relative intensities of 2.6 and 0.0, respectively. Therefore, the Western blot analyses of polymerized and soluble tubulin fractions of 3617.4 cells showed that the dynein inhibitors did not alter the microtubule content of cells.

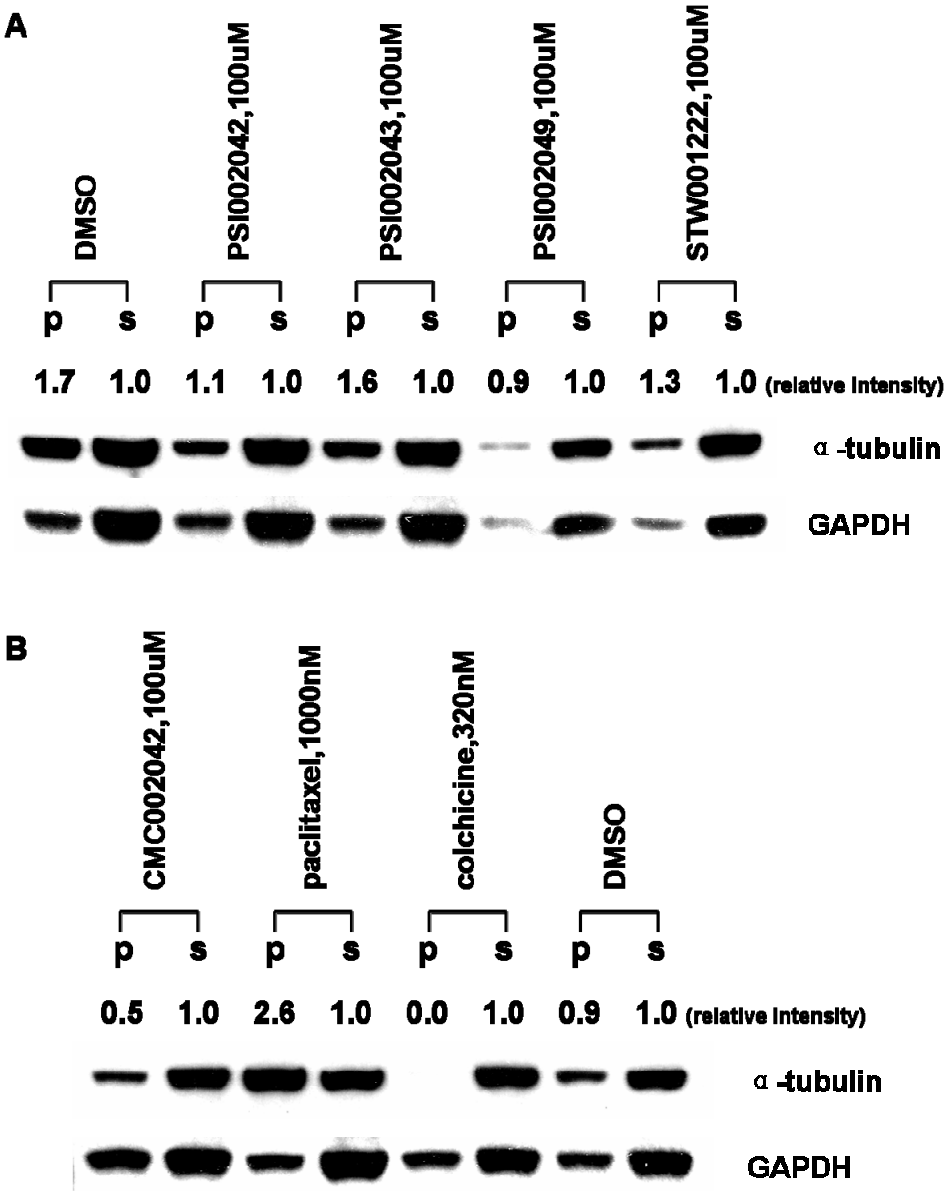

Figure 61. Western blot analysis of polymerized (p) and soluble (s) tubulin fractions of 3617.4 cells with treatment of dynein inhibitors.

The compounds' abilities to disturb tubulin polymerization *in vitro* was also tested. Tubulin (from bovine brain) assembly reactions under various conditions were performed in the presence of 20 and 100μM PSI002049 (Figure 62). Polymer development was determined in temperature-controlled spectrophotometers by measuring turbidity at 350 nm. The experimental procedure is described in Chapter 2. Briefly, reaction mixtures consisting of tubulin (1 mg/ml), GTP (400 μM, if present) in 1M monosodium glutamate, pH 6.9, were prepared. Baselines were established after addition of all reaction components, except the test agents, to the cuvettes held at 0 ^{o}C. Test agents predissolved in DMSO were added and each reaction mixture (0.25 mL final volume) was subjected to the sequential temperature change studies at the indicated temperatures. The hypernucleating potencies of the test agents were also evaluated by turbidimetry, but in the absence of GTP.

Tubulin with GTP. Test agent-induced turbidity profiles in the tubulin plus GTP system are shown in Figure 62A. In the presence of GTP and with no test agent, an increase in temperature to 30 ^{o}C resulted in a extensive assembly reaction as shown by the rapid rise in turbidity readings. When the temperature was rapidly dropped from 30 ^{o}C back to 0 ^{o}C, the polymer disassembled and the turbidity reading concordantly dropped quickly. A similar turbidimetry profile was observed with 20 and 100μM PSI002049. However, with 10μM colchicine, no polymer was observed from the beginning to the end of the experiment. The result illustrated that PSI002049 did not inhibit the GTP-induced polymerization of tubulin.

Tubulin with no GTP. Test agent-induced turbidity profiles in the tubulin without GTP system are shown in Figure 62B. In the presence of DMSO, when temperature was increased to 30 ^{o}C and was rapidly dropped from 30 ^{o}C back to 0 ^{o}C, the turbidity reading remained unchanged. A similar turbidimetry profile was observed with 20 and 100μM PSI002049.

However, with paclitaxel (10μM and 20μM), an increase in temperature to 30 °C resulted in an extensive assembly reaction as shown by the rapid rise in turbidity readings. When the temperature was rapidly dropped from 30 °C back to 0 °C, the turbidity reading slowly and incompletely dropped. The result illustrated that PSI002049 did not induce the polymerization of tubulin.

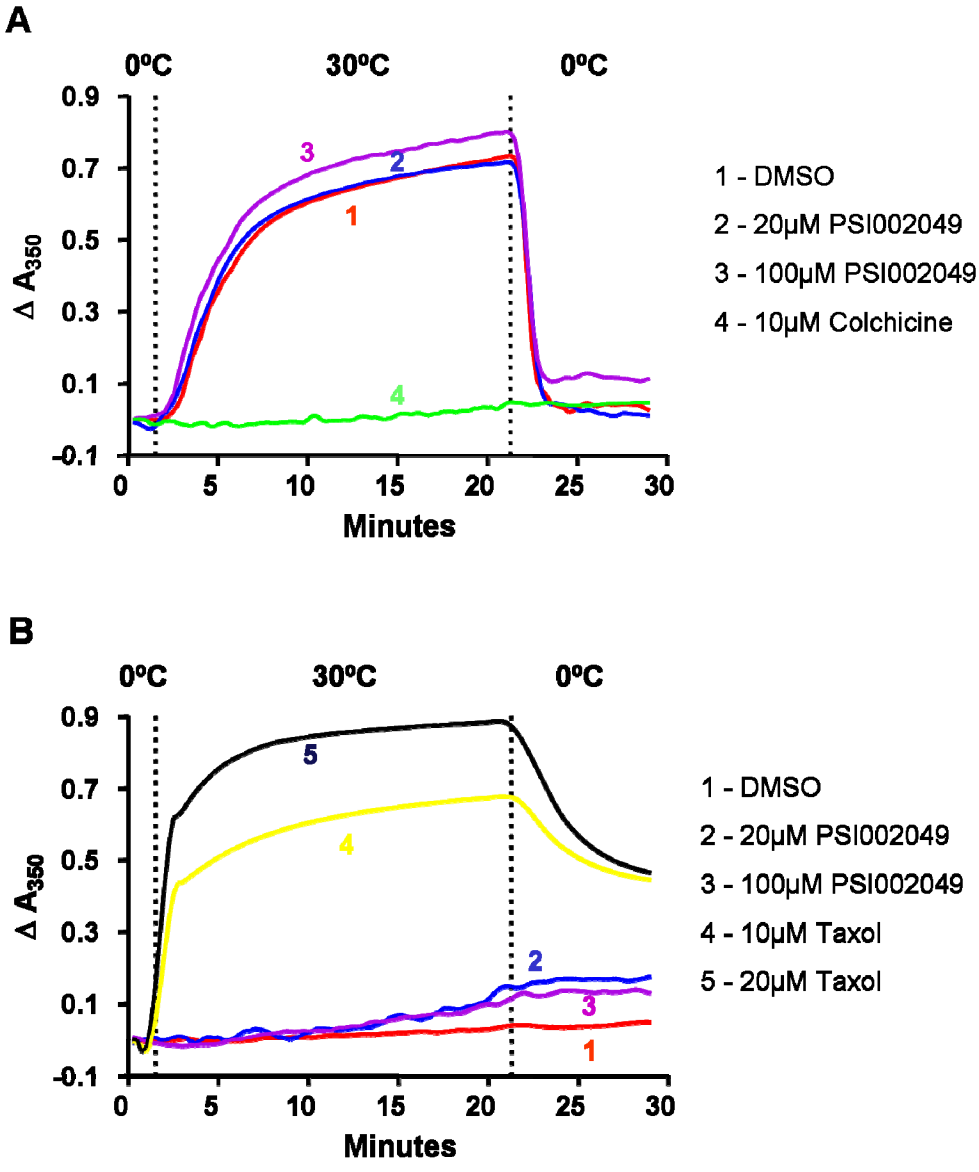

Figure 62. Turbidity profiles of tubulin polymerization assay with stepwise temperature changes in the presence of PSI002049.
A: In the presence of GTP. B: In the absence of GTP.

4.8 Antiproliferative activity of the UPCMLD hit compounds

Finally, examination of the antiproliferative activities of the agents against the expansion of 3617.4 mouse mammary adenocarcinoma cells cultures (24 h or 72 h) showed that most of the six compounds had weak antiproliferative activity. Fifty percent growth inhibitory concentrations were in the mid-micromolar range (Table 13). In contrast, previous results showed synthetic purealin has no antiproliferative activity against human carcinoma cells[75].

Table 13. Antiproliferative activities of the test agents against 3617.4 cells.

Compound	GI_{50} (μM)	
	24h	72h
PSI002049	24 ± 2	27 ± 2
PSI002043	40 ± 7	>50
STW001222	>50	>50
CMC002042	>50	42 ± 5
PSI002042	20 ± 8	29 ± 2
STW001150	40 ± 5	21 ± 5
Paclitaxel	0.17 ± 0.05	>0.25

4.9 Discussion

The strategy outlined here indicates that screening for compounds that block the transport of dynein's cargo could be an efficient way to find new dynein inhibitors. Moreover, the

advantage of the initial cell-based strategy is that cell-permeating small molecules can be identified; i.e., those that give a phenotypic readout of dynein inhibition. Importantly, the new dynein inhibitors exhibited specificity, as they did not interfere with GR binding, nor Hsp70 and Hsp90 ATPase activity. Since the one non-ATP-mimicking small molecule previously known to inhibit dynein, purealin, also has effects on myosin ATPase activity, it was considered prudent to screen the hits against this target as well. None of the new compounds here inhibited myosin.

An important aspect of the small molecule inhibitors described here is that they do not compete for the nucleotide-binding site of the dynein motor domain. These cell-permeating dynein inhibitors are not ATP analogues and have very different chemical structures/scaffolds than previously identified dynein inhibitors; they are, therefore, a promising starting point for investigation of structure-activity relationships. The lead compound, PSI002043, has dynein ATPase inhibitory effect with an IC_{50} in the micromolar range. This compound could be a valuable tool to study detailed kinetics of the dynein motor and to dissect the mechanism of dynein-based cargo transport. Since dynein is related to many diseases, particularly neurodegenerative diseases and cancer[28,104,105], a drug-like dynein inhibitor could also have therapeutic potential.

Since the skeletal muscle myosin II inhibitor BTS[12] and the Eg5 kinesin inhibitor monastrol[10] have shown the potential for use as therapeutic agents, the present results identify an additional motor protein as a potential target for small molecule therapeutics. Further screening of libraries with diverse structures for inhibition of GFP-GR nuclear translocation, followed by validation with the biochemical assays described herein, will hopefully lead to a dynein inhibitor useful as a cell biology tool or perhaps even as a therapeutic agent.

The leading compound, PSI002049, showed effective inhibition against dynein motor domain ATPase (IC_{50}=2.0μM). The compound was resynthesized by Dr. Stefan Werner in order to perform more cell based assays. However, the resynthesized PSI002049 showed pretty weak inhibitory effect against dynein motor domain ATPase with IC_{50} greater than 50μM. Therefore, old DMSO stock of PSI002049 was analyzed in LC-MS to check its purity. Unfortunately, the result showed that PSI002049 decomposed to different fractions upon current storage condidtion (-20°C) in DMSO (Figure 63). Different fractions (F1-F6) were collected and some of the fractions (F2, F3, F5 and F6) were also tested against dynein motor domain. The most active fraction F6 has IC_{50} = 36 ± 1 μg/mL.

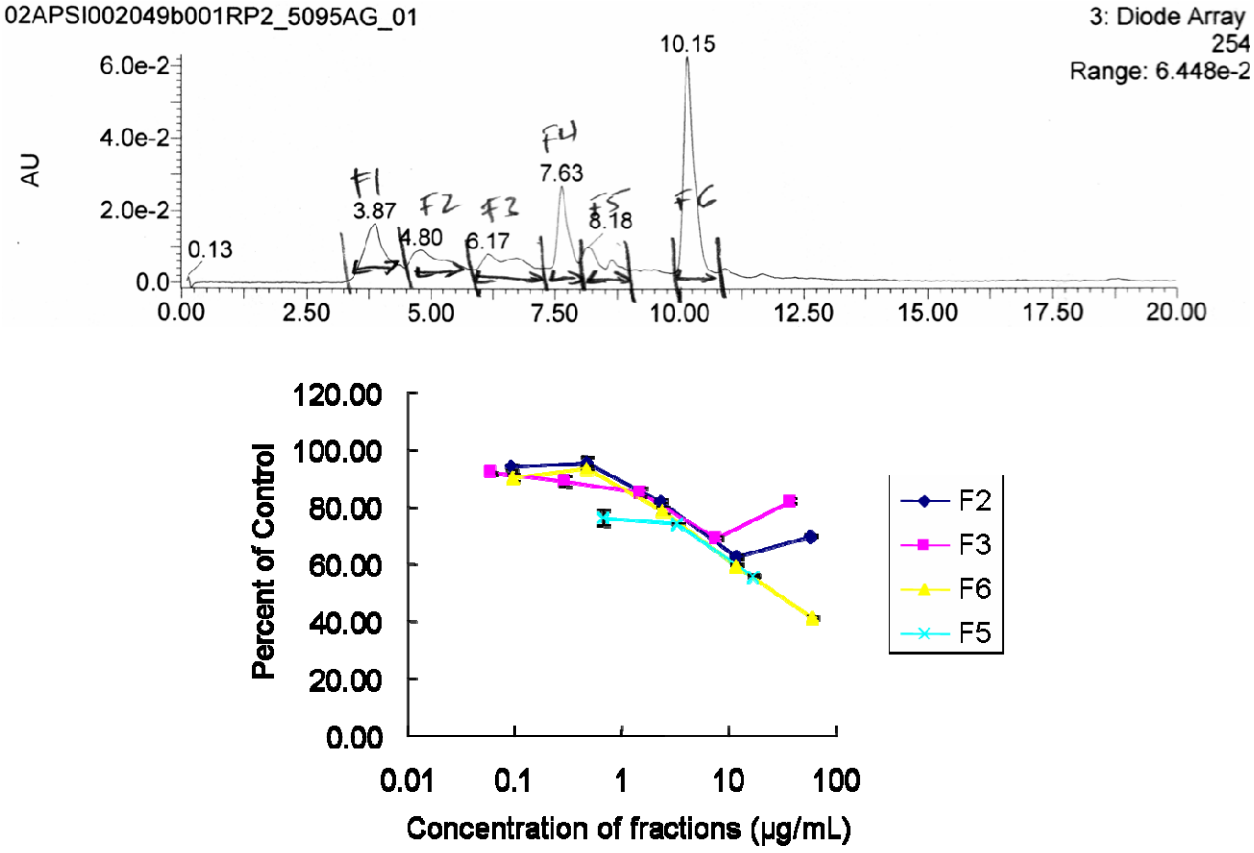

Figure 63. Dynein motor domain ATPase in the presence of different concentration of PSI002049 fractions.

5.0 BIOLOGICAL EALUATION OF HSP70 INHIBITORS

5.1 Introduction

The molecular chaperone Hsp70 plays very important roles in the cellular machinery for protein folding, for transport in concert with dynein (see previous chapters), and helps to protect cells from stress. It is known that overexpression of Hsp70 can lead to cellular transformation and tumorigenesis. Recent reports also show that inhibition of Hsp70 synthesis induces massive death of the breast cancer cells MDA-MB-468, MCF-7, SK-BR3 and BT-549, but has very little effect on WI-38 fibroblasts and HBL-100 nontumorigenic breast epithelial cells. Therefore, Hsp70 is a reasonable target for chemotherapeutic agents[56].

It is known that the Ugi-Biginelli compound MAL3-101 inhibits Tag-stimulated Hsp70 ATPase activity[67]. However, there no data regarding the antiproliferative activity of MAL3-101, or even its other cellular activities, has so far been determined. This chapter describes the screening of compounds related to MAL3-101 for activity against breast cancer cell proliferation.

MAL3-101 is structurally considered as three parts: the Biginelli tetrahydropyrimidone part (shown as in red in Figure 64A); the Ugi part (shown as in blue in Figure 64A) and the linker between the above (shown as in purple in Figure 64A). The Biginelli part was synthesized by the Biginelli multicomponent reaction, a acid-catalyzed reaction between a β-ketoester **1**, an

aldehyde **2** and urea **3** (Figure 64B). Then the Ugi part was obtained from an Ugi four component reaction (U-4CC), a condensation of the carboxylic acid **4** from Biginelli reaction, an isocyanide **5**, an aldehyde **6** and an amine **7** to form α-aminoacyl amide derivatives (Figure 63C).

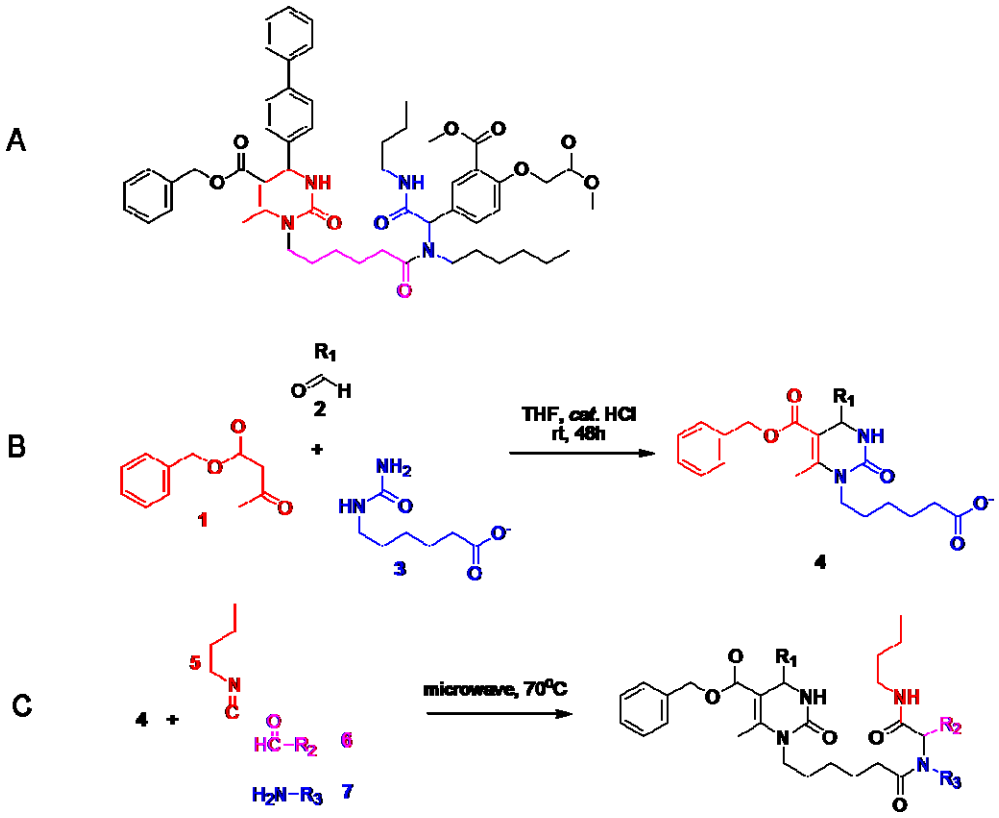

Figure 64. General synthetic scheme of MAL3-101 analogues.
A. Chemical structure of MAL3-101. Different color represents different part of the molecule. B. General scheme of Biginelli reaction. C. General scheme of Ugi reaction.

5.2 Antiproliferative activity of the first library

First, seven Biginelli/Ugi compounds, including MAL3-101, were obtained from the UPCMLD (Figure 65). Since biological inhibition of Hsp70 activity inhibits cell proliferation in different breast cancer cells, chemical inhibition of Hsp70 ATPase activity should also lead to

the same effect. SK-BR3 cells were used to test if the library had effects on cell proliferation. The MTS assay was used for determination of cell viability and cell counting. The procedure is described in Chapter 2. In short, cells were plated in 96-well plate and allowed to attach for 72 h. The cells were then treated with test agents for another 72 or 96 h and the MTS reagents were added. The results indicated that MAL3-101 has GI_{50}s against SK-BR3 cells of 9.3 and 11 μM for 72 and 96 h, respectively, of drug treatment. However, the other six structurally related compounds did not show effective antiproliferative activity against SK-BR3 cells, especially when the cells were treated for 72 h (Table 14). Paclitaxel was used as a positive control in the MTS assay and it gave a GI_{50} in the low nanomolar range. This result supported the hypothesis that chemical inhibition of Hsp70 ATPase activity will inhibit breast cancer cell proliferation. The result also showed that MAL3-101 could be used as the starting point for breast cancer chemotherapeutic agent, although its structural related compounds failed antiproliferation assay.

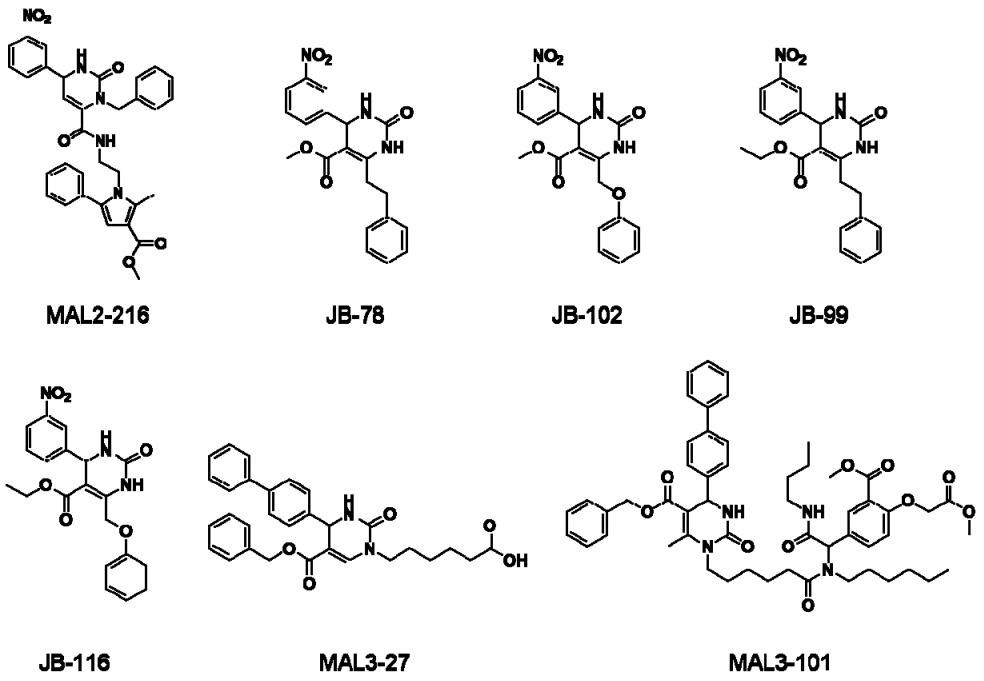

Figure 65. Chemical structure of MAL3-101 structural related compounds.

Table 14. Antiproliferative activity of MAL3-101 and structural related compounds against SK-BR3 cells.

GI_{50}/μM	SK-BR3 (1st trial)	SK-BR3 (2nd trial)
Exposure time/h	72	96
MAL3-27	>50	41±2
JB-99	38±4	38±8
JB-78	>50	41±2
MAL2-216	>50	ND*
JB-116	>50	37±2
JB-102	>50	40±0
MAL3-101	9.3±2.2	11±2
paclitaxel(nM)	3.7±0.5	5.9±0.8

The antiproliferative activity of MAL3-101 against another human breast cancer cell line, MDA-MB468, as well as against WI-38 fibroblast (a model for non-breast, "normal" cells) was also tested (Table 15). MAL3-101 gave a GI_{50} of 8.4μM against MDA-MB468 cell proliferation. However, MAL3-101 also showed antiproliferative activity against the WI-38 "normal" fibroblasts, with a GI_{50} of 15μM. Paclitaxel was again used as a positive control and it had a GI_{50} of 1.7nM against MDA-MB468 cells but a value of >100 nM against WI-38 cells.

Table 15. Antiproliferative activity of MAL3-101 against MDA-MB468 and WI-38 cell proliferation.

GI_{50}/μM	MDA-MB468	WI-38
Exposure time/d	6	5
MAL3-101	8.4±1.0	15±12
Paclitaxel(nM)	1.7±0.4	>100

5.3 Antiproliferative activity of Ugi-Biginelli compounds

More MAL3-101 analogues were synthesized by the UPCMLD in order to look for more active and more drug-like Hsp70 inhibitors. The compounds were first screened against SK-BR3 cell proliferation with the MTS assay and GI_{50}s were obtained. The results given below are classified according to chemical structural classes in order to help provide information about structure-activity relationships.

A

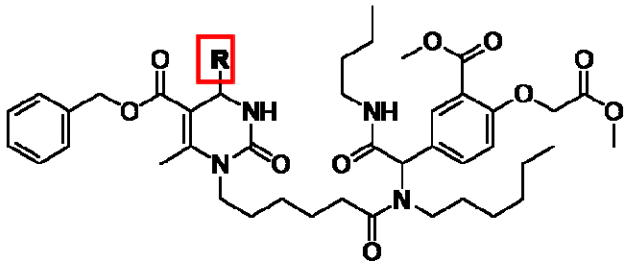

B

GI_{50}/μM	COMPOUND TYPE		SK-BR3/72h	Tag-stimulated Hsp70 ATP hydrolysis with 300μM compound/fold
DMT003082	Ugi-1	para-trifluoromethylbenzaldehyde	>50	-4.8
DMT003084	Ugi-1	para-tert-butylbenzaldehyde	29±0	-5.2
DMT003086	Ugi-1	meta-nitrobenzaldehyde	6.0±0.4	-1.5
DMT003088	Ugi-1	benzaldehyde	6.5⊥0.7	-1.1
DMT003090	Ugi-1	para-chlorobenzaldehyde	16⊥6	-5.1
DMT003092	Ugi-1	para-nitrobenzaldehyde	6.9±0.4	-1.1
DMT003094	Ugi-1	naphthaldehyde	10±1	-1.1
DMT003096	Ugi-1	ortho-biphenylcarboxaldehyde	17±3	-4.0
DMT003100	Ugi-1	cyclohexylcarboxaldehyde	6.3±1.0	-2.1
DMT003132	Ugi-1	cyclopropylcarboxaldehyde	6.2±0.4	-2.6
DMT003134	Ugi-1	para-cyclohexylbenzaldehyde	42±6	-1.6

Figure 66. Antiproliferative activity of Ugi-1 compounds.
A. General chemical structure of Ugi-1 compounds. B. Antiproliferative activity of Ugi-1 compounds against SK-BR3 cells for 72 h and the fold change of Tag-stimulated Hsp70 ATP hydrolysis in the presence of 300μM compounds (The Hsp70 data are courtesy of Prof. Brodsky group.)

The Ugi-1 compounds were MAL3-101 analogues with different aldehyde groups in the Biginelli part. The antiproliferative activities of the Ugi-1 compounds illustrated that most were active against SK-BR3 cells. Five out of 11 of the Ugi-1 compounds gave GI_{50}s of less than 10μM when the cells were treated for 72 h (Figure 66).

A

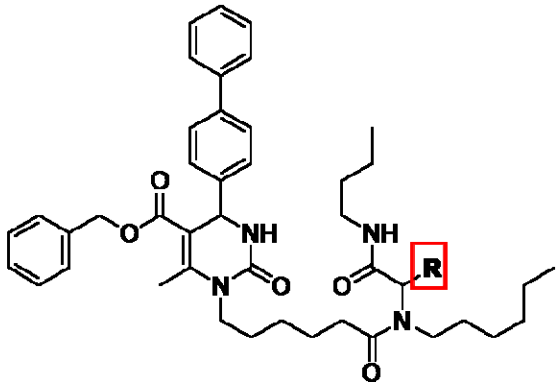

B

GI_{50}/μM	COMPOUND TYPE		SK-BR3/72h	Tag-stimulated Hsp70 ATP hydrolysis with 300μM compound/fold
DMT002218	Ugi-2	benzaldehyde	>50	1.1
DMT002220	Ugi-2	para-hydroxybenzaldehyde	>50	9.2
DMT002222	Ugi-2	para-biphenylcarboxaldehyde	>50	6.0
DMT002260	Ugi-2	meta-ester-benzaldehyde	>50	-2.0
DMT002262	Ugi-2	acetaldehyde	>50	1.0
DMT002264	Ugi-2	cyclohexylcarboxaldehyde	>50	1.1
DMT003058	Ugi-2	2-pyridinecarboxaldehyde	>50	5.5
DMT003112	Ugi-2	3-ester-4-hydroxybenzaldehyde	>50	2.1
DMT003114	Ugi-2	para-oxymethylester	48±5	1.2

Figure 67. Antiproliferative activity of Ugi-2 compounds.
A. General chemical structure of Ugi-2 compounds. B. Antiproliferative activity of Ugi-2 compounds against SK-BR3 cells for 72 h and the fold change of Tag-stimulated Hsp70 ATP hydrolysis in the presence of 300μM compounds (The Hsp70 data are courtesy of Prof. Brodsky group.)

The Ugi-2 compounds were MAL3-101 analogues with different aldehyde groups in the Ugi part. The results showed that most of the Ugi-2 compounds were not effective against SK-

BR3 cell proliferation (Figure 67). Apparently, a changing in aldehyde group in the Ugi part of MAL3-101 causes a loss of antiproliferative activity.

A

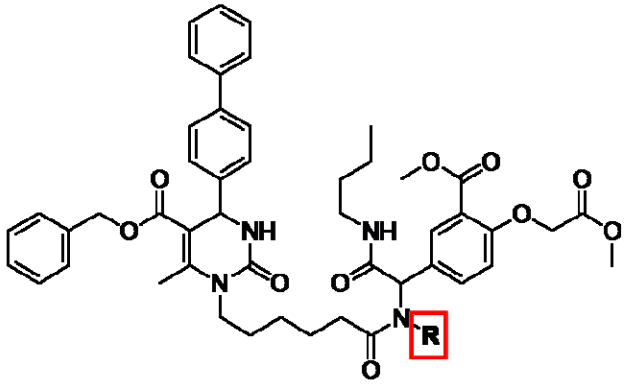

B

GI_{50}/μM	COMPOUND TYPE		SK-BR3/72h	Tag-stimulated Hsp70 ATP hydrolysis with 300μM compound/fold
DMT002286	Ugi-3	cyclohexenylethylamine	39±6	-1.2
DMT003052	Ugi-3	methoxyethylamine	8.8±0.3	-1.8
DMT003102	Ugi-3	benzylamine	14±2	-1.9
DMT003104	Ugi-3	phenethylamine	32±2	1.3
DMT003106	Ugi-3	2-pyridinemethylamine	7.1±0.4	-1.1
DMT003108	Ugi-3	2-pyridineethylamine	7.5±0.8	-1.1
DMT003110	Ugi-3	tryptamine	>50	-1.3

Figure 68. Antiproliferative activity of Ugi-3 compounds.
A. General chemical structure of Ugi-3 compounds. B. Antiproliferative activity of Ugi-3 compounds against SK-BR3 cells for 72 h and the fold change of Tag-stimulated Hsp70 ATP hydrolysis in the presence of 300μM compounds (The Hsp70 data are courtesy of Prof. Brodsky group.)

Seven Ugi-3 compounds, which were MAL3-101 analogues with different amine groups in the Ugi part, were also examined. The antiproliferative activity of Ugi-3 compounds are shown in Figure 68. Most of Ugi-3 compounds were effective against SK-BR3 cell proliferation. The GI_{50} values for them were between 8.8 and 39μM (Figure 68).

A

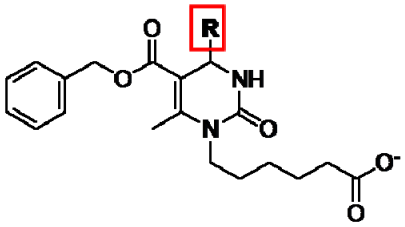

B

GI_{50}/μM	COMPOUND TYPE		SK-BR3/72h	Tag-stimulated Hsp70 ATP hydrolysis with 300μM compound/fold
DMT002272	Biginelli acid	ortho-biphenylcarboxaldehyde	>50	-5.0
DMT003034	Biginelli acid	cyclohexylcarboxaldehyde	>50	1.5
DMT003036	Biginelli acid	para-tert-butylbenzaldehyde	>50	-3.5
DMT003038	Biginelli acid	cyclopropylcarboxaldehyde	>50	1.0
DMT003116	Biginelli acid	para-cyclohexylbenzaldehyde	>50	-2.4
MAL1-274	Biginelli acid	para-cchlorobenzaldehyde	>50	-1.6
MAL2-06A	Biginelli acid	2-naphthaldehyde	>50	-1.4
MAL2-10A	Biginelli acid	benzaldehyde	>50	-1.1
MAL2-116-17	Biginelli acid	meta-nitrobenzaldehyde	>50	1.1
MAL2-116-20	Biginelli acid	para-trifluoromethylbenzaldehyde	>50	1.1
MAL2-11B	Biginelli acid	para-biphenylcarboxaldehyde	>50	-3.5
MAL2-13	Biginelli acid	para-nitrobenzaldehyde	>50	1.1

Figure 69. Antiproliferative activity of Biginelli acids.
A. General chemical structure of Biginelli acids. B. Antiproliferative activity of Biginelli acids against SK-BR3 cells for 72 h and the fold change of Tag-stimulated Hsp70 ATP hydrolysis in the presence of 300μM compounds (The Hsp70 data are courtesy of Prof. Brodsky group.)

The antiproliferative activity of the Biginelli acids, which were MAL3-101 analogues without the Ugi part in an acid form, were also examined. None of the Biginelli acids showed effective antiproliferative activity against SK-BR3 cells, giving GI_{50}s greater than 50 μM(Figure 69).

A

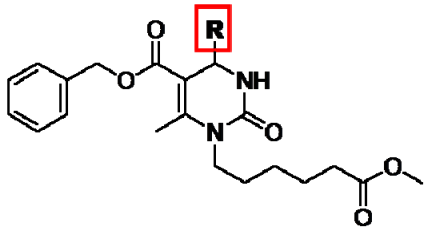

B

GI_{50}/μM	COMPOUND TYPE		SK-BR3/72h	Tag-stimulated Hsp70 ATP hydrolysis with 300μM compound/fold
DMT003042	Biginelli ester	para-biphenylcarboxaldehyde	>50	-1.2
DMT003044	Biginelli ester	benzaldehyde	>50	-1.7
DMT003046	Biginelli ester	cyclopropylcarboxaldehyde	>50	1.0

Figure 70. Antiproliferative activity of Biginelli esters.

A. General chemical structure of Biginelli esters. B. Antiproliferative activity of Biginelli esters against SK-BR3 cells for 72 hrs. and the fold change of Tag-stimulated Hsp70 ATP hydrolysis in the presence of 300μM compounds (The Hsp70 data are courtesy of Prof. Brodsky group.)

As the Biginelli acids might not pass cell membranes, the Biginelli esters, MAL3-101 analogues without the Ugi part in an ester form, were also examined. Again, GI_{50}s were greater than 50 μM, the highest concentration used in the antiproliferation assay (Figure 70).

5.4 Conclusions and discussion

The Hsp70 and Hsp90 families of molecular chaperones play important roles in cellular processes, including protein folding, synthesis, transport and degradation. Hsp70 and Hsp90 chaperones are also related to many human diseases, including cancer, cystic fibrosis, heart disease and some neurodegenerative syndromes (for review, see ref.[58]). Although there are

relatively more known Hsp90 inhibitors, and even some of them are currently used clinically, very few Hsp70 modulators have been identified (for review, see ref.[106]). The first efforts towards the discovery of more potent Hsp70 inhibitors as antibreast cancer agents is described here. Starting from the lead compound MAL3-101, which was prepared by the Wipf group and its biological discovered by the Day and Brodsky groups[67], analogues of MAL3-101 were evaluated. The test of the first small library containing a small number of MAL3-101-related compounds did not provide agents with antiproliferative activity in SK-BR3 human breast cancer cells. A much larger library of MAL3-101 analogues was then obtained and screened against SK-BR3 cells. The antiproliferative activity of the MAL3-101 provided a practical structure-activity relationship analysis based on the GI_{50}s (Figure 71): the structure of the aldehyde group in Biginelli part is changeable, based on the results from Ugi-1 compounds; the structure of aldehyde group in Ugi part is required, based on the results from Ugi-2 compounds; the structure of the amine group in the Ugi part is changeable, based on the results of Ugi-3 compounds; the tetrahydropyrimidone part might be required to maintain the biological activity; the α-aminoacyl amide part is required; and the length of the linker might be important.

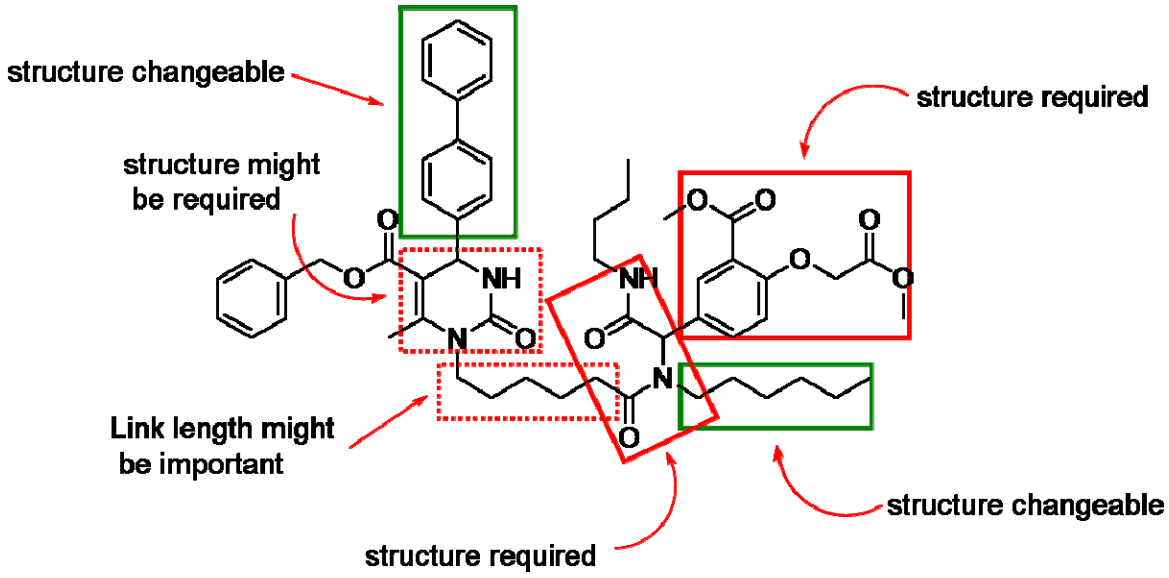

Figure 71. Structure-activity relationship of MAL3-101 analogues.

6.0 CONCLUSIONS AND DISCUSSIONS

The work described here is the first practical evaluation for inhibitors of cytoplasmic dynein, and one of the first for inhibitors of its interacting protein Hsp70. Although dynein plays very important role in cells, especially in many types of cellular organelle transportation, very little is known about small molecule dynein inhibitors. This work started from purealin, a bromotyrosine-derived natural product isolated from the sea sponge *Psammaplysilla purea*, which inhibits the ATPase activity of isolated axonemal dynein and skeletal muscle myosin without competing for the ATP site on these motor proteins. A small library of synthetic purealin derivatives was examined for inhibition of cytoplasmic dynein heavy chain and cell growth. The compounds showed effective antiproliferative activity against L1210 mouse leukemia cells, but selective activities against a small panel of human carcinoma cell lines (MDA-MB231, PC-3. 2008 and HT-29). Cytoplasmic dynein heavy chain was then purified from bovine brain and identified by MALDI-TOF-MS. Purealin and some of its analogues showed inhibitory effects against microtubule-stimulated ATPase activity of bovine cytoplasmic dynein heavy chain. A recombinant form of rat cytoplasmic dynein heavy chain motor domain was obtained and the purealin library was tested for inhibition of the ATPase activity of the motor domain. Purealin and a few of its analogues also showed inhibitory effects on microtubule-stimulated ATPase activity of the motor domain. The inhibitory effect of purealin was concentration-dependent and uncompetitive, supporting the hypothesis that it does not compete with the binding of ATP.

Since dynein is responsible for transport of the tumor suppressor protein p53 to the nucleus when DNA is damaged, a p53 nuclear translocation assay was established for evaluation of dynein inhibitors. A549 lung carcinoma cells were used for the p53 translocation assay. Cells were treated with a sub-lethal dose of a DNA damaging agent, camptothecin, to stimulate p53 accumulation into the nucleus. Purealin showed weak inhibitory effects of p53 nuclear accumulation after DNA damage. An ArrayScan-based p53 nuclear translocation assay was set up in a HTS format. Dynein heavy chain knockdown experiments were also evaluated and optimized with dynein heavy chain siRNA, but this RNAi method proved not to be useful as a positive control in this assay due to the apparent long lifetime of dynein heavy chain in cells.

It is known that ligand-bound glucocorticoid receptor (GR) is translocated to the nucleus by dynein, via linkages provided by Hsp90, in concert with Hsp70 to immunophilins bound to the region of the dynactin-associated portion of the dynein complex. Chemical inhibition of dynein activity was envisioned as a useful means to block nuclear transportation of GR. A strategy for screening new dynein inhibitors was built based on a GFP-GR nuclear translocation assay using a mouse mammary adenocarcinoma cell line (3617.4) stably expressing GFP-rat GR.

A library of compounds was obtained from the University of Pittsburgh Center for Chemical Methodology and Library Development (UPCMLD) that contained synthetic compounds wisely chosen as representatives from a larger set with considerable scaffold and physicochemical property variety. The 3617.4 cells stably expressing GFP-GR were used to screen for compounds that block hormone -stimulated GFP-GR nuclear translocation. Some of the compounds showed inhibitory effects in this asay. A GR competitor assay and a GR binding assay showed that the compounds active in the GFP-GR nuclear translocation assay did not compete for GR binding nor affected the GR complex.

Dynein motor domain ATPase assays were then performed to determine the compounds' direct effects on the target, and five were found to be new dynein ATPase inhibitors. The leading compound gave an IC_{50} value against dynein ATPase in the micromolar range. Kinetic study of these compounds showed that they did not compete for the ATP binding site on cytoplasmic dynein's motor domain. The new dynein inhibitors also showed no significant effect on Hsp70 and Hsp90 ATPase activities. Furthermore, results from an assay for myosin ATPase indicated that the new dynein inhibitors had no observable effect on Ca^{2+}-ATPase activity of skeletal muscle myosin II. The results therefore suggest that this strategy provides a practical way to find new cell-permeable dynein inhibitors via screening the compounds that could block the transportation of dynein's cargo.

Molecular chaperones are required for protein maturation and play critical roles in the pathogenesis of many human diseases. Previous data indicate that the Hsp70 chaperone class is induced in breast cancer cells and that antisense-mediated knock-down of Hsp70 triggers breast cancer cell apoptosis *in vitro*. These results indicate that Hsp70s represent a new target for breast cancer therapy and that small molecule inhibitors of Hsp70s might similarly trigger breast cancer cell death. To test this hypothesis, breast cancer cell growth was examined in the presence or absence of a small molecule inhibitor of Hsp70 co-chaperone interaction, MAL3-101, as well as several compounds structurally related to MAL3-101. Varying concentrations of each compound were added to SK-BR3 breast cancer cells in two independent experiments and their GI_{50}s were determined. The GI_{50} for MAL3-101 was 10 ± 2μM; as a positive control, paclitaxel was shown to inhibit growth with a GI_{50} of 3.7 ± 0.5nM. A first small library of MAL3-101-related compounds were less effective than MAL3-101, most likely because their impact on Hsp70 ATPase activity and modulation by Hsp70 co-chaperones was less pronounced.

A larger library of MAL3-101 compounds was prepared by the UPCMLD and evaluated for inhibition of SK-BR3 cell proliferation. Some of the analogues showed effective antiproliferative activities, providing a valuable first qualitiative structure-activity relationship. These data support the importance of future efforts to identify new and more potent chaperone modulators that may prove valuable to combat breast cancer.

The research provided here showed the rationality of screening for dynein-specific inhibitors via phenotypic screening assays. However, there is still a need to find more potent dynein inhibitors. Theoretically, any phenotypic assay showing the inhibition of transportation of dynein's cargo (e.g., p53, GR, adenovirus, HIV-Vpr, VSVG-GFP[107], etc.) could be used to set up a high throughput screen for dynein ATPase inihibtiors. Since the p53 and GR nuclear translocation assays were implemented here into at worst what could be considerd a medium throughput format, those two assays should be transferred to high throughput first. The assays can be performed in 384-well format, cells plated with a liquid handling plate processor (e.g., the Titertek MAP-C plate processor) and cell density optimized. Compound/reagent addition could be performed with Biomek2000 or SymBiot I (single channel) or XVI (16 channel) liquid handlers. DMSO tolerance, the time course for appropriate responses from the positive and negative controls, the concentration-dependence of the nuclear translocation stimulator (camptothecin/etoposide in the p53 nuclear translocation assay, dexamethasone in GFP-GR nuclear translocation assay) should be determined next for optimization. The assay with different conditions and different controls, e.g., known dynein inhibitors, should be repeated several times. Maximum signal (with the positive control) and minimum signal (with the negative control), signal-to-background, signal-to-noise, coefficients of variance (CV), and Z'-factors should also be obtained. The CV and Z'-factor can be used to evaluate the suitability and compatibility of the

assay for HTS. The hits from the cellular phenotype HTS assay should be tested for validation following the strategy described: inhibition of dynein heavy chain ATPase activity; inhibition of Hsp90, Hsp70 and myosin ATPase; perturbation of tubulin assembly; and GR binding by fluorescence polarization.

Adenovirus is a 70-100 nm diameter non-enveloped dsDNA virus that replicates in the cell nucleus. It is known that dynein is responsible for the transportation of the naked virus particle after adenovirus escapes from the endosome[13]. It is also known that the addition of the microtubule-disrupting agent nocodazole, microinjection of an antibody to the dynein intermediate chain, and overexpression of the dynamitin subunit of dynactin will prevent perinuclear accumulation of adenovirus[32-34]. Therefore, a cytoplasmic dynein inhibitor shold give a similar effect. The adenovirus nuclear translocation assay should be performed in the A549 human lung carcinoma cell line, as these cells have a large cytoplasm that enables clear determination of viral accumulation at the nucleus or otherwise. A form of Cy3 could be covalently coupled to adenovirus as described[33] and the resulting fluorescent virus can be produced in amounts suitable for use in high-throughput assays. The A549 cells would be infected with the Cy3-adenovirus at a multiplicity of infection (m.o.i.) of 100 and incubated at 4°C for 40 min. The cells would then be washed to remove unbound virus and incubated at 37°C for 60 min. The 4°C incubation followed by washing enables the infectious process to be synchronized because microtubules partially disassemble at this temperature. Such synchronization would result in a very clear end point for the assay. Nucleus-localized fluorescent virus should be easily visible in both live and fixed cells. The cells should as be fixed and stained for microtubules as described above to insure that the test agent does not perturb cellular tubulin assembly/disassembly.

BIBLIOGRAPHY

1. Mollinedo, F.; Gajate, C., Microtubules, microtubule-interfering agents and apoptosis. *Apoptosis* **2003,** 8, (5), 413-50.

2. Rowinsky, E. K.; Onetto, N.; Canetta, R. M.; Arbuck, S. G., Taxol: the first of the taxanes, an important new class of antitumor agents. *Semin Oncol* **1992,** 19, (6), 646-62.

3. Eckardt, J. R., Antitumor activity of docetaxel. *Am J Health Syst Pharm* **1997,** 54, (24 Suppl 2), S2-6.

4. Neuss, N.; Mallett, G. E.; Brannon, D. R.; Mabe, J. A.; Horton, H. R.; Huckstep, L. L., Vinca alkaloids XXXIII [1]. Microbiological conversions of vincaleukoblastine (VLB, vinblastine), an antitumor alkaloid from Vinca rosea. Linn. *Helv Chim Acta* **1974,** 57, (6), 1886-90.

5. ter Haar, E.; Kowalski, R. J.; Hamel, E.; Lin, C. M.; Longley, R. E.; Gunasekera, S. P.; Rosenkranz, H. S.; Day, B. W., Discodermolide, a cytotoxic marine agent that stabilizes microtubules more potently than taxol. *Biochemistry* **1996,** 35, (1), 243-50.

6. Mandelkow, E.; Mandelkow, E. M., Microtubules and microtubule-associated proteins. *Curr Opin Cell Biol* **1995,** 7, (1), 72-81.

7. Ookata, K.; Hisanaga, S.; Bulinski, J. C.; Murofushi, H.; Aizawa, H.; Itoh, T. J.; Hotani, H.; Okumura, E.; Tachibana, K.; Kishimoto, T., Cyclin B interaction with microtubule-associated protein 4 (MAP4) targets p34cdc2 kinase to microtubules and is a potential regulator of M-phase microtubule dynamics. *J Cell Biol* **1995,** 128, (5), 849-62.

8. Schliwa, M.; Woehlke, G., Molecular motors. *Nature* **2003,** 422, (6933), 759-65.

9. Sakowicz, R.; Berdelis, M. S.; Ray, K.; Blackburn, C. L.; Hopmann, C.; Faulkner, D. J.; Goldstein, L. S., A marine natural product inhibitor of kinesin motors. *Science* **1998,** 280, (5361), 292-5.

10. Mayer, T. U.; Kapoor, T. M.; Haggarty, S. J.; King, R. W.; Schreiber, S. L.; Mitchison, T. J., Small molecule inhibitor of mitotic spindle bipolarity identified in a phenotype-based screen. *Science* **1999,** 286, (5441), 971-4.

11. Kwok, B. H.; Kapitein, L. C.; Kim, J. H.; Peterman, E. J.; Schmidt, C. F.; Kapoor, T. M., Allosteric inhibition of kinesin-5 modulates its processive directional motility. *Nat Chem Biol* **2006,** 2, (9), 480-5.

12. Cheung, A.; Dantzig, J. A.; Hollingworth, S.; Baylor, S. M.; Goldman, Y. E.; Mitchison, T. J.; Straight, A. F., A small-molecule inhibitor of skeletal muscle myosin II. *Nat Cell Biol* **2002,** 4, (1), 83-8.

13. Paschal, B. M.; Shpetner, H. S.; Vallee, R. B., MAP 1C is a microtubule-activated ATPase which translocates microtubules in vitro and has dynein-like properties. *J Cell Biol* **1987,** 105, (3), 1273-82.

14. Pazour, G. J.; Dickert, B. L.; Witman, G. B., The DHC1b (DHC2) isoform of cytoplasmic dynein is required for flagellar assembly. *J Cell Biol* **1999,** 144, (3), 473-81.

15. Porter, M. E.; Bower, R.; Knott, J. A.; Byrd, P.; Dentler, W., Cytoplasmic dynein heavy chain 1b is required for flagellar assembly in Chlamydomonas. *Mol Biol Cell* **1999,** 10, (3), 693-712.

16. Goshima, G.; Vale, R. D., The roles of microtubule-based motor proteins in mitosis: comprehensive RNAi analysis in the Drosophila S2 cell line. *J Cell Biol* **2003,** 162, (6), 1003-16.

17. Mocz, G.; Gibbons, I. R., Model for the motor component of dynein heavy chain based on homology to the AAA family of oligomeric ATPases. *Structure (Camb)* **2001,** 9, (2), 93-103.

18. Gibbons, I. R.; Lee-Eiford, A.; Mocz, G.; Phillipson, C. A.; Tang, W. J.; Gibbons, B. H., Photosensitized cleavage of dynein heavy chains. Cleavage at the "V1 site" by irradiation at 365 nm in the presence of ATP and vanadate. *J Biol Chem* **1987,** 262, (6), 2780-6.

19. Mocz, G.; Gibbons, I. R., Phase partition analysis of nucleotide binding to axonemal dynein. *Biochemistry* **1996,** 35, (28), 9204-11.

20. Mazumdar, M.; Mikami, A.; Gee, M. A.; Vallee, R. B., In vitro motility from recombinant dynein heavy chain. *Proc Natl Acad Sci U S A* **1996,** 93, (13), 6552-6.

21. Asai, D. J.; Koonce, M. P., The dynein heavy chain: structure, mechanics and evolution. *Trends Cell Biol* **2001,** 11, (5), 196-202.

22. Burgess, S. A.; Walker, M. L.; Sakakibara, H.; Knight, P. J.; Oiwa, K., Dynein structure and power stroke. *Nature* **2003,** 421, (6924), 715-8.

23. Giannakakou, P.; Sackett, D. L.; Ward, Y.; Webster, K. R.; Blagosklonny, M. V.; Fojo, T., p53 is associated with cellular microtubules and is transported to the nucleus by dynein. *Nat Cell Biol* **2000,** 2, (10), 709-17.

24. Puthalakath, H.; Huang, D. C.; O'Reilly, L. A.; King, S. M.; Strasser, A., The proapoptotic activity of the Bcl-2 family member Bim is regulated by interaction with the dynein motor complex. *Mol Cell* **1999,** 3, (3), 287-96.

25. Tai, A. W.; Chuang, J. Z.; Bode, C.; Wolfrum, U.; Sung, C. H., Rhodopsin's carboxy-terminal cytoplasmic tail acts as a membrane receptor for cytoplasmic dynein by binding to the dynein light chain Tctex-1. *Cell* **1999,** 97, (7), 877-87.

26. Ishibashi, M.; Tsuda, M.; Ohizumi, Y.; Sasaki, T.; Kobayashi, J., Purealidin A, a new cytotoxic bromotyrosine-derived alkaloid from the Okinawan marine sponge Psammaplysilla purea. *Experientia* **1991,** 47, (3), 299-300.

27. Dohner, K.; Wolfstein, A.; Prank, U.; Echeverri, C.; Dujardin, D.; Vallee, R.; Sodeik, B., Function of dynein and dynactin in herpes simplex virus capsid transport. *Mol Biol Cell* **2002,** 13, (8), 2795-809.

28. LaMonte, B. H.; Wallace, K. E.; Holloway, B. A.; Shelly, S. S.; Ascano, J.; Tokito, M.; Van Winkle, T.; Howland, D. S.; Holzbaur, E. L., Disruption of dynein/dynactin inhibits axonal transport in motor neurons causing late-onset progressive degeneration. *Neuron* **2002,** 34, (5), 715-27.

29. Kawaguchi, Y.; Kovacs, J. J.; McLaurin, A.; Vance, J. M.; Ito, A.; Yao, T. P., The deacetylase HDAC6 regulates aggresome formation and cell viability in response to misfolded protein stress. *Cell* **2003,** 115, (6), 727-38.

30. Galigniana, M. D.; Harrell, J. M.; O'Hagen, H. M.; Ljungman, M.; Pratt, W. B., Hsp90-binding immunophilins link p53 to dynein during p53 transport to the nucleus. *J Biol Chem* **2004,** 279, (21), 22483-9.

31. Galigniana, M. D.; Radanyi, C.; Renoir, J. M.; Housley, P. R.; Pratt, W. B., Evidence that the peptidylprolyl isomerase domain of the hsp90-binding immunophilin FKBP52 is involved in both dynein interaction and glucocorticoid receptor movement to the nucleus. *J Biol Chem* **2001,** 276, (18), 14884-9.

32. Mabit, H.; Nakano, M. Y.; Prank, U.; Saam, B.; Dohner, K.; Sodeik, B.; Greber, U. F., Intact microtubules support adenovirus and herpes simplex virus infections. *J Virol* **2002,** 76, (19), 9962-71.

33. Leopold, P. L.; Kreitzer, G.; Miyazawa, N.; Rempel, S.; Pfister, K. K.; Rodriguez-Boulan, E.; Crystal, R. G., Dynein- and microtubule-mediated translocation of adenovirus serotype 5 occurs after endosomal lysis. *Hum Gene Ther* **2000,** 11, (1), 151-65.

34. Suomalainen, M.; Nakano, M. Y.; Keller, S.; Boucke, K.; Stidwill, R. P.; Greber, U. F., Microtubule-dependent plus- and minus end-directed motilities are competing processes for nuclear targeting of adenovirus. *J Cell Biol* **1999,** 144, (4), 657-72.

35. Suikkanen, S.; Aaltonen, T.; Nevalainen, M.; Valilehto, O.; Lindholm, L.; Vuento, M.; Vihinen-Ranta, M., Exploitation of microtubule cytoskeleton and dynein during parvoviral traffic toward the nucleus. *J Virol* **2003,** 77, (19), 10270-9.

36. McDonald, D.; Vodicka, M. A.; Lucero, G.; Svitkina, T. M.; Borisy, G. G.; Emerman, M.; Hope, T. J., Visualization of the intracellular behavior of HIV in living cells. *J Cell Biol* **2002,** 159, (3), 441-52.

37. Lakadamyali, M.; Rust, M. J.; Babcock, H. P.; Zhuang, X., Visualizing infection of individual influenza viruses. *Proc Natl Acad Sci U S A* **2003,** 100, (16), 9280-5.

38. Kelkar, S. A.; Pfister, K. K.; Crystal, R. G.; Leopold, P. L., Cytoplasmic dynein mediates adenovirus binding to microtubules. *J Virol* **2004,** 78, (18), 10122-32.

39. Blum, J. J.; Hayes, A., Effect of thiourea and substituted thioureas on dynein ATPase and on the turbidity response of Tetrahymena cilia. *J Supramol Struct* **1979,** 12, (1), 23-34.

40. Tanabe, K.; Tokumoto, T.; Ishikawa, N.; Shimizu, T.; Okuda, H.; Ito, S.; Shimmura, H.; Inui, M.; Harano, M.; Ohtsubo, S.; Manu, M.; Shiroyanagi, Y.; Yagisawa, T.; Fuchinoue, S.; Toma, H., Effect of Deoxyspergualin on the long-term outcome of renal transplantation. *Transplant Proc* **2000,** 32, (7), 1745-6.

41. Bouchard, P.; Penningroth, S. M.; Cheung, A.; Gagnon, C.; Bardin, C. W., erythro-9-[3-(2-Hydroxynonyl)]adenine is an inhibitor of sperm motility that blocks dynein ATPase and protein carboxylmethylase activities. *Proc Natl Acad Sci U S A* **1981,** 78, (2), 1033-6.

42. Nakamura, Y.; Kobayashi, M.; Nakamura, H.; Wu, H.; Kobayashi, J.; Ohizumi, Y., Purealin, a novel activator of skeletal muscle actomyosin ATPase and myosin EDTA-ATPase that enhanced the superprecipitation of actomyosin. *Eur J Biochem* **1987,** 167, (1), 1-6.

43. Fang, Y. I.; Yokota, E.; Mabuchi, I.; Nakamura, H.; Ohizumi, Y., Purealin blocks the sliding movement of sea urchin flagellar axonemes by selective inhibition of half the ATPase activity of axonemal dyneins. *Biochemistry* **1997,** 36, (50), 15561-7.

44. Takito, J.; Nakamura, H.; Kobayashi, J.; Ohizumi, Y.; Ebisawa, K.; Nonomura, Y., Purealin, a novel stabilizer of smooth muscle myosin filaments that modulates ATPase activity of dephosphorylated myosin. *J Biol Chem* **1986,** 261, (29), 13861-5.

45. Wu, H.; Nakamura, H.; Kobayashi, J.; Nakamura, Y.; Ohizumi, Y., *Tetrahedron Lett.* **1985,** 26, 4517.

46. Wu, H.; Nakamura, H.; Kobayashi, J.; Ohizumi, Y.; Hirata, Y., *Experientia* **1986,** 42, 855.

47. Flaherty, K. M.; DeLuca-Flaherty, C.; McKay, D. B., Three-dimensional structure of the ATPase fragment of a 70K heat-shock cognate protein. *Nature* **1990,** 346, (6285), 623-8.

48. Palleros, D. R.; Shi, L.; Reid, K. L.; Fink, A. L., hsp70-protein complexes. Complex stability and conformation of bound substrate protein. *J Biol Chem* **1994,** 269, (18), 13107-14.

49. Suh, W. C.; Burkholder, W. F.; Lu, C. Z.; Zhao, X.; Gottesman, M. E.; Gross, C. A., Interaction of the Hsp70 molecular chaperone, DnaK, with its cochaperone DnaJ. *Proc Natl Acad Sci U S A* **1998,** 95, (26), 15223-8.

50. Brodsky, J. L., Chaperoning the maturation of the cystic fibrosis transmembrane conductance regulator. *Am J Physiol Lung Cell Mol Physiol* **2001,** 281, (1), L39-42.

51. Gelman, M. S.; Kopito, R. R., Rescuing protein conformation: prospects for pharmacological therapy in cystic fibrosis. *J Clin Invest* **2002,** 110, (11), 1591-7.

52. Jolly, C.; Morimoto, R. I., Role of the heat shock response and molecular chaperones in oncogenesis and cell death. *J Natl Cancer Inst* **2000,** 92, (19), 1564-72.

53. Beere, H. M.; Green, D. R., Stress management - heat shock protein-70 and the regulation of apoptosis. *Trends Cell Biol* **2001,** 11, (1), 6-10.

54. Volloch, V. Z.; Sherman, M. Y., Oncogenic potential of Hsp72. *Oncogene* **1999,** 18, (24), 3648-51.

55. Seo, J. S.; Park, Y. M.; Kim, J. I.; Shim, E. H.; Kim, C. W.; Jang, J. J.; Kim, S. H.; Lee, W. H., T cell lymphoma in transgenic mice expressing the human Hsp70 gene. *Biochem Biophys Res Commun* **1996,** 218, (2), 582-7.

56. Nylandsted, J.; Rohde, M.; Brand, K.; Bastholm, L.; Elling, F.; Jaattela, M., Selective depletion of heat shock protein 70 (Hsp70) activates a tumor-specific death program that is independent of caspases and bypasses Bcl-2. *Proc Natl Acad Sci U S A* **2000,** 97, (14), 7871-6.

57. Elbi, C.; Walker, D. A.; Lewis, M.; Romero, G.; Sullivan, W. P.; Toft, D. O.; Hager, G. L.; DeFranco, D. B., A novel in situ assay for the identification and characterization of soluble nuclear mobility factors. *Sci STKE* **2004,** 2004, (238), pl10.

58. Brodsky, J. L.; Chiosis, G., Hsp70 molecular chaperones: emerging roles in human disease and identification of small molecule modulators. *Curr Top Med Chem* **2006,** 6, (11), 1215-25.

59. Garrido, C.; Schmitt, E.; Cande, C.; Vahsen, N.; Parcellier, A.; Kroemer, G., HSP27 and HSP70: potentially oncogenic apoptosis inhibitors. *Cell Cycle* **2003,** 2, (6), 579-84.

60. Polla, B. S.; Kantengwa, S.; Francois, D.; Salvioli, S.; Franceschi, C.; Marsac, C.; Cossarizza, A., Mitochondria are selective targets for the protective effects of heat shock against oxidative injury. *Proc Natl Acad Sci U S A* **1996,** 93, (13), 6458-63.

61. Nadler, S. G.; Tepper, M. A.; Schacter, B.; Mazzucco, C. E., Interaction of the immunosuppressant deoxyspergualin with a member of the Hsp70 family of heat shock proteins. *Science* **1992,** 258, (5081), 484-6.

62. Nadeau, K.; Nadler, S. G.; Saulnier, M.; Tepper, M. A.; Walsh, C. T., Quantitation of the interaction of the immunosuppressant deoxyspergualin and analogs with Hsc70 and Hsp90. *Biochemistry* **1994,** 33, (9), 2561-7.

63. Brodsky, J. L., Selectivity of the molecular chaperone-specific immunosuppressive agent 15-deoxyspergualin: modulation of Hsc70 ATPase activity without compromising DnaJ chaperone interactions. *Biochem Pharmacol* **1999,** 57, (8), 877-80.

64. Jiang, C.; Fang, S. L.; Xiao, Y. F.; O'Connor, S. P.; Nadler, S. G.; Lee, D. W.; Jefferson, D. M.; Kaplan, J. M.; Smith, A. E.; Cheng, S. H., Partial restoration of cAMP-stimulated CFTR chloride channel activity in DeltaF508 cells by deoxyspergualin. *Am J Physiol* **1998,** 275, (1 Pt 1), C171-8.

65. Mamelak, D.; Lingwood, C., The ATPase domain of hsp70 possesses a unique binding specificity for 3'-sulfogalactolipids. *J Biol Chem* **2001,** 276, (1), 449-56.

66. Whetstone, H.; Lingwood, C., 3'Sulfogalactolipid binding specifically inhibits Hsp70 ATPase activity in vitro. *Biochemistry* **2003,** 42, (6), 1611-7.

67. Fewell, S. W.; Smith, C. M.; Lyon, M. A.; Dumitrescu, T. P.; Wipf, P.; Day, B. W.; Brodsky, J. L., Small molecule modulators of endogenous and co-chaperone-stimulated Hsp70 ATPase activity. *J Biol Chem* **2004,** 279, (49), 51131-40.

68. Hamel, E.; Lin, C. M., Separation of active tubulin and microtubule-associated proteins by ultracentrifugation and isolation of a component causing the formation of microtubule bundles. *Biochemistry* **1984,** 23, (18), 4173-84.

69. Walker, D.; Htun, H.; Hager, G. L., Using inducible vectors to study intracellular trafficking of GFP-tagged steroid/nuclear receptors in living cells. *Methods* **1999,** 19, (3), 386-93.

70. Galigniana, M. D.; Scruggs, J. L.; Herrington, J.; Welsh, M. J.; Carter-Su, C.; Housley, P. R.; Pratt, W. B., Heat shock protein 90-dependent (geldanamycin-inhibited) movement of the glucocorticoid receptor through the cytoplasm to the nucleus requires intact cytoskeleton. *Mol Endocrinol* **1998,** 12, (12), 1903-13.

71. Hook, P.; Mikami, A.; Shafer, B.; Chait, B. T.; Rosenfeld, S. S.; Vallee, R. B., Long range allosteric control of cytoplasmic dynein ATPase activity by the stalk and C-terminal domains. *J Biol Chem* **2005,** 280, (38), 33045-54.

72. Youker, R. T.; Walsh, P.; Beilharz, T.; Lithgow, T.; Brodsky, J. L., Distinct roles for the Hsp40 and Hsp90 molecular chaperones during cystic fibrosis transmembrane conductance regulator degradation in yeast. *Mol Biol Cell* **2004,** 15, (11), 4787-97.

73. Isaacs, J. S.; Xu, W.; Neckers, L., Heat shock protein 90 as a molecular target for cancer therapeutics. *Cancer Cell* **2003,** 3, (3), 213-7.

74. Balachandran, R.; Welsh, M. J.; Day, B. W., Altered levels and regulation of stathmin in paclitaxel-resistant ovarian cancer cells. *Oncogene* **2003,** 22, (55), 8924-30.

75. Madiraju, C.; Edler, M. C.; Hamel, E.; Raccor, B. S.; Balachandran, R.; Zhu, G.; Giuliano, K. A.; Vogt, A.; Shin, Y.; Fournier, J. H.; Fukui, Y.; Bruckner, A. M.; Curran, D. P.; Day, B. W., Tubulin assembly, taxoid site binding, and cellular effects of the microtubule-stabilizing agent dictyostatin. *Biochemistry* **2005,** 44, (45), 15053-63.

76. Barltrop, J. A.; Owen, T. C., 5-(3-carboxymethoxyphenyl)-2-(4,5-dimenthylthiazoly)-3-(4-sulfophenyl)tetrazolium, inner salt (MTS) and related analogs of 3-(4,5-dimethylthiazolyl)-2,5-diphenyltetrazolium bromide (MTT) reducing to purple water-soluble formazans a cell-viability indicators. *Bioorg. & Med. Chem. Lett.* **1991,** 1, (11), 611.

77. Berridge, M. V.; Tan, A. S., Characterization of the cellular reduction of 3-(4,5-dimethylthiazol-2-yl)-2,5-diphenyltetrazolium bromide (MTT): subcellular localization, substrate dependence, and involvement of mitochondrial electron transport in MTT reduction. *Arch Biochem Biophys* **1993,** 303, (2), 474-82.

78. Cory, A. H.; Owen, T. C.; Barltrop, J. A.; Cory, J. G., Use of an aqueous soluble tetrazolium/formazan assay for cell growth assays in culture. *Cancer Commun* **1991,** 3, (7), 207-12.

79. Paschal, B. M.; Shpetner, H. S.; Vallee, R. B., Purification of brain cytoplasmic dynein and characterization of its in vitro properties. *Methods Enzymol* **1991,** 196, 181-91.

80. Shpetner, H. S.; Vallee, R. B., Purification and characterization of dynamin. *Methods Enzymol* **1991,** 196, 192-201.

81. Shpetner, H. S.; Vallee, R. B., Identification of dynamin, a novel mechanochemical enzyme that mediates interactions between microtubules. *Cell* **1989,** 59, (3), 421-32.

82. Lanzetta, P. A.; Alvarez, L. J.; Reinach, P. S.; Candia, O. A., An improved assay for nanomole amounts of inorganic phosphate. *Anal Biochem* **1979,** 100, (1), 95-7.

83. Roepstorff, P., Mass spectrometry in protein studies from genome to function. *Curr Opin Biotechnol* **1997,** 8, (1), 6-13.

84. Karas, M.; Hillenkamp, F., Laser desorption ionization of proteins with molecular masses exceeding 10,000 daltons. *Anal Chem* **1988,** 60, (20), 2299-301.

85. Pappin, D. J.; Hojrup, P.; Bleasby, A. J., Rapid identification of proteins by peptide-mass fingerprinting. *Curr Biol* **1993,** 3, (6), 327-32.

86. Martin, M.; Doty, M., *Anal Biochem* **1949,** 21, 965-967.

87. Romer, L.; Klein, C.; Dehner, A.; Kessler, H.; Buchner, J., p53--a natural cancer killer: structural insights and therapeutic concepts. *Angew Chem Int Ed Engl* **2006,** 45, (39), 6440-60.

88. Burkhardt, J. K.; Echeverri, C. J.; Nilsson, T.; Vallee, R. B., Overexpression of the dynamitin (p50) subunit of the dynactin complex disrupts dynein-dependent maintenance of membrane organelle distribution. *J Cell Biol* **1997,** 139, (2), 469-84.

89. Hirokawa, N., Kinesin and dynein superfamily proteins and the mechanism of organelle transport. *Science* **1998,** 279, (5350), 519-26.

90. http://nobelprize.org/nobel_prizes/medicine/laureates/2006/index.html.

91. Reck-Peterson, S. L.; Vale, R. D., Molecular dissection of the roles of nucleotide binding and hydrolysis in dynein's AAA domains in Saccharomyces cerevisiae. *Proc Natl Acad Sci U S A* **2004,** 101, (6), 1491-5.

92. Dell, K. R.; Turck, C. W.; Vale, R. D., Mitotic phosphorylation of the dynein light intermediate chain is mediated by cdc2 kinase. *Traffic* **2000,** 1, (1), 38-44.

93. Skop, A. R.; White, J. G., The dynactin complex is required for cleavage plane specification in early Caenorhabditis elegans embryos. *Curr Biol* **1998,** 8, (20), 1110-6.

94. Uetake, Y.; Terada, Y.; Matuliene, J.; Kuriyama, R., Interaction of Cep135 with a p50 dynactin subunit in mammalian centrosomes. *Cell Motil Cytoskeleton* **2004,** 58, (1), 53-66.

95. Shu, T.; Ayala, R.; Nguyen, M. D.; Xie, Z.; Gleeson, J. G.; Tsai, L. H., Ndel1 operates in a common pathway with LIS1 and cytoplasmic dynein to regulate cortical neuronal positioning. *Neuron* **2004,** 44, (2), 263-77.

96. Tsai, J. W.; Chen, Y.; Kriegstein, A. R.; Vallee, R. B., LIS1 RNA interference blocks neural stem cell division, morphogenesis, and motility at multiple stages. *J Cell Biol* **2005,** 170, (6), 935-45.

97. Kon, T.; Nishiura, M.; Ohkura, R.; Toyoshima, Y. Y.; Sutoh, K., Distinct functions of nucleotide-binding/hydrolysis sites in the four AAA modules of cytoplasmic dynein. *Biochemistry* **2004,** 43, (35), 11266-74.

98. Brummond, K. M.; Curran, D. P.; Mitasev, B.; Fischer, S., Heterocyclic alpha-alkylidene cyclopentenones obtained via a Pauson-Khand reaction of amino acid derived allenynes. A scope and limitation study directed toward the preparation of a tricyclic pyrrole library. *J Org Chem* **2005,** 70, (5), 1745-53.

99. Lazo, J. S.; Nemoto, K.; Pestell, K. E.; Cooley, K.; Southwick, E. C.; Mitchell, D. A.; Furey, W.; Gussio, R.; Zaharevitz, D. W.; Joo, B.; Wipf, P., Identification of a potent and selective pharmacophore for Cdc25 dual specificity phosphatase inhibitors. *Mol Pharmacol* **2002,** 61, (4), 720-8.

100. Nishiyama, S.; Yamamura, S., *Bull. Chem. Soc. Jpn.* **1985,** 58, 3453.

101. Werner, S.; Iyer, P. S.; Fodor, M. D.; Coleman, C. M.; Twining, L. A.; Mitasev, B.; Brummond, K. M., Solution-phase synthesis of a tricyclic pyrrole-2-carboxamide discovery library applying a stetter-Paal-Knorr reaction sequence. *J Comb Chem* **2006,** 8, (3), 368-80.

102. Czar, M. J.; Galigniana, M. D.; Silverstein, A. M.; Pratt, W. B., Geldanamycin, a heat shock protein 90-binding benzoquinone ansamycin, inhibits steroid-dependent translocation of the glucocorticoid receptor from the cytoplasm to the nucleus. *Biochemistry* **1997,** 36, (25), 7776-85.

103. Pratt, W. B.; Morishima, Y.; Murphy, M.; Harrell, M., Chaperoning of glucocorticoid receptors. *Handb Exp Pharmacol* **2006**, (172), 111-38.

104. Sasaki, S.; Shionoya, A.; Ishida, M.; Gambello, M. J.; Yingling, J.; Wynshaw-Boris, A.; Hirotsune, S., A LIS1/NUDEL/cytoplasmic dynein heavy chain complex in the developing and adult nervous system. *Neuron* **2000,** 28, (3), 681-96.

105. Vadlamudi, R. K.; Bagheri-Yarmand, R.; Yang, Z.; Balasenthil, S.; Nguyen, D.; Sahin, A. A.; den Hollander, P.; Kumar, R., Dynein light chain 1, a p21-activated kinase 1-interacting substrate, promotes cancerous phenotypes. *Cancer Cell* **2004,** 5, (6), 575-85.

106. Soti, C.; Nagy, E.; Giricz, Z.; Vigh, L.; Csermely, P.; Ferdinandy, P., Heat shock proteins as emerging therapeutic targets. *Br J Pharmacol* **2005,** 146, (6), 769-80.

107. Presley, J. F.; Cole, N. B.; Schroer, T. A.; Hirschberg, K.; Zaal, K. J.; Lippincott-Schwartz, J., ER-to-Golgi transport visualized in living cells. *Nature* **1997,** 389, (6646), 81-5.